The Dissertation Committee for Mark Jeffrey Pond
certifies that this is the approved version of the following dissertation:

Structure and dynamics of fluids: From molecular to colloidal perspectives

Committee:

Thomas M. Truskett, Supervisor

Christopher J. Ellison

Venkat Ganesan

Dmitrii E. Makarov

Isaac C. Sanchez

Structure and dynamics of fluids: From molecular to colloidal perspectives

by

Mark Jeffrey Pond, B.S.Ch.E.; B.A.

DISSERTATION

Presented to the Faculty of the Graduate School of

The University of Texas at Austin

in Partial Fulfillment

of the Requirements

for the Degree of

DOCTOR OF PHILOSOPHY

THE UNIVERSITY OF TEXAS AT AUSTIN

August 2011

Dedicated to J. Edwin Faris and in memory of Zorita J. Faris

Acknowledgments

Above all, I would like to thank Prof. Thomas Truskett for guiding me during my graduate studies. In addition to his numerous ideas and writing gifts, he also created a comfortable and welcoming work environment that encourages research and discussion. I would also like to thank Prof. Jeffrey Errington for acting like secondary advisor. None of this work would have been possible without his timely simulations and suggestions. Vincent Shen also helped greatly with his contributions of Monte Carlo simulations of binary systems. Vince and Jeff allowed me to build a dynamic story on top of their structural foundation.

In addition to my advisor and collaborators, the Truskett research group has been wonderful to me over the past 5 years. James Carmer has been great to share an office with. Our conversations on life, research and football have kept me sane. Bill Krekelberg was an incredible source of bash scripts, FORTRAN programming tricks and interesting thoughts. Garuav Goel gave me a great appreciation for doing theoretical work instead of just brute forcing simulations and greatly embodied both Indian and American culture. Avni Jain and Kyle Hollingshead have brought good, young energy into the lab and I'm looking forward to seeing what they will produce in their graduate careers.

I'm grateful to the winter school on glasses and glass formers at the

JNCASR in Bangalore, which allowed me to interact with many great minds and inspired my work back at UT.

In addition to the research opportunities, my time at UT has been enriched by all of the other opportunities I've been able to take advantage of here. My roommates have been consistently amazing and intelligent people that have shaped the person I have become. The dance communities I've been involved with have brought out an expressive, artistic side of my personality I never knew existed. The wonderful Bible study groups and church group I have been involved in have shaped my worldview and provided wonderful examples of what it means to have a relationship with God. In addition to all of these communities, there are many more people that I've shared a beer with or been able to hang out with that have made my time here in Austin unforgettable. Thanks to all of you.

Finally, I would like to thank my true backbone, my family. Their consistent love, phone calls, research discussions and general presence keep me grounded. I know that no matter where I go and what I do, my family will be there to support me and lift me up.

Structure and dynamics of fluids: From molecular to colloidal perspectives

Publication No. _____

Mark Jeffrey Pond, Ph.D.
The University of Texas at Austin, 2011

Supervisor: Thomas M. Truskett

Relationships between structure and dynamics have been well studied in molecular fluids, both in computer simulations and in experiments. However, the development of simple structure-dynamics relationships would also be useful in understanding colloidal fluids. Colloidal fluids display differentiated component dynamics, are made of polydisperse particles, have soft interactions and have a separation of length and time scales. In this dissertation work, we have used computer simulations to generalize some structure-dynamics scaling laws, originally formulated for molecular fluids, in a way that successfully accounts for these important aspects of colloidal suspensions.

To begin, we examine a two-component mixture of ultrasoft Gaussian-core particles through molecular dynamics simulations. This fluid shows an anomalous dynamic crossover where the larger particles become more diffusive

than the smaller particles. However, this dynamic crossover is accompanied by a corresponding structural crossover for a component-specific structural order metric. In the light of this structural order metric, the fluid is non-anomalous with respect to the relationship between static structuring and diffusivity.

Next, we show that accounting for the many-component nature of even modestly polydisperse fluids is important for accurately characterizing their structure-dynamics relationships. We demonstrate this for colloids with short-range attractions through new Monte Carlo simulation techniques and through theoretical calculations carried out in the dilute limit.

From here, we present a new generalized framework to non-dimensionalize diffusivity so that it will have an approximately one-to-one relationship with excess entropy. This method involves rescaling diffusivity with dilute-limit analyses that can be analytically and systematically executed. We tested this framework through a combination of molecular dynamics simulations, Brownian dynamics simulations and Monte Carlo simulations. The results of the simulations demonstrate that this framework can account for particle size asymmetry, particle additivity, interaction strength and some solvent effects.

Finally, we present a new, simple equation that relates non-dimensionalized forms of diffusivity from molecular dynamics and Brownian dynamics simulations. This simple relationship is tested for inverse power law fluids, as well as a suite of ultrasoft fluids that show structural and dynamic anomalies.

Table of Contents

List of Figures

Chapter 1

Introduction

For my dissertation work, I have explored the relationship between structure and dynamics in fluids with the aim of extending existing models from a molecular perspective towards a broader colloidal perspective. To do this, I have analyzed computer simulations of systems similar to a simple molecular model, but each with an isolated change to make a controlled investigation of the effects of looking at different elements of colloidal systems.

Understanding a system's dynamic behaviors has applications in food science, membrane design, glass transitions and a variety of other transport-dominated phenomena. There is a wide range of literature tying the dynamic behavior of molecular liquids to their static structuring.[5, 6, 7, 8, 9] This is shown in computer simulations of effective molecular components and in experiments on high pressure molecular fluids.[10, 1, 11] Understanding these relationships has helped us understand underlying dynamic processes and even design idealized dynamics from molecular interactions that take advantage of these relationships.[12]

However, many systems that use dynamic design are not molecular in length scale. They are colloidal systems that are mixtures of non-idealized

particles that can show a wide range of dynamic behavior. In contrast to molecular systems, colloidal systems show anomalous mixture behavior, show polydispersity in the construction of the solutes, have softer interactions between particles and have a separation of length and time scales between their solvent and solutes.[13, 14, 15] In my thesis, I have explored the behavior of soft fluid systems and analyzed the effect of the differences that come up in the study of colloidal fluids. I have done this through a combination of molecular dynamics simulations, Brownian dynamics simulations, Monte Carlo simulations and dilute-limit expansions of dynamic and static fluid behavior.

1.1 Relationships between structure and dynamics

Intuitively, dynamics in a liquid should be tied to the fluid's ordering. However, finding the correct framework to put the two on an equal footing is still an unsolved and active problem.[16] Static ordering has been well studied in fluids and there are robust methods to predict the ordering from first principles.[17] However, understanding of dynamic relaxation is still subject to investigation from many – at times contradictory – angles.[5, 6, 7, 8, 9] Finding a consistent framework that relates structure and dynamics would allow us to understand, predict and control the dynamic properties of fluids with increased precision and speed.

This dissertation focuses on excess-entropy-based relationships between structuring and dynamics. These relationships were first noted by Rosenfeld[5] in his study of the low-density dynamic behavior of simple inverse-power-

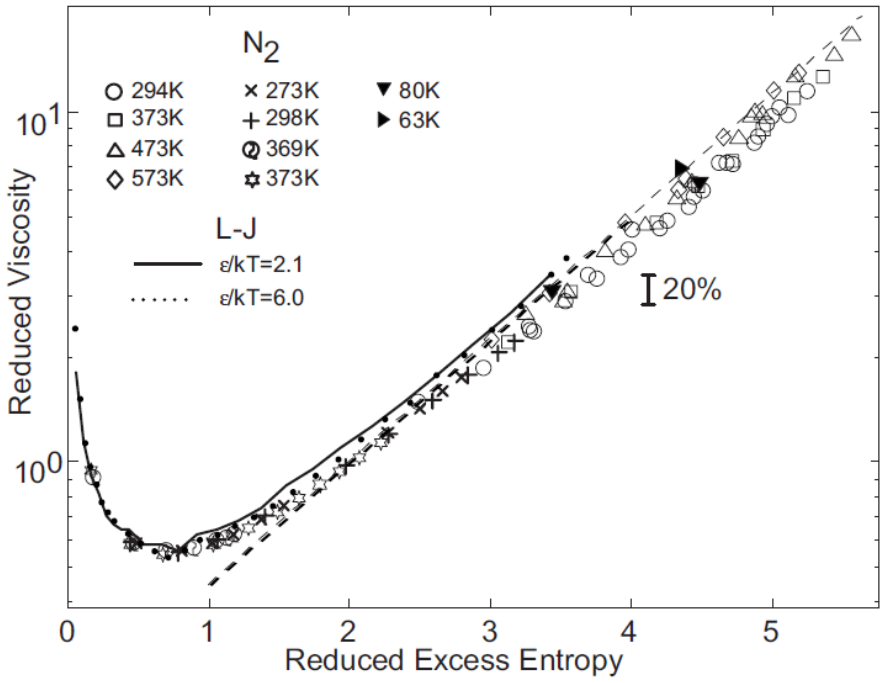

Figure 1.1: Reduced viscosity plotted against reduced excess entropy. The solid and dotted lines are results from molecular dynamics simulations of a Lennard-Jones fluid at reduced temperatures of 2.1 and 6.0, respectively. The dashed line represents Rosenfeld's hypothesis. Figure is reproduced with permission from Abramson et al.[1]. Copyright 2008 by The American Physical Society.

law (IPL) fluids. He noted that, through appropriate non-dimensionalization, diffusivity was approximately a single-valued function of excess entropy for all of the IPL fluids, from hard-spheres to a one-component-plasma. These scalings have turned out to be robust enough to apply not just to fluids in-silico, but also to molecular fluids at high densities and temperatures (see Figure 1.1).[10, 1, 11] The Rosenfeld scaling has been extended in analogous directions and applied to new fluids,[7, 18, 19, 2, 20] but even these have not been well-analyzed for their universality. The work in Chapters 2-6 address new angles for excess-entropy scalings that help shine light on the subject and advance our understanding of the relationship between structure and dynamics.

1.2 Characteristics of colloidal fluids

Colloids are mixtures of two separate components that coexist with one phase dispersed in the other. Colloidal mixtures are ubiquitous in technological applications and processing of everyday materials. These dispersions typically involve particles that are on the nanoscale or microscale, which brings forth complications that do not exist in a molecular fluid.[13] Until now, all of the studies on the connection between excess entropy and dynamics have been focused on molecular systems. In order to extend that connection to colloidal systems, we examine systems that have slight changes from well-studied molecular systems. From this framework, we can understand potential pitfalls in applying excess-entropy scalings to colloidal systems and work to find methods of dealing with those pitfalls. The following subsections will introduce the

specific changes that we have decided to focus on in our studies.

1.2.1 Multicomponent fluids

Colloids are inherently mixtures and the treatment of multiple components with respect to excess-entropy scalings has been largely unstudied. There exist treatments to analyze the individual-component behavior of collective mixtures.[21, 22] However, these treatments do not study colloidal systems that display differentiated component behavior, such as the single-glass state of star polymer mixtures where one component is glassy and the other is still ergodic.[23] In addition, the existing analyses depend on the additivity of the individual components. However, in some colloidal fluids – such as polymer blends – the individual components act in a non-additive manner.[24] Some extensions to understanding the connection between structure and dynamics for mixtures with these kinds of dynamic anomalies are addressed in Chapters 2 and 4 of this work.

1.2.2 Polydisperse solutes

Colloidal particles are inherently mildly polydisperse, even when considered to be effectively monodisperse.[25] In addition, many solutes are intentionally polydisperse so that they can avoid the freezing transition and remain in suspension at higher particle concentrations.[26, 27, 28] However, this polydispersity can lead to misleading apparent softening of scattering and structural information.[29, 25, 30] Despite this, many studies of the dynamics

and real-space structuring of colloidal fluid models have neglected adjusting for the effects of polydispersity in their treatments.[31, 3] In Chapter 3, we address whether polydispersity changes the fundamental relationship between structure and dynamics for simplified colloidal models.

1.2.3 Soft effective interactions

One method for determining interparticle potentials between solutes in colloidal mixtures is to analyze their structuring at low densities and back-calculate what potential interaction would give an equivalent pair distribution function.[32, 33, 14] For colloids of varying sizes and solvent interactions, these effective interactions can be quite soft. For interpenetrable polymer chains[34] or similar colloidal fluids, their ultrasoft effective interactions can even have a finite energy at total overlap. If these soft, interpenetrable fluids don't cluster at high densities,[35] they will form a high-density fluid phase that shows water-like dynamic anomalies. Chapters 2, 4, 5 and 6 deal with these soft fluids and analyze them within the context of Rosenfeld's excess-entropy scalings.

1.2.4 Separation of length and time scales

Many studies of the dynamics of colloidal systems utilize Newtonian molecular dynamics routines to obtain dynamic data. This approach can be comprehensive if the solvent can be approximated in the simulation. However, in many colloidal systems, there is a separation of length scales and relaxation

time scales between the solvent and solute such that including both in a simulation becomes intractable.[13] There are numerous methods to include the effects of solvent in computer simulations,[13, 36, 37, 38, 39] but the question arises as to whether we can take the molecular dynamics general behavior and use it to understand colloidal dynamics. We address this question in Chapters 5 and 6.

1.3 Thesis Organization

Chapter 2: Composition and concentration anomalies for structure and dynamics of Gaussian-core mixtures[40]

In this chapter, we report molecular dynamics simulation results for two-component fluid mixtures of Gaussian-core particles, focusing on how tracer diffusivities and static pair correlations depend on temperature, particle concentration, and composition. At low particle concentrations, these systems behave like simple atomic mixtures. However, for intermediate concentrations, the single-particle dynamics of the two species largely decouple, giving rise to the following anomalous trends. Increasing either the concentration of the fluid (at fixed composition) or the mole fraction of the larger particles (at fixed particle concentration) enhances the tracer diffusivity of the larger particles, but decreases that of the smaller particles. In fact, at sufficiently high particle concentrations, the larger particles exhibit higher mobility than the smaller particles. Each of these dynamic behaviors is accompanied by a corresponding structural trend that characterizes how either concentration

or composition affects the strength of the static pair correlations. Specifically, the dynamic trends observed here are consistent with a single empirical scaling law that relates an appropriately normalized tracer diffusivity to its pair-correlation contribution to the excess entropy.

Chapter 3: Implications of the effective one-component analysis of pair correlations in colloidal fluids with polydispersity[41]

Partial pair-correlation functions of colloidal suspensions with continuous polydispersity can be challenging to characterize from optical microscopy or computer simulation data due to inadequate sampling. As a result, it is common to adopt an effective one-component description of the structure that ignores the differences between particle types. Unfortunately, whether this kind of simplified description preserves or averages out information important for understanding the behavior of the fluid depends on the degree of polydispersity and can be difficult to assess, especially when the corresponding multicomponent description of the pair correlations is unavailable for comparison. Here, we present a computer simulation study that examines the implications of adopting an effective one-component structural description of a polydisperse fluid. The square-well model that we investigate mimics key aspects of the experimental behavior of suspended colloids with short-range, polymer-mediated attractions. To characterize the partial pair-correlation functions and thermodynamic excess entropy of this system, we introduce a Monte Carlo sampling strategy appropriate for fluids with a large number of pseudo-components. The data from our simulations at high particle concentrations, as well as exact

theoretical results for dilute systems, show how qualitatively different trends between structural order and particle attractions emerge from the multicomponent and effective one-component treatments, even with systems characterized by moderate polydispersity. We examine consequences of these differences for excess-entropy-based scalings of shear viscosity, and we discuss how use of the multicomponent treatment reveals similarities between the corresponding dynamic scaling behaviors of attractive colloids and liquid water that the effective one-component analysis does not capture.

Chapter 4: Generalized Rosenfeld scalings for tracer diffusivities in not-so-simple fluids: Mixtures and soft particles[42]

Rosenfeld[5] originally noticed that casting the transport coefficients of simple monatomic, equilibrium fluids in a specific dimensionless form makes them approximately single-valued functions of excess entropy. This observation has predictive value because, while the transport coefficients of dense fluids can be difficult to estimate from first principles, the excess entropy can often be accurately predicted from liquid-state theory. In this chapter, we use molecular simulations to investigate whether Rosenfeld's observation is a special case of a more general scaling law relating the tracer diffusivities of particles in mixtures to the excess entropy. Specifically, we study the tracer diffusivities, static structure, and thermodynamic properties of a variety of one- and two-component model fluid systems with either additive or non-additive interactions of the hard-sphere or Gaussian-core form. The results of the simulations demonstrate that the effects of mixture concentration and

composition, particle-size asymmetry and additivity, and strength of the interparticle interactions in these fluids are consistent with an empirical scaling law relating the excess entropy to a new dimensionless (generalized Rosenfeld) form of tracer diffusivity, which we introduce here. The dimensionless form of the tracer diffusivity follows from knowledge of the intermolecular potential and the transport/thermodynamic behavior of fluids in the dilute limit. The generalized Rosenfeld scaling requires less information, and provides more accurate predictions, than either Enskog theory or scalings based on the pair-correlation contribution to the excess entropy. As we show, however, it also suffers from some limitations, especially for systems that exhibit significant decoupling of individual component tracer diffusivities.

Chapter 5: Generalizing Rosenfeld's excess-entropy scaling to predict long-time diffusivity in dense fluids of Brownian particles: From hard to ultrasoft interactions[43]

Computer simulations are used to test whether a generalization of Rosenfeld's excess-entropy scaling method for estimating transport coefficients in systems obeying molecular dynamics can be extended to predict long-time diffusivities in fluids of particles undergoing Brownian dynamics in the absence of interparticle hydrodynamic forces. Model fluids with inverse-power-law, Gaussian-core, and Hertzian pair interactions are considered. Within the generalized Rosenfeld scaling method, long-time diffusivities of ultrasoft Gaussian-core and Hertzian particle fluids, which display anomalous trends with increasing density, are predicted (to within 20%) based on knowledge

of interparticle interactions, excess entropy, and scaling behavior of simpler inverse-power-law fluids.

Chapter 6: Mapping between long-time molecular and Brownian dynamics[44]

We use computer simulations to test a simple idea for mapping between long-time self diffusivities obtained from molecular and Brownian dynamics. The strategy we explore is motivated by the behavior of fluids comprising particles that interact via inverse-power-law pair potentials, which serve as good reference models for dense atomic or colloidal materials. Based on our simulation data, we present an empirical expression that semi-quantitatively describes the "atomic" to "colloidal" diffusivity mapping for inverse-power-law fluids, but also for model complex fluids with considerably softer (star-polymer, Gaussian-core, or Hertzian) interactions. As we show, the anomalous structural and dynamic properties of these latter, ultrasoft systems pose problems for other strategies designed to relate Newtonian and Brownian dynamics of hard-sphere-like particles.

Chapter 7: Future work

This chapter addresses questions that have been generated from the results in the dissertation and suggests possible angles to explore those new questions.

Chapter 2

Composition and concentration anomalies for structure and dynamics of Gaussian-core mixtures

2.1 Introduction

Fluids of identical particles interacting via the Gaussian-core (GC) pair potential have been the subject of many recent investigations.[45, 46, 47, 48, 49, 50, 51, 52, 2] Continued interest in this model system, introduced by Stillinger in 1976,[53] can be attributed in part to the fact that the GC potential is a simple and computationally tractable idealization of the soft, effective interparticle repulsions that can exist between large molecular species (e.g., star polymers) or self-assembled structures (e.g., micelles) in solution.[14] The GC fluid is also a compelling model to study because it exhibits several unusual physical properties that are typically associated with molecular or complex-fluid systems with more complicated interactions. For example, at low temperature, the GC fluid displays a re-entrant freezing transition [48, 49, 51, 53] negative thermal expansivity,[45, 54] and its isothermal compressibility increases upon isobaric cooling.[50] Although the structural and dynamic properties of the GC fluid are qualitatively similar to those of simpler fluids at low particle concentrations, they become anomalous

at sufficiently high particle concentrations. For example, the single-particle dynamics, quantified by, e.g., the self diffusivity, become progressively faster upon increasing particle concentration (diffusivity anomaly). [50, 52, 2, 54] The static pair correlations,[46, 47, 49, 50, 51, 52, 2, 53] quantified by, e.g., the two-body excess entropy $s^{(2)}$, also weaken upon increasing particle concentration (structural anomaly).[2]

The differences between the structural behavior of the GC fluid at low versus high particle concentration can be qualitatively understood by considering the Gaussian form of the repulsion. At low concentration and low temperature, the average interparticle separation is larger than the range of the interaction. Thus, the part of the GC potential that the particles typically sample when they "collide" is steeply repulsive. Under these conditions, small increases in concentration lead to the build up of short-range static correlations (i.e., coordination shell structure), similar to what occurs in the hard-sphere fluid.[46, 47, 49, 50, 51, 52, 2, 53] However, at sufficiently high concentration, the bounded form of the GC potential allows the average interparticle separation to become much smaller than the range of the interaction. As a result, particles are effectively penetrable and constantly experience soft repulsive forces from many neighbors. These forces largely cancel one another, creating a "mean field". Further increasing the concentration only makes this effect more pronounced, paradoxically driving the high-density system toward an ideal-gas-like structure. [46, 47, 49, 50, 51, 52, 2, 53]

Less is understood about the microscopic origins of the anomalous re-

lationship between diffusivity and particle concentration, although the results of recent investigations indicate that the unusual dynamical trends are closely linked to the aforementioned structural anomalies.[52, 2] In particular, the equilibrium GC fluid exhibits a semi-quantitative scaling relation[2] between self diffusivity D and the two-body excess entropy $s^{(2)}$. Interestingly, this relationship is "normal" in the sense that it is similar to that observed for a wide variety of simpler fluids that do not exhibit either structural or dynamic anomalies. [2, 5, 6, 7, 55] Stated differently, the diffusivity anomaly of the equilibrium GC fluid disappears when one plots D versus $s^{(2)}$ instead of particle concentration.[2] Similar trends have also recently been reported for other equilibrium fluids with dynamic and structural anomalies, e.g., models with water-like interactions [56, 19, 57] or colloid-like, short-range attractions. [58, 3]

In this paper, we further explore the relationship between structure and dynamics in simple models for complex fluids by studying, via molecular simulation, binary mixtures of GC particles. The fluid phase behavior of these systems has already been studied extensively. [24] However, here we present, to our knowledge, the first investigation of the relationships between the static pair correlations of the fluid and the tracer diffusivities of the two components.

Specifically, we study the following questions about how these quantities depend on particle concentration and mixture composition. Are the trends in the tracer diffusivities of the two components of the GC mixture closely coupled? Do they scale in a simple way with a single measure of the

overall strength of the pair correlations (e.g., $s^{(2)}$)? Or, alternatively, is there a significant decoupling of the single-particle dynamics of the two species? If this latter scenario holds, do the resulting trends in tracer diffusivities track decoupled, species-dependent measures of static structure? Finally, what are the implications of the answers to the above for the compositional dependencies of structural order and tracer diffusivity at low versus high particle concentration?

2.2 Methods

To address these questions, we use molecular dynamics simulations to investigate equilibrium two-component fluid mixtures of particles that interact via pair potentials of the GC form, $\phi_{ij}(r) = \epsilon_{ij} \exp[-(r/\sigma_{ij})^2]$. Here, r is the interparticle separation, and the parameters ϵ_{ij} and σ_{ij} characterize the energy scale and range of the interactions, respectively, between particles of type i and j with $i, j \in \{A, B\}$. Since we want to understand the behavior of uniform binary fluids, we assign numerical values to the parameters that favor mixing. Specifically, we adopt a set[24] introduced earlier ($\sigma_{BB} = 0.665\sigma_{AA}$; $\sigma_{AB} = (0.5[\sigma_{AA}^2 + \sigma_{BB}^2])^{0.5}$; $\epsilon_{AA} = \epsilon_{BB}$; $\epsilon_{AB} = 0.944\epsilon_{AA}$), in which the σ_{ij} were chosen to mimic binary mixtures of self-avoiding polymers in solution. [47] We truncate all pair potentials at an interparticle separation of $3.2\sigma_{AA}$, and treat the particles of the two species as having equal masses ($m_A = m_B$).

We carry out the simulations in the microcanonical ensemble, numerically integrating Newton's equations of motion with the velocity-Verlet scheme [17]

using a time step of $0.05\sqrt{m_A\sigma_{AA}^2/\epsilon_{AA}}$. We use $N = 3000$ GC particles and a periodically replicated simulation cell, the volume V of which is chosen to realize specific values of reduced total concentrations (i.e., particle densities) in the range $0.05 \leq \rho\sigma_{AA}^3 \leq 1$, where $\rho = N/V$. We investigate mixtures over a wide range of composition ($0.1 \leq x_A \leq 0.9$, where x_A is the mole fraction of species A) and reduced temperature ($0.05 \leq k_BT/\epsilon_{AA} \leq 0.40$). To characterize the single-particle dynamics of species i, we compute its tracer diffusivity D_i by fitting the long-time ($t \to \infty$) behavior of its average mean-squared displacement $\langle \Delta {r_i}^2 \rangle$ to the Einstein formula, $D_i = \langle \Delta {r_i}^2 \rangle / 6t$.[1]

We compute the two-body excess entropy $s^{(2)}$ directly from the partial radial distribution functions $g_{ij}(r)$ of the fluid using the expression,[59, 22]

$$s^{(2)} = \sum_i x_i s_i^{(2)} \tag{2.1}$$

where $s_i^{(2)}$ is given by

$$\frac{s_i^{(2)}}{k_\mathrm{B}} = -\sum_j \frac{x_j \rho}{2} \int [g_{ij}(\mathbf{r}) \ln g_{ij}(\mathbf{r}) - g_{ij}(\mathbf{r}) + 1] d\mathbf{r} \tag{2.2}$$

Both $-s^{(2)}$ and $-s_i^{(2)}$ are non-negative and can be viewed as translational structural order metrics.[60] The former characterizes the overall strength of the pair correlations in the fluid,[60] while the latter quantifies the amount of pair structuring surrounding particles of type i.

[1] We use Student's t distribution together with the tracer diffusivities from five independent runs to estimate 95% confidence intervals for the D_i.

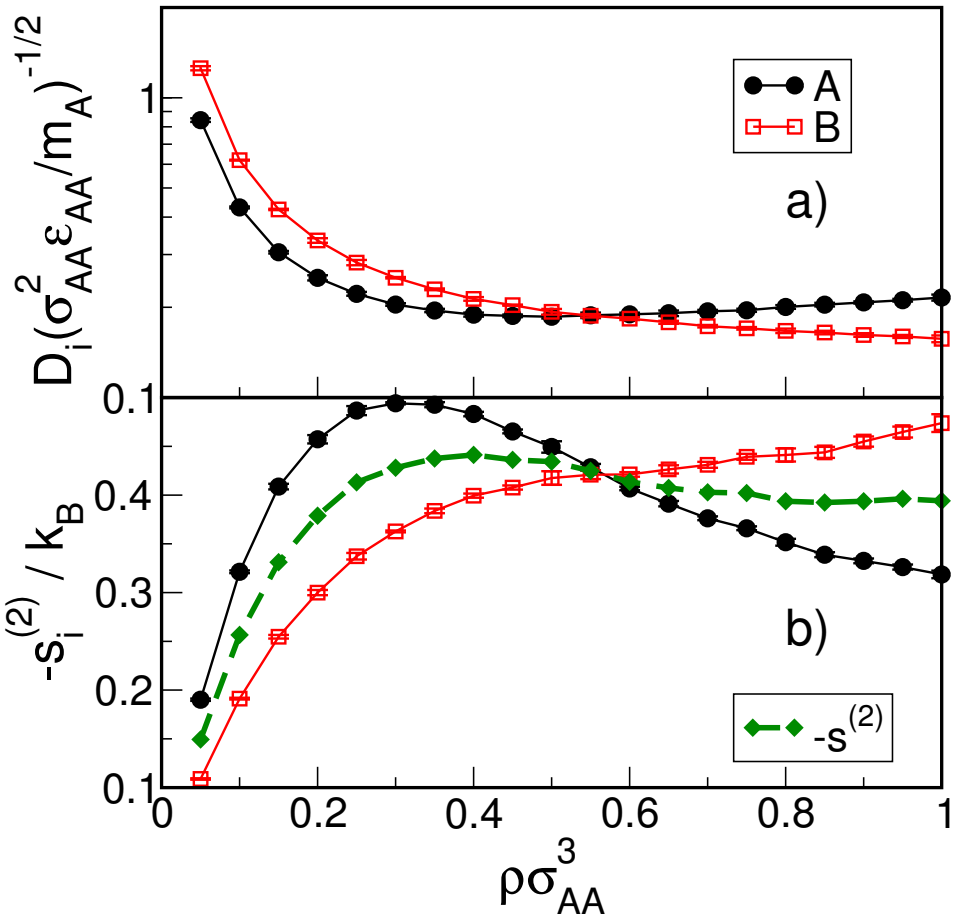

Figure 2.1: (a)Tracer diffusivity D_i and (b) structural order metric -$s_i^{(2)}$, with $i \in \{A, B\}$, versus concentration $\rho\sigma_{AA}^3$ for the binary Gaussian-core fluid mixture discussed in the text. The collective structural order metric -$s^{(2)}$ is also included in (b). The temperature is $k_{\rm B}T/\epsilon_{AA} = 0.1$ and the mole fraction is $x_A = 0.5$.

2.3 Decoupling of small and large particle behavior

The first issue that we investigate using our simulation data is how closely the single-particle dynamics of the two species are coupled. Figure 2.1(a) shows how the computed tracer diffusivities, D_A and D_B, depend on density $\rho\sigma_{AA}^3$ for an equimolar ($x_A = 0.5$) mixture at a temperature of $k_{\mathrm{B}}T/\epsilon_{AA} = 0.1$. As can be seen, D_A follows the same type of non-monotonic trend observed for the self diffusivity of the single-component GC fluid,[2] displaying an anomalous dependency on particle concentration $[(\partial D_A/\partial\rho)_{T,x_A} > 0]$ for densities greater than $\rho\sigma_{AA}^3 \approx 0.4$. On the other hand, D_B shows behavior consistent with that of simple fluids, monotonically decreasing with $\rho\sigma_{AA}^3$ over the density range examined here. The fact that D_A and D_B decouple in this way gives rise to a dynamic crossover density, above which the larger A particles exhibit higher mobility than the smaller B particles. It also suggests that one cannot trivially correlate both the D_A and D_B trends with a single, collective measure of structural order for the fluid, such as $s^{(2)}$ [see, e.g., Figure 2.1(b)], a point we examine further below.

Does increasing particle concentration result in a corresponding decoupling of species-specific structural metrics that, in turn, correlate with the dynamical trends of A and B particles? To examine this possibility, we first plot in Figure 2.1(b) the density dependencies of $-s_A^{(2)}$ and $-s_B^{(2)}$. As can be seen, there is indeed a structural decoupling. While both $-s_A^{(2)}$ and $-s_B^{(2)}$ increase with density at low values of $\rho\sigma_{AA}^3$, the increase in ordering is initially more pronounced for the structure surrounding the A particles. This is to

be expected because A particles have larger effective contact diameters with their neighbors, and thus respond by building up stronger static pair correlations at low density. However, the large size of the A particles, coupled with the bounded nature of the GC interaction, means that A particles are also forced into more interparticle overlaps than the B particles as the density is increased. This ultimately leads to a weakening of the static correlations (i.e., coordination shell structure) of the A particles, and hence a maximum in $-s_A^{(2)}$ at an intermediate value of $\rho\sigma_{AA}^3$. As should be expected based on the smaller size of the B particles, a maximum in $-s_B^{(2)}$ (and a corresponding minimum in D_B) can also occur at significantly higher densities, if phase separation of the mixture does not occur first.[2] Interestingly, similar to what is observed for the tracer diffusivities, one of the consequences of the $s_i^{(2)}$ decoupling described above is the presence of a structural crossover density above which the smaller B particles exhibit stronger pair correlations than the larger A particles.

2.4 Correlation between structure and dynamics

The data in Figure 2.1(a) and (b) suggests a negative correlation between D_A and $-s_A^{(2)}$ (and also between D_B and $-s_B^{(2)}$), in which the structural crossover ($s_A^{(2)} = s_B^{(2)}$) occurs at approximately the same density as the dynamic

[2]In the limit of pure B ($x_A = 0$), one observes[2] both $(\partial D_B/\partial\rho)_{T,x_A} > 0$ and $(\partial s_B^{(2)}/\partial\rho)_{T,x_A} > 0$ for reduced densities greater than $\rho\sigma_{AA}^3 \approx 1.4$. However, we have found in our studies of this system that, for non-zero values of x_A, the binary GC fluid will often phase separate at densities below where the onset of anomalous dynamic and structural behavior occurs.

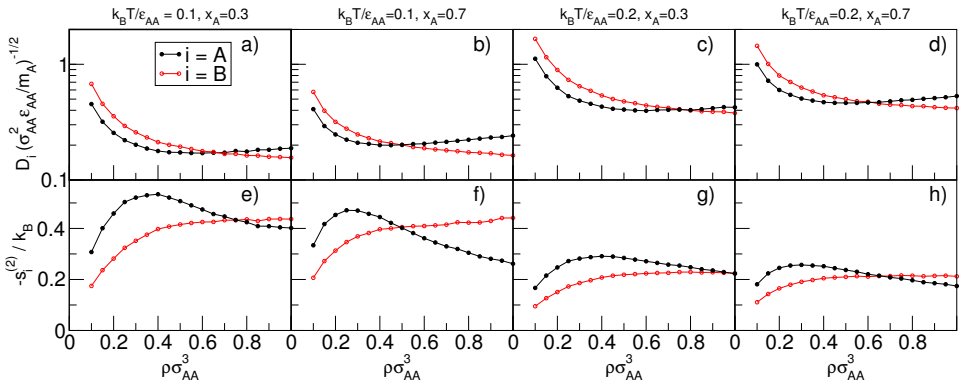

Figure 2.2: (a-d)Tracer diffusivity D_i and (e-h) structural order metric -$s_i^{(2)}$, with $i \in \{A, B\}$, versus concentration $\rho\sigma_{AA}^3$ for the binary Gaussian-core fluid mixture discussed in the text. The columns are systems at different temperatures and mole fractions, which are listed above the respective column.

crossover ($D_A = D_B$). In fact, although we focus on one particular pairing of composition and temperature in Figure 2.1, these trends are exhibited by this system for a wide range of compositions and temperatures, as demonstrated in Figure 2.2.

To quantitatively examine the correlation between single-particle dynamics and structure, we studied possible generalizations of a scaling relationship that describes the behavior of the single-component GC fluid. In the case of the single-component fluid, the so-called Rosenfeld scaled[6] self diffusivity $D^R = D\rho^{1/3}(k_\mathrm{B}T/m)^{-1/2}$ is approximately a single-valued function of $-s^{(2)}$ across a wide range of temperature and density.[2] Figure 2.3(a), however, shows that a naïve extension of this result for mixtures, $D_i^R = D_i\rho^{1/3}(k_\mathrm{B}T/m_i)^{-1/2}$ versus $-s^{(2)}$, does not adequately collapse the data for either of the two species. This should not be particularly surprising, given the

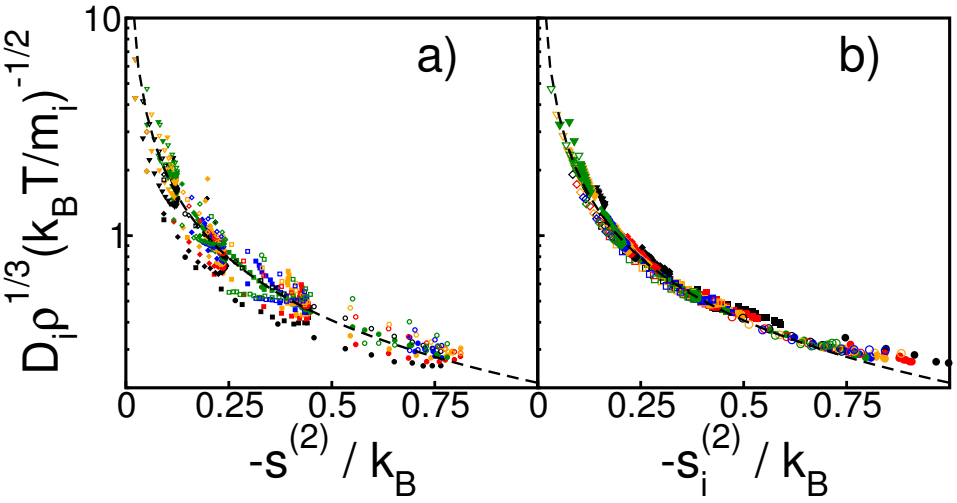

Figure 2.3: Rosenfeld scaled tracer diffusivity $D_i^R = D_i\rho^{1/3}(k_BT/m_i)^{-1/2}$ versus (a) two body excess entropy $-s^{(2)}$ and (b) its contribution from structuring around type i particles $-s_i^{(2)}$, with $i \in \{A, B\}$, for the binary Gaussian-core fluid mixture discussed in the text. Shown are mole fractions $x_A = 0.1$ (black), 0.3 (red), 0.5 (orange), 0.7 (blue), and 0.9 (green) and temperatures $k_BT/\epsilon_{AA} = 0.05$ (circles), 0.1 (squares), 0.2 (diamonds) and 0.4 (triangles). Filled and open shapes represent A and B particles, respectively. The dashed line indicates a least-square fit to a power law relationship for the single-component GC fluid[2], $D^R = 0.208{s^{(2)}}^{-0.972}$.

dynamical and structural decouplings shown in Figure 2.1(a) and (b).

On the other hand, Figure 2.3(b) examines a species-specific extension of the single-component scaling law, D_i^R versus $-s_i^{(2)}$. Interestingly, not only does this generalization collapse the temperature, density, and compositional dependencies of tracer diffusivity for each individual particle type, but the behaviors of the two species are, to a good approximation, accounted for by the mathematical form of the scaling law for the single-component GC fluid.

2.5 Compositional anomaly

We now explore what this correlation implies about how mixture composition affects the tracer diffusivities [Figure 2.4(a),(b)] and species-specific pair-correlation contributions to excess entropy [Figure 2.4(c),(d)]. As should be expected, at low values of density ($\rho\sigma_{AA}^3 < 0.2$), the response of the system to changes in composition is normal, i.e., qualitatively similar to that of simple atomic or hard-sphere-like mixtures where interparticle "collisions" dominate. Under these conditions, increasing the mole fraction of the larger A particles effectively increases the "packing fraction" of the fluid, which in turn decreases the mobility and increases the local structural order surrounding both types of particles.

At high values of density, on the other hand, the fact that the bounded GC potential allows for significant interparticle overlaps changes the physics. Since increasing the mole fraction of the larger particles (at constant density) here increases the number of overlaps and nudges the system toward the mean-field fluid, one expects anomalous behavior in dynamics and structure, i.e. a corresponding increase in D_i and decrease in $-s_i^{(2)}$ for both species. Indeed, Figure 2.4 shows that these anomalous compositional trends for dynamics and structure do occur for $\rho\sigma_{AA}^3 > 0.4$.

In closing, we note a final manifestation of the decoupled behavior for the two species of this GC mixture. Specifically, the densities at which the compositional trends for structure and dynamics transition from normal to anomalous are significantly different for the two species, with the larger species

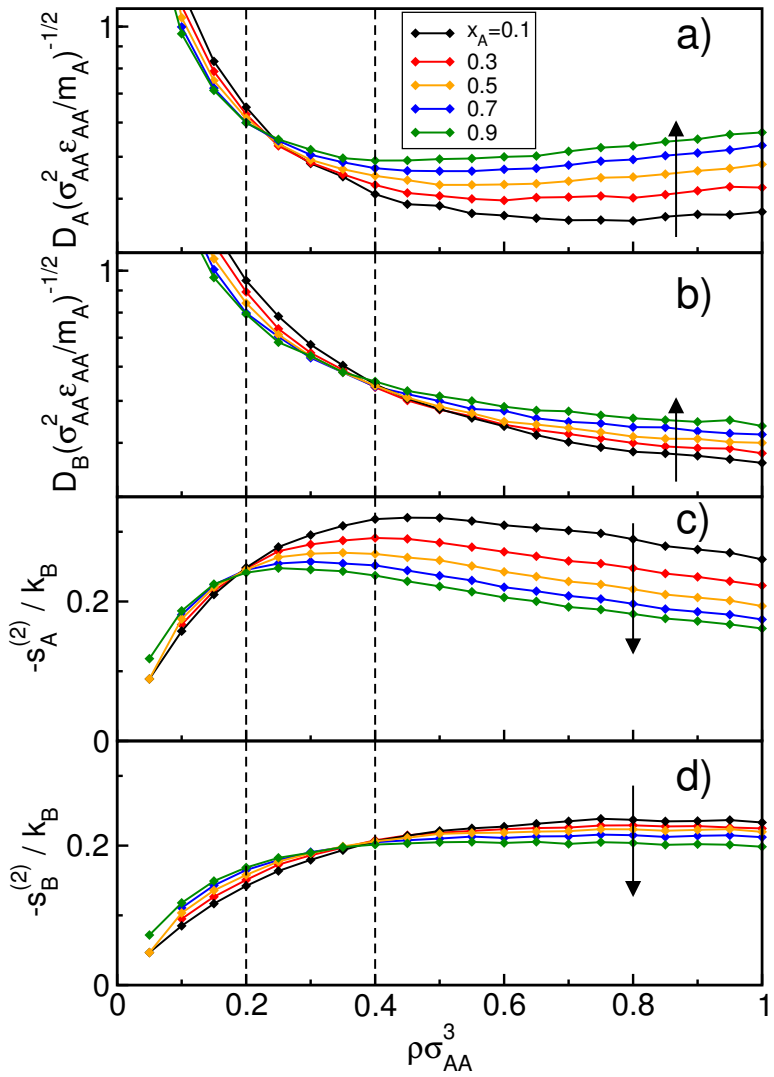

Figure 2.4: Tracer diffusivity D_i for (a) A particles and (b) B particles and structural order metric $-s_i^{(2)}$ for (c) A particles and (d) B particles for the binary Gaussian-core mixture discussed in the text. All are plotted versus density $\rho\sigma_{AA}^3$. Data shown is for temperature $k_{\rm B}T/\epsilon_{AA} = 0.2$ and mole fractions $x_A = 0.1$, 0.3, 0.5, 0.7 and 0.9. Arrows indicate increasing x_A. The dashed lines separate the approximate low, intermediate and high density ranges described in the text.

logically becoming anomalous at a lower overall density. The implication is that there is a fairly wide range of intermediate fluid densities (approximately $0.2 < \rho\sigma_{AA}^3 < 0.4$) for which the structure and dynamics of the A particles behave anomalously, while those of the B particles behave normally, with respect to changes in composition.

2.6 Author Contributions

The work in this chapter was originally published in 2009 [40]. Thomas M. Truskett designed the research and helped write the document. William P. Krekelberg provided molecular dynamics simulations of the monodisperse Gaussian-core fluid. Jeffrey R. Errington and Vincent K. Shen provided Monte Carlo simulations for thermodynamic insights to the system which helped develop the narrative. Mark J. Pond provided molecular dynamics simulations of the binary Gaussian-core fluid, analyzed data and wrote the core of the document.

Chapter 3

Implications of the effective one-component analysis of pair correlations in colloidal fluids with polydispersity

Fluid suspensions of natural and technological interest are inevitably polydisperse. Their constituent particles–each of which comprise a large number of smaller atoms, molecular, or ions–exhibit distinct geometric and chemical features (size, shape, charge, etc.) and hence represent different species of a many-component mixture. As might be expected, the composition of such a mixture can strongly affect its structural, thermodynamic, and dynamic behavior. [26, 61, 62, 63, 64, 65, 66, 67, 68, 69, 70, 71, 72, 73, 74, 75] For example, suspensions with narrowly distributed (e.g., approximately monodisperse) particle characteristics often readily crystallize and thus can be interesting candidates for applications like colloidal self assembly. [27, 28] In contrast, fluids with more diverse particle populations that suppress crystallization [74, 76, 77, 78] are more useful in applications which call for good glass-forming materials.

Characterizing the properties of systems with a large number of components can be a formidable technical challenge. Insufficient sampling typically limits the species-specific information that can be directly obtained via experiments and computer simulations. In fact, for suspensions with apparently

"weak" polydispersity, it is common practice to ignore particle differences altogether, adopting an effective one-component description. The latter is tantamount to assuming a fictitious pure-fluid model, whose (typically softer) interparticle interactions are those that, under equilibrium conditions, would reproduce some globally averaged behavior of the original polydisperse material. [29, 25, 30] An obvious drawback of this simplification is that one generally does not know in advance whether a system's polydispersity is weak enough (as it pertains to the properties of interest) to justify use of an average description that washes out species-specific contributions. Moreover, it is difficult to assess the impact of averaging *a posteriori*, especially when statistically meaningful information about the component contributions to the polydisperse material's properties is unavailable. This type of dilemma, though far from resolved, has long been appreciated and studied in colloid science. For example, it arises in considering the trade-offs between characterizing polydisperse colloidal suspensions by partial (species-specific) versus total (average) structure factors inferred from scattering data. [66, 79, 80, 81, 82, 83, 84, 85, 86, 87] Although a multicomponent description is ideally desired, it cannot generally be obtained from experiments without invoking a number of approximations that compromise its reliability.

In this study, we use computer simulations and exact theoretical results to examine how the static structure of a model polydisperse fluid differs when quantified based on multicomponent versus effective one-component descriptions of its pair correlations. Similar in spirit to, e.g., related work of Pangburn

and Bevan,[25, 30] we focus exclusively on the real-space counterpart to the reciprocal-space scattering problem discussed above, the former being especially critical for the interpretation of data from computer simulations and optical microscopy experiments[88, 89, 90, 91, 92, 93] of complex fluids.

The model we investigate here is a fluid of polydisperse hard-sphere particles with short-range, square-well attractions. Earlier simulations[3] show that it reproduces key static and dynamic behavior of suspended colloids with polymer-mediated depletion interactions. Most notably, in agreement with experiments[94, 95] it displays strikingly anomalous dynamic behaviors at high particle concentrations near the so-called "repulsive glass" transition (e.g., diffusivity increases and viscosity decreases with *increasing* particle attractions). Interestingly, an effective one-component analysis[3] suggests these behaviors emerge under conditions where the fluid also displays structural anomalies (e.g., static correlations apparently weaken with *increasing* particle attractions). Of course, it is important to note that polydispersity is an important feature of this and similar models because it suppresses crystallization that would otherwise restrict access to the deeply supercooled fluid states where the anomalous behavior is most pronounced. Here, in order to fully characterize the structure of this system in an efficient manner, we introduce Monte Carlo sampling techniques that allow us to accurately determine the $m(m+1)/2$ partial radial distribution functions as well as the free energy for a fluid mixture of m pseudo-components [in this case, $m = 60$; $m(m+1)/2 = 1830$] at each state point of interest.

The main findings of this study are as follows. (1) The multicomponent (i.e., partial) and effective one-component radial distribution functions show qualitatively different behavior as a function of the magnitude of the inter-particle attractions, even for this moderately polydisperse model. This should serve as a cautionary note regarding conclusions that one might otherwise draw about structure in polydisperse systems based on trends exhibited by the latter globally-averaged, static correlations. (2) The pair-correlation contribution to the excess entropy of the polydisperse fluid based on the multicomponent description, in contrast to the estimate based on the one-component model, very closely approximates the full thermodynamic excess entropy of the system. This suggests that techniques which allow one to accurately determine the partial radial distribution functions of dense, polydisperse colloids studied will also furnish information key for understanding their thermodynamic behavior. (3) Finally, the excess entropy scaling for the shear viscosity of this polydisperse fluid is similar in some key ways to that of liquid water, another system known to exhibit anomalous thermodynamic and dynamic properties. Importantly, such similarities are not apparent if the effective one-component is used in the excess entropy estimation for the polydisperse colloidal fluid.

3.1 Methods

3.1.1 Model for the polydisperse fluid

We consider a previously introduced model[3] comprising hard-sphere particles with short-range, square-well (SW) attractions. The pair potential

between particles i and j (with diameters σ_i and σ_j, respectively) is given by

$$\mathcal{V}_{ij}(r) = \begin{cases} \infty & r \leq \sigma_{ij} \\ -\epsilon & \sigma_{ij} < r \leq 1.03\sigma_{ij} \\ 0 & r > 1.03\sigma_{ij} \end{cases} \tag{3.1}$$

Here, r is the separation between particle centers, $\sigma_{ij} = (\sigma_i + \sigma_j)/2$ is the hard-core contact separation, and ϵ is the depth of the attractive well. The particle diameters σ_i of this polydisperse fluid follow a truncated normal distribution with a mean value of σ and a standard deviation of 0.1σ. The truncation ensures that all particle diameters of the fluid are within 3 standard deviations of the mean ($0.7\sigma - 1.3\sigma$). This degree of polydispersity in the particle population, while still modest, is significant enough to discourage crystallization in simulations, allowing access to deeply supercooled fluid states.[3]

As discussed extensively elsewhere,[3, 96, 97] short-range attractions like those exhibited by this model can give rise to unusual dependencies of shear viscosity (which decreases) and self diffusivity (which increases) with $\epsilon/k_{\mathrm{B}}T$, where k_{B} is the Boltzmann constant and T is temperature. These trends capture what is observed experimentally[94, 95] for suspensions of hard-sphere-like colloids with polymer-mediated depletion attractions. Interestingly, an effective one-component analysis of this model's pair correlations[3] suggests that the aforementioned dynamic anomalies are accompanied by a structural anomaly (i.e., increasing $\epsilon/k_{\mathrm{B}}T$ *weakens* the effective pair correlations). In this work, we test whether this feature also emerges from a multicomponent analysis.

3.1.2 Monte Carlo simulations

For the Monte Carlo (MC) simulations, we approximate the model introduced in Section 3.1.1 by a closely related mixture of 60 pseudo-components. Particle diameters in the pseudo-component mixture exhibit continuous polydispersity, and their pairwise interactions $\mathcal{V}_{ij}(r)$ are described by eq. 3.1. The pseudo-components each comprise nearly identical particles (e.g., diameter differences of less than 0.01σ). Specifically, particles with diameters greater than $[0.7 + 0.01(k-1)]\sigma$ and less than $[0.7 + 0.01k]\sigma$ are considered members of the k^{th} pseudo-component with chemical potential μ_k, where $k \in [1, 60]$. In what follows, subscripts on variables refer to pseudo-component numbers rather than particle identities. We have found that specifying the mole fraction of the k^{th} pseudo-component, x_k^n, by the relation

$$x_k^n = \frac{\exp\left[-\left(k-30.5\right)^2/\,200\right]}{\sum_{l=1}^{60}\exp\left[-\left(l-30.5\right)^2/200\right]} \tag{3.2}$$

results in a mixture with properties virtually identical to the model described in Section 3.1.1. As we discuss below, the pseudo-component mixture is very convenient to simulate within the semi-grand (SG) ensemble.[98]

In our SG MC simulations of this mixture, temperature T, total particle number $N = 1000$, volume V (or density $\rho = N/\mathrm{V}$), and all pseudo-component chemical potential differences $\Delta\mu_{rk} = \mu_k - \mu_r$ (relative to that of an arbitrarily chosen r^{th} pseudo-component reference) are held constant. In what follows, we express chemical potential differences in terms of activity ratios $\xi_{rk} = \xi_k/\xi_r$,

where the activity of a particle of the k^{th} pseudo-component with molecular partition function q_k is given by $\xi_k = q_k e^{\mu_k/k_{\rm B}T}$.

In order to study a fluid with a specified pseudo-component composition $x_k^{\rm n}$ within the SG ensemble, we must first solve for the activity distribution $\xi_{rk}^{\rm n}$ that produces the desired $x_k^{\rm n}$ at the temperature and density of interest. In general, this is a highly nontrivial task because $\xi_{rk}^{\rm n}$ is an unknown functional of $x_k^{\rm n}$. Fortunately, this inverse problem has received considerable attention,[99, 100, 101] and robust methods are now available for computing $\xi_{rk}^{\rm n}$ given $x_k^{\rm n}$.

Here, we use an efficient nonequilibrium potential refinement scheme introduced by Wilding[101] to obtain $\xi_{rk}^{\rm n}$. We take advantage of the efficient sampling of composition space facilitated by SG MC simulation techniques and allow particles to adopt *any* diameter within the range $0.7\sigma - 1.3\sigma$. We begin the potential refinement scheme by setting $\ln \xi_{rk} = 0$ and subsequently adjust the activity distribution during an eight-stage SG MC simulation. At regular intervals during the i^{th} stage, $\ln \xi_{rk}$ is incremented by the relative difference between the instantaneous x_k and target $x_k^{\rm n}$ discretized particle-size distributions scaled by a modification factor γ_i,

$$\ln \xi_{rk}^{\rm new} = \ln \xi_{rk}^{\rm old} - \gamma_i \left(\frac{x_k - x_k^{\rm n}}{x_k^{\rm n}} \right). \tag{3.3}$$

A given stage terminates when the maximum relative difference

$$\zeta = \max \left[\left| \left(x_k^{\rm agg} - x_k^{\rm n} \right) / x_k^{\rm n} \right| \right] \tag{3.4}$$

between the target ($x_k^{\rm n}$) and stage-averaged ($x_k^{\rm agg}$) particle size distributions drops below a tolerance of $\zeta^* = 0.01$. We set $\gamma_1 = 0.001$ and reduce the

modification factor by a factor of two after the completion of each stage. The activity distribution that emerges after the eighth stage is taken to be $\xi^{\rm n}_{rk}$.

3.1.3 Static pair correlations

Perhaps the most basic measure of real-space structure is the partial radial distribution function (PRDF), $g_{ij}(r)$. The PRDF characterizes the frequency of various pair separations r that occur between particles of "type" i and j in the fluid. Specifically, the mean number of particle centers of type i located in a spherical shell of differential thickness dr a distance r away from a type j particle center is $4\pi r^2 \rho_i g_{ij}(r) dr$, where ρ_i is the overall number density of particle type i. Note that symmetry requires $g_{ij}(r) = g_{ji}(r)$. Below, we use the labels i and j to indicate specific choices of the $m = 60$ pseudo-components, i.e., $i, j \in [1, 60]$. Note that there are $m(m+1)/2 = 1830$ distinct pseudo-component PRDFs in the mixture we study here, highlighting the statistical challenge associated with characterizing the structure, even at the pseudo-component level of description.

The effective one-component treatment for pair correlations, on the other hand, ignores all differences between the various particle types. Its radial distribution function $g_{\rm eff}(r)$ is defined such that the mean total number of particle centers located in a spherical shell of differential thickness dr a distance r away from other centers is $4\pi r^2 \rho g_{\rm eff}(r) dr$, where ρ is the total particle number density. Expressed differently, $g_{\rm eff}(r) = \sum_{i=1}^{M} \sum_{j=1}^{M} x_i x_j g_{ij}(r)$. In other words, as should be expected, the effective one-component description provides a

highly averaged representation of the fluid's pair correlations. This makes it easier to characterize statistically, but more challenging to interpret.

3.1.4 Structural order metrics

We examine the behavior of two different structural order metrics that characterize the degree of local translational order of a fluid based on the strength of its pair correlations. To understand the implications of adopting the effective one-component description for our polydisperse model, we compare the value that these scalar parameters take on when the structure is described by $g_{\text{eff}}(r)$ versus the full set of pseudo-component PRDFs, i.e., $g_{ij}(r)$, where $i, j \in [1, 60]$.

The first structural metric we consider is $-s^{(2)}/k_{\text{B}}$,[60] where $s^{(2)}$ comes from the leading term in the multiparticle expansion of the fluid's molar excess entropy (over ideal gas), $s^{\text{ex}} = s^{(2)} + s^{(3)} + \cdots$.[59, 22] The explicit connection between $-s^{(2)}/k_{\text{B}}$ and the PRDFs of a fluid mixture can be seen when the former is expressed as

$$-\frac{s^{(2)}}{k_{\text{B}}} = \sum_i \sum_j \frac{x_i x_j \rho}{2} \int [g_{ij}(r) \ln g_{ij}(r) - g_{ij}(r) + 1] d\mathbf{r} \tag{3.5}$$

Note that $-s^{(2)}/k_{\text{B}}$ is a non-negative quantity that vanishes for an ideal gas and is considerably larger for dense liquids and glasses that exhibit stronger interparticle correlations.[60] Since 3- and higher-body correlations are challenging to characterize in a fluid, the thermodynamic quantity s^{ex} is commonly approximated by $s^{(2)}$ for pure fluids or binary mixtures. Here, we compute s^{ex}

and $s^{(2)}$ (at the pseudo-component level) directly from simulation. The corresponding structural order metric in the effective one-component description is given by

$$-\frac{s_{\rm eff}^{(2)}}{k_{\rm B}} = \frac{\rho}{2}\int [g_{\rm eff}(r)\ln g_{\rm eff}(r) - g_{\rm eff}(r) + 1]d\mathbf{r} \tag{3.6}$$

As discussed earlier, it was this quantity that was used in previous computer simulation studies to characterize the average strength of the interparticle correlations for the system considered here[3] and related models of polydisperse colloids[58]. The second structural order metric τ studied here is defined as

$$\tau = y_c^{-1}\sum_i\sum_j x_i x_j \int_0^{y_c} |g_{ij}(y) - 1|dy \tag{3.7}$$

where $y = r\rho^{1/3}$ and y_c is a cut-off value (here, we chose $y_c = 4$). This measure is a straightforward generalization of a parameter introduced earlier to study the local translational order of fluid, glassy, and crystalline states of single-component materials based on their static pair correlations.[60, 102] The version of this metric for the effective one-component model is given by

$$\tau_{\rm eff} = y_c^{-1}\int_0^{y_c} |g_{\rm eff}(y) - 1|dy \tag{3.8}$$

where, as before, $y = r\rho^{1/3}$ and $y_c = 4$.

3.1.5 Thermodynamic excess entropy

A two-step process is used to compute the excess entropy per particle $s^{\rm ex}\left(\rho\sigma^3\ , \epsilon/k_{\rm B}T\right)$ of our pseudo-component SW fluid. In the first step, we obtain thermodynamic properties as a function of $\rho\sigma^3$ for polydisperse hard-spheres ($\epsilon/k_{\rm B}T = 0$) in contact with a reservoir of particles with an ideal-gas

activity distribution $\xi_{rk}^{\mathrm{ig}} = x_k^{\mathrm{n}}$. In the second step, we move along a path that takes the system from ξ_{rk}^{ig} and $\epsilon/k_{\mathrm{B}}T = 0$ to ξ_{rk}^{n} and nonzero $\epsilon/k_{\mathrm{B}}T$ at constant density.

To obtain the density dependence of the entropy, we perform a multicomponent grand canonical (GC) simulation with $V = 1000\sigma^3$ and $\xi_k = \xi_r \xi_{rk}^{\mathrm{ig}}$, with $\xi_r = q_r$. Following the strategy outlined above, we allow the individual particle diameters to take on values that span the range 0.7σ to 1.3σ and treat ξ_k as a stepwise function. Transition matrix MC methods [103, 104] are used to determine the probability $\Pi_{\mathrm{GC}}(N)$ of observing the system with a total number of particles N. The density probability distribution is related to the SG partition function Υ and GC partition function Ξ as follows[104]

$$\Pi_{\mathrm{GC}}(N) = \frac{\Upsilon(N, \xi_{rk}, V, T)}{\Xi(\xi_j, V, T)} \left(\frac{\xi_r}{q_r}\right)^N. \tag{3.9}$$

The relevant bridge equation $Y = -k_{\mathrm{B}}T \ln \Upsilon$ provides the SG potential

$$Y(N) = -k_{\mathrm{B}}T \left[\ln\left(\frac{\Pi_{\mathrm{GC}}(N)}{\Pi_{\mathrm{GC}}(0)}\right) - N \ln\left(\frac{\xi_r}{q_r}\right)\right], \tag{3.10}$$

where we have used the zero-particle limit to express the GC partition function in terms of the particle number probability distribution, $\ln \Xi = -\ln \Pi(0)$. The SG potential and Helmholtz free energy F are linked by the relationship[98]

$$F(N) = Y(N) + N \sum_{k=1}^{m} \bar{x}_k(N)(\mu_k - \mu_r), \tag{3.11}$$

where $\bar{x}_k(N)$ is the ensemble-averaged discretized particle size distribution within a system described by T, V, N, and ξ_{rk}. For the $\epsilon/k_{\mathrm{B}}T = 0$ case, the

intensive entropy s and Helmholtz free energy f are now

$$\frac{s\left(\rho\sigma^3\,,0\right)}{k_{\mathrm{B}}}=-\frac{f\left(\rho\sigma^3,0\right)}{k_{\mathrm{B}}T}=-\frac{1}{N}\ln\left(\frac{\Pi_{\mathrm{GC}}\left(N\right)}{\Pi_{\mathrm{GC}}\left(0\right)}\right)+\sum_{k=1}^{m}\bar{x}_k\left(N\right)\ln\left(\frac{\xi_k}{q_k}\right),\quad(3.12)$$

Within the GC simulations employed here , we have $\xi_{rk}=x_k^{\mathrm{n}}$, and therefore $\bar{x}_k\left(N\right)$ deviates from the normal particle size distribution. For the polydisperse hard-sphere fluid ($\epsilon/k_{\mathrm{B}}T=0$), increasing N causes the $\bar{x}_k\left(N\right)$ distribution to shift such that the populations of pseudo-components with smaller particle diameters increase. This feature of the system allows us to sample high particle number densities with relative ease. To summarize, within the first stage of the two-step scheme employed here, we use GC simulation to obtain the density dependence of thermodynamic properties for a hard-sphere polydisperse fluid ($\epsilon/k_{\mathrm{B}}T=0$) subject to $\xi_{rk}=x_k^{\mathrm{n}}$, and we perform just one of these simulations.

In the second step of our approach an expanded ensemble (EE) MC procedure[105] is used to determine the difference in the thermodynamic properties of a polydisperse SW fluid with ξ_{rk}^{n} and the reference polydisperse hard-sphere fluid with ξ_{rk}^{id} at a $\rho\sigma^3$ and $\epsilon/k_{\mathrm{B}}T$ of interest. The two systems are connected through a series of subensembles described by λ, which spans from $\lambda=0$ to 1 in increments of $\Delta\lambda=0.001$ (i.e., $\lambda_i=0.001i$, where $i\in[0,1000]$). To obtain the relative entropy of the system along this path, we perform SG simulations with fixed $N=1000$ and $\rho\sigma^3=N\sigma^3/V$. Within subensemble i, the activity distribution $\xi_{rk,i}$ and well depth $\epsilon_i/k_{\mathrm{B}}T$ are

$$\ln\xi_{rk,i}=\ln\xi_{rk,i}^{\mathrm{id}}+\lambda_i\left(\ln\xi_{rk}^{\mathrm{n}}-\ln\xi_{rk}^{\mathrm{id}}\right)\quad(3.13)$$

and

$$\epsilon_i/k_{\mathrm{B}}T = \lambda_i \epsilon/k_{\mathrm{B}}T. \tag{3.14}$$

Transition matrix MC methods[106, 107] are used to evaluate the probability $\Pi_{EE}(\lambda)$ of finding the system in a subensemble defined by λ. The difference in the SG potential over the entire path evaluates to

$$\Delta Y = Y\left(\xi^{\mathrm{n}}_{rk}, \epsilon/k_{\mathrm{B}}T\right) - Y\left(\xi^{\mathrm{id}}_{rk}, 0\right) = -k_{\mathrm{B}}T \ln\left(\frac{\Pi_{\mathrm{EE}}(\lambda=1)}{\Pi_{\mathrm{EE}}(\lambda=0)}\right). \tag{3.15}$$

The corresponding change in the Helmholtz free energy per particle is

$$\begin{array}{l}\Delta f\left(\rho\sigma^3, \epsilon/k_{\mathrm{B}}T\right) = \\ -\frac{k_{\mathrm{B}}T}{N}\left[\ln\left(\frac{\Pi_{\mathrm{EE}}(1)}{\Pi_{\mathrm{EE}}(0)}\right) - N\sum_{k=1}^{m}\bar{x}_k(1)\ln\left(\frac{\xi^{\mathrm{n}}_{rk}}{q_k}\right) - \bar{x}_k(0)\ln\left(\frac{\xi^{\mathrm{ig}}_{rk}}{q_k}\right)\right]\end{array} \tag{3.16}$$

where $\bar{x}_k(0)$ and $\bar{x}_k(1)$ are the ensemble-averaged discretized particle size distributions within the $\lambda = 0$ and 1 subensembles, respectively. By further considering the ensemble-averaged intensive configurational energies $\bar{e}(\lambda)$, we arrive at the entropy difference Δs

$$\frac{\Delta s\left(\rho\sigma^3, \epsilon/k_{\mathrm{B}}T\right)}{k_{\mathrm{B}}} = \frac{1}{k_{\mathrm{B}}T}\left[\bar{e}(1) - \bar{e}(0) - \Delta f\left(\rho\sigma^3, \epsilon/k_{\mathrm{B}}T\right)\right], \tag{3.17}$$

where, in our case $\bar{e}(0) = 0$. An EE simulation is completed for each $\rho\sigma^3$ and $\epsilon/k_{\mathrm{B}}T$ of interest. Collectively, the GC and EE simulations provide the absolute entropy

$$s\left(\rho\sigma^3, \epsilon/k_{\mathrm{B}}T\right) = s\left(\rho\sigma^3, 0\right) + \Delta s\left(\rho\sigma^3, \varepsilon/k_{\mathrm{B}}T\right). \tag{3.18}$$

We now turn our attention to the ideal gas contribution to the excess entropy. The entropy of a multicomponent ideal gas is

$$\frac{s^{\mathrm{ig}}}{k_{\mathrm{B}}} = 1 - \ln\rho - \sum_{k=1}^{m} x_k \ln\left(\frac{x_k}{q_k}\right). \tag{3.19}$$

To be consistent with the analysis above, we evaluate the expression above with $x_k = \bar{x}_k(1)$, which, of course, closely approximates x_k^{n}. Finally, we arrive at the excess entropy

$$s^{\mathrm{ex}} = s - s^{\mathrm{ig}}. \tag{3.20}$$

We note that the algorithm outlined here is rather general and we expect it to prove useful for computing the free energy of a wide range of polydisperse fluids.

3.2 Results and discussion

The first results that we consider pertain to the behavior of a dilute ($\rho \to 0$) polydisperse fluid of SW particles that interact through the potential given by eq. 3.1 and that exhibit a Gaussian distribution of particle diameters (with mean σ and standard deviation $\sigma/10$). This is an interesting case to study because–while simple enough to allow for an exact theoretical description of the polydisperse fluid's static properties–it is also rich enough to illustrate some of the key consequences of adopting the effective one-component description. Analytical expressions for the structural quantities discussed below can be found in the Appendix.

Fig. 3.1 shows how the strength of the static interparticle correlations of the dilute fluid depends on the magnitude of the interparticle attraction $\epsilon/k_{\mathrm{B}}T$. Two levels of structural characterization are considered: one that takes into account the full set of PRDFs (i.e., the exact multicomponent description), and one based on the effective one-component structure. The key point of Fig. 3.1a

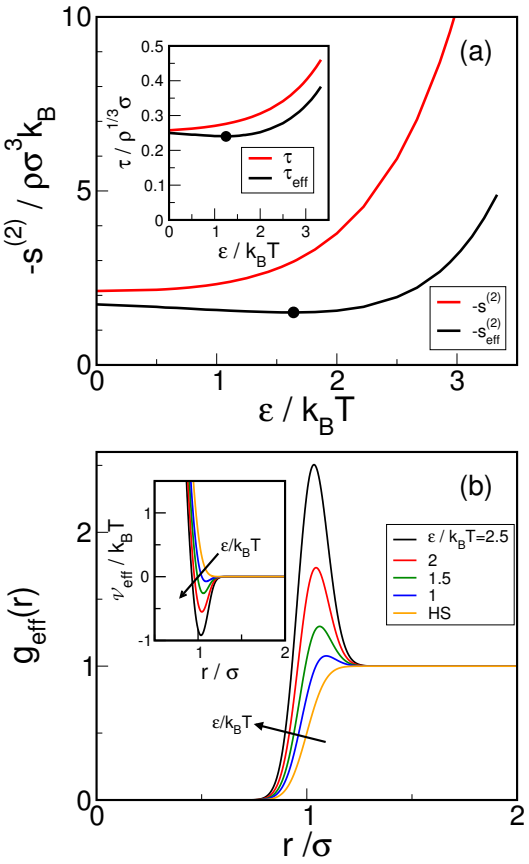

Figure 3.1: Effect that the magnitude of the interparticle attraction $\epsilon/k_{\rm B}T$ has on the static structure of the polydisperse SW fluid described in the text in the dilute ($\rho\sigma^3 \to 0$) limit. (a) [Main panel] Comparison of the reduced two-body excess entropy, $-s^{(2)}/\rho\sigma^3 k_{\rm B}$ (identical to $-s^{\rm ex}/\rho\sigma^3 k_{\rm B}$ in this limit), computed using eq. 1.3, as well its effective one-component counterpart, $-s^{(2)}_{\rm eff}\rho\sigma^3 k_{\rm B}$, calculated using eq. 3.6 and 1.5. [Inset] Comparison of the reduced structural order metric, $\tau/\rho^{1/3}\sigma$, computed using eq.1.4, as well its effective one-component counterpart, $\tau_{\rm eff}/\rho^{1/3}\sigma$, calculated using eq. 3.8 and 1.5. Effective one-component quantities spuriously indicate the presence of structural anomalies (attractions apparently weaken structure) for energies $\epsilon/k_{\rm B}T$ less than the values indicated by the black dots. (b) [Main panel] The effective one-component radial distribution function $g_{\rm eff}(r)$, computed using eq. 1.5, plotted versus reduced interparticle separation r/σ. [Inset] The interparticle potential, $\mathcal{V}_{\rm eff}(r) = -k_{\rm B}T \ln g_{\rm eff}(r)$, of the effective one-component fluid.

is that the structural order metrics that properly account for the polydisperse nature of the fluid ($-s^{(2)}/\rho\sigma^3 k_{\rm B}$ and $\tau/\rho^{1/3}\sigma$) show qualitatively different behavior than their effective one-component counterparts ($-s^{(2)}_{\rm eff}/\rho\sigma^3 k_{\rm B}$ and $\tau_{\rm eff}/\rho^{1/3}\sigma$). The former display the expected monotonic behavior; i.e., static correlations strengthen with increasing magnitude of the interparticle attractions. In fact, in the Appendix, we demonstrate that this monotonic trend must always be observed in the dilute limit for this system, independent of the width of the diameter distribution. In contrast, the effective one-component quantities both spuriously indicate the presence of a structural anomaly; i.e., conditions where static correlations apparently weaken with increasing interparticle attractions.

Why do $-s^{(2)}_{\rm eff}/\rho\sigma^3 k_{\rm B}$ and $\tau_{\rm eff}/\rho^{1/3}\sigma$ predict qualitatively different behavior than $-s^{(2)}/\rho\sigma^3 k_{\rm B}$ and $\tau/\rho^{1/3}\sigma$, respectively? The basic mathematical reason is that the structural metrics are nonlinear functionals of the PRDFs. Thus, their behaviors can depend sensitively on whether the latter "inputs" are treated in a multicomponent or a pre-averaged (effective one-component) manner. From a physical perspective, as illustrated in Fig. 3.1b, averaging the PRDFs to obtain $g_{\rm eff}(r)$ softens the apparent pair correlations in the fluid, as well as the effective interactions between the particles, $\mathcal{V}_{\rm eff}(r) = -k_{\rm B}T \ln g_{\rm eff}(r)$. As a result, the effective one-component metrics significantly underestimate the effect that the attractions have on static structure. For example, the magnitude of $-s^{(2)}_{\rm eff}/\rho\sigma^3 k_{\rm B}$ is much smaller than that of $-s^{(2)}/\rho\sigma^3 k_{\rm B}$ (which is equal to $-s^{\rm ex}/\rho\sigma^3 k_{\rm B}$ in this dilute limit) for $\epsilon/k_{\rm B}T > 1$, illustrating

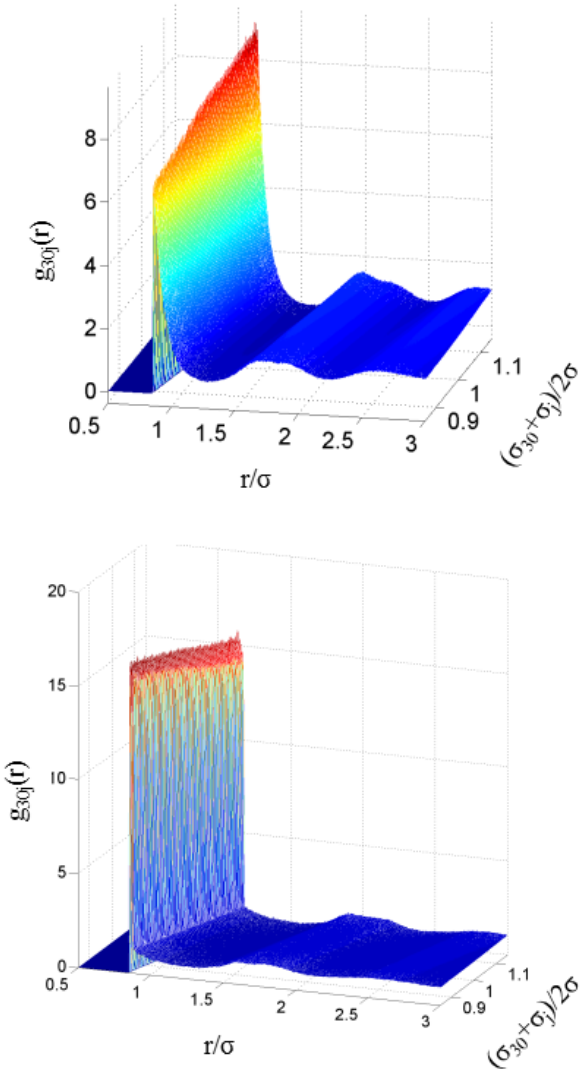

Figure 3.2: Partial radial distribution functions $g_{30j}(r)$ describing correlations between the 30^{th} and the j^{th} pseudo-components ($j \in [1, 60]$) of the polydisperse SW fluid obtained via MC simulations. Results are shown as a function of reduced interparticle separation r/σ and interaction diameter $(\sigma_{30} + \sigma_j)/2$. Color (red-to-blue) corresponds to magnitude of $g_{30j}(r)$ (high-to-low). Data are for a reduced density of $\rho\sigma^3 = 1.05$ and interparticle attractions of (a) $\epsilon/k_{\mathrm{B}}T = 0$ (hard-sphere limit) and (b) $\epsilon/k_{\mathrm{B}}T = 2.5$.

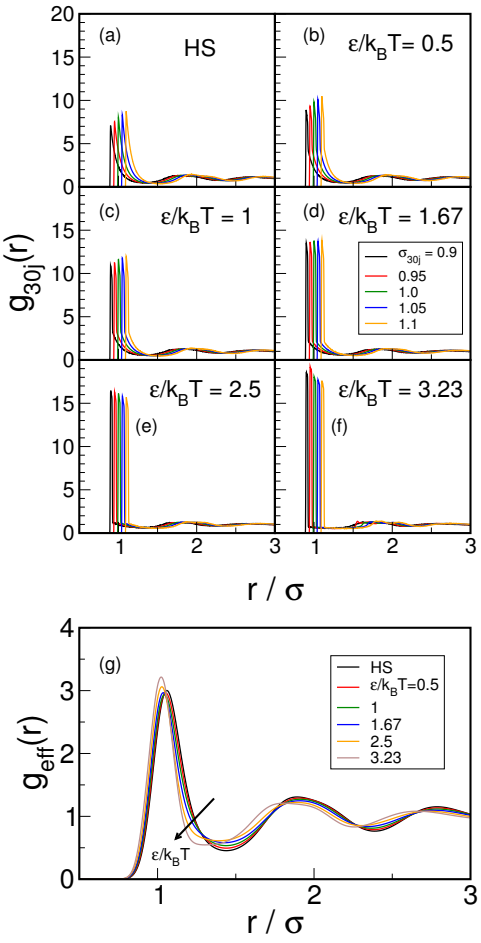

Figure 3.3: Effect that magnitude of the interparticle attraction $\epsilon/k_{\rm B}T$ has on the static pair correlations of the polydisperse SW fluid at a reduced density of $\rho\sigma^3 = 1.05$. Data obtained via MC simulations. (a)-(f) Partial radial distribution functions $g_{30j}(r)$ between 30^{th} and the j^{th} pseudo-components for j = 10, 20, 30, 40, and 50 (with corresponding characteristic interaction diameters $\sigma_{30j} = 0.90$, 0.95, 1.0, 1.05 and 1.10, respectively) and various values of $\epsilon/k_{\rm B}T$. (g) Radial distribution function for the effective one-component description of the fluid, $g_{\rm eff}(r)$, as a function of reduced particle center separation r/σ for conditions used to generate the data for panels (a)-(f).

that one cannot readily estimate the thermodynamic excess entropy from the effective one-component approximation.

In order to compare this behavior to that of concentrated SW fluids, we analyze results from our MC simulations. Fig. 3.2 displays 60 of the 1830 PRDFs that we collected for the polydisperse SW fluid described in Section 3.1 at a reduced density $\rho\sigma^3 = 1.05$ (particle packing fraction of 0.567) and two extreme levels of interparticle attractions: $\epsilon/k_{\mathrm{B}}T = 0$ (Fig. 3.2a) and $\epsilon/k_{\mathrm{B}}T = 2.5$ (Fig. 3.2b). The functions presented in Fig. 3.2, labeled $g_{30j}(r)$, characterize the partial pair correlations between particles with diameters close to the median size (the 30^{th} pseudo-component) and particles of other sizes (the j^{th} pseudo-component with $j \in [1, 60]$). In the case of $\epsilon/k_{\mathrm{B}}T = 0$ (i.e., the hard-sphere limit), there is a clear relationship between the contact value $g_{30j}(r = \sigma_{30j})$ and the contact diameter $\sigma_{30j} = (\sigma_{30} + \sigma_j)/2$; larger particles have higher probabilities of contact configurations. This is the expected trend and is a classic manifestation of the depletion effect.[108, 109] Contact configurations of big spheres are entropically favorable because they increase the volume accessible to smaller spheres. A weak splitting of the second peak of the PRDFs is also apparent–as is commonly observed for dense hard-sphere fluids[110]–the precise shape of which depends on the identities of the participating pseudo-components. Interestingly, for $\epsilon/k_{\mathrm{B}}T = 2.5$ (Fig. 3.2b), the aforementioned entropic packing preferences have all but vanished. The strong attractions in this limit dominate the pair correlations, and there are only very minor differences between PRDFs involving different pseudo-components. The

main point is that the sensitivity of the distribution of PRDFs to $\epsilon/k_{\rm B}T$ suggests that the pre-averaging required for the effective one-component description may also be problematic for this high-density system, as it was for the dilute case.

The data of Fig. 3.3 clarify this point. Specifically, panels 3.3a-3.3f illustrate how 5 characteristic PRDFs for this system–$g_{30j}(r)$ for j = 10, 20, 30, 40, and 50–evolve with increasing strength of the interparticle attraction. The pronounced changes of these functions [e.g., the contact values $g_{30j}(r = \sigma_{30j})$ triple in magnitude with increasing $\epsilon/k_{\rm B}T$] should be contrasted with the behavior of the corresponding effective one-component quantity $g_{\rm eff}(r)$ shown in Figure 3.3g, which not only looks qualitatively different (considerably softer than the PRDFs) but also is remarkably insensitive to the value of $\epsilon/k_{\rm B}T$ considered. In other words, the averaging involved in forming $g_{\rm eff}(r)$ has the effect of hiding some significant changes that attractions have on the static structure of the polydisperse fluid.

The consequences of the aforementioned averaging become clearer in Fig. 3.4 where we directly compare how the structural order metrics–based on multi-component versus one-component descriptions of the systems–depend on $\epsilon/k_{\rm B}T$. The first point to note is that, as in the dilute fluid, the metrics $-s^{(2)}/k_{\rm B}$ and $-s^{(2)}_{\rm eff}/k_{\rm B}$ show different behavior, both quantitatively and qualitatively. The former provides an excellent approximation to the thermodynamic excess entropy $-s^{\rm ex}/k_{\rm B}$, while the latter is too small by factor of between 1.8 and 3.5 (depending on $\epsilon/k_{\rm B}T$). Also, as observed in the dilute case, the

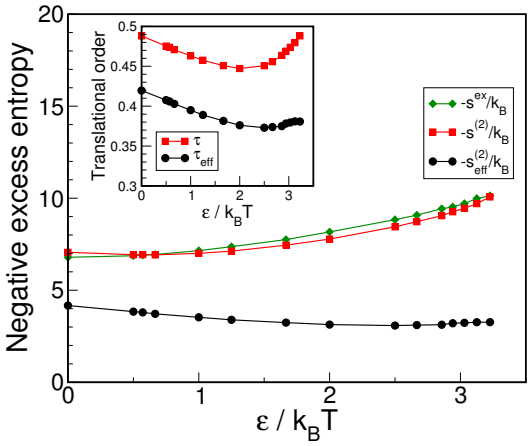

Figure 3.4: Effect that magnitude of interparticle attraction $\epsilon/k_{\mathrm{B}}T$ has on different structural order metrics for the polydisperse SW fluid at a reduced density of $\rho\sigma^3 = 1.05$ Data obtained via MC simulations. [Main panel] Negative thermodynamic excess entropy, $-s^{\mathrm{ex}}/k_{\mathrm{B}}$ (diamonds), and its two-body approximation based on multicomponent, $-s^{(2)}/k_{\mathrm{B}}$ (squares), and effective one-component, $-s^{(2)}_{\mathrm{eff}}/k_{\mathrm{B}}$ (circles), descriptions of the system. [Inset] Translational structure metrics based on the effective one-component, τ_{eff} (circles), and multicomponent, τ (squares), descriptions of the system. Curves are guides to the eye.

effective one-component quantity reports that the fluid is structurally anomalous (attractions apparently weaken pair correlations) across a wide range of $\epsilon/k_{\mathrm{B}}T$. In contrast, $-s^{(2)}/k_{\mathrm{B}}$ shows normal behavior (attractions strengthen correlations) except for a very narrow range of conditions at low values of $\epsilon/k_{\mathrm{B}}T$, where a weak structural anomaly is present. Similar trends are apparent when comparing τ and τ_{eff}. The latter underestimates the magnitude of the structural order, and it overestimates the range of conditions where structural anomalies occur.

As a final point, we examine the implications of the one-component

analysis for scaling relationships between static structure and dynamics. In particular, we plot in Fig. 3.5 reduced shear viscosity $\eta\rho^{-2/3}(mk_{\mathrm{B}}T)^{-1/2}$ (here η shear viscosity and m is particle mass) for the polydisperse SW fluid as a function of the various structural order metrics analyzed above. The shear viscosity data we use for this plot was extracted from the earlier molecular dynamics investigation of Krekelberg et al.[3]. As Rosenfeld[5, 6] originally observed, the non-dimensionalized form $\eta\rho^{-2/3}(mk_{\mathrm{B}}T)^{-1/2}$ is strictly a single-valued function of $-s^{\mathrm{ex}}/k_{\mathrm{B}}$ for a fluid of classical particles interacting via a pair potential of the inverse-power-law form and obeying Newton's equations of motion. For fluids with more complex structures and interactions, the scaling can only be expected to approximately hold.

The key point of Fig. 3.5 is that one sees qualitatively different trends for the scaling relation depending on whether the multicomponent ($-s^{(2)}/k_{\mathrm{B}}$ or τ) or effective one-component quantities ($-s_{\mathrm{eff}}^{(2)}/k_{\mathrm{B}}$ or τ_{eff}) are used. When the former are adopted, one finds that a single scaling curve describes all data for which $\epsilon/k_{\mathrm{B}}T > 2$ (i.e., the data for which η follows the "dynamically normal" trend of increasing with $\epsilon/k_{\mathrm{B}}T$; see Fig. 2 of ref. [3]). Only dynamically anomalous state points with $\epsilon/k_{\mathrm{B}}T < 2$ (i.e., for which η decreases with increasing $\epsilon/k_{\mathrm{B}}T$) deviate from the scaling curve. This is analogous to the excess entropy scaling behavior observed in recent simulations of liquid water.[111] Specifically, deviations from excess entropy scaling were also observed for dynamically anomalous state points (where water's relaxation times decrease with increasing density). As can be seen from the insets of Fig. 3.5 (also in the data of

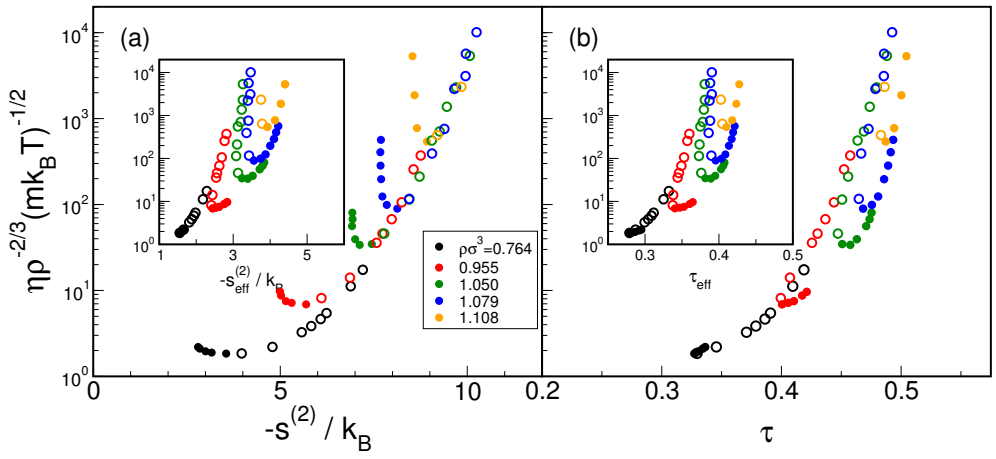

Figure 3.5: Reduced shear viscosity $\eta\rho^{-2/3}(mk_BT)^{-1/2}$ plotted versus various structural order metrics based on static pair correlations for the polydisperse SW fluid: (a) [main panel] negative two-body excess entropy, $-s^{(2)}/k_B$ and [inset] its effective one-component counterpart, $-s^{(2)}_{eff}/k_B$; (b) [main panel] translational structure metric, τ, and [inset] its effective one-component counterpart, τ_{eff}. Structural data were obtained via the MC simulations of this study, and the dynamic data were extracted from the earlier molecular dynamics investigation of Krekelberg et al.[3]. Open symbols represent data for $\epsilon/k_BT > 2$ and filled symbols for $\epsilon/k_BT < 2$. For the latter conditions, shear viscosity anomalously increases with ϵ/k_BT (see Fig. 2 of ref. [3])

ref. [3]), different trends emerge when the effective one-component quantities $-s^{(2)}_{eff}/k_B$ or τ_{eff} are adopted in the analysis, which obscure the aforementioned qualitative connection between the scaling behaviors of two different types of fluids that exhibit dynamic anomalies.

3.3 Conclusions

This investigation highlights some significant problems that arise when characterizing real-space, static pair correlations of moderately polydisperse

colloidal fluids by a commonly-used effective one-component approach. Specifically, our analysis of a model fluid that mimics the experimental behavior of colloids with short-range attractions shows that trends based on the one-component treatment are qualitatively inconsistent with those of the full multicomponent description; e.g., the former spuriously indicates that pair correlations weaken with increasing attractions over a wide range of conditions. A key problem associated with the effective one-component analysis is an artificial, polydispersity-induced "softening" of the apparent static correlations–due to averaging over different particle sizes–which in turn causes the entropic consequences of structural ordering to be significantly underestimated. As an example of the implications of this issue, we demonstrate how excess entropy scalings for the shear viscosity of our model fluid show expected behavior only when the full multicomponent structural analysis is employed. Finally, we show that characterization of the partial radial distribution functions in concentrated suspensions of model colloidal fluid allows for a quantitatively accurate estimate of the thermodynamic excess entropy, a quantity that cannot be reliably estimated from an effective one-component analysis.

On the theoretical front, our study demonstrates that both analytical results from statistical mechanics and Monte Carlo simulations can provide insights into some of the key polydispersity-related issues for the structural characterization of model colloidal fluids. An important open question is how to carry out a similar multicomponent analysis for data obtained via, e.g., optical microscopy experiments, where one is inevitably limited by inadequate

sampling. We are currently exploring the prospects of using maximum likelihood estimation techniques together with liquid-state theory for accomplishing this, and we will report on our findings in a future study.

3.4 Author Contributions

The work in this chapter was submitted to be published in 2011. [41] Thomas M. Truskett designed the research and helped write the document. Jeffrey R. Errington designed and executed the new Monte Carlo simulations techniques and helped write the document. Mark J. Pond provided the dilute-limit analysis, analyzed data and wrote the core of the document.

Chapter 4

Generalized Rosenfeld scalings for tracer diffusivities in not-so-simple fluids: Mixtures and soft particles

4.1 Introduction

Many computational and experimental studies have now provided empirical evidence of a strong correlation between transport coefficients and the excess entropy of equilibrium fluids (see, e.g., [5, 6, 7, 55, 10, 1, 11]). The transport coefficients (e.g., diffusivity, viscosity, and thermal conductivity) quantify the dynamic response of a fluid to a small perturbation in the associated field variables, while the excess entropy is a negative quantity that characterizes the number of microstates rendered inaccessible to the fluid (relative to an ideal gas) due to static interparticle correlations. Changes to macrostate variables that strengthen the interparticle correlations, and hence make excess entropy more negative, typically result in slower dynamical processes [6]. This is true even for confined fluids [18, 55, 112, 113, 114, 115] and for systems that show anomalous dependencies of transport coefficients on density, temperature, or the strength of the interparticle attractions [56, 116, 117, 118, 119, 120, 121, 58, 57, 122, 123, 124, 125, 126, 127, 128, 3, 2, 40, 129].

The connection between transport coefficients and excess entropy is of

fundamental interest because it provides a clue in the long-standing puzzle concerning what structural and thermodynamic properties correlate with the dynamics of equilibrium fluids. The link also has practical consequences. For example, if the transport coefficients of a fluid, cast in an appropriately reduced form, can be approximately represented as a single-valued function of the excess entropy, then knowledge of the latter allows indirect "prediction" of the former [114]. The value of this approach lies in the fact that, while it is difficult to directly estimate transport coefficients from first principles, the excess entropy can often be accurately predicted from liquid-state theories.

At present, a rigorous and general statistical mechanical justification for the empirically observed relationship between transport coefficients and excess entropy is lacking. However, even in the absence of a formal justification, there are a number of practical questions that deserve further investigation. Here, we present new calculations that address key aspects of two such questions.

- For what types of fluid systems is tracer diffusivity, when cast in an appropriately reduced form, approximately a single-valued function of excess entropy?

- Can we develop a strategy for determining the aforementioned "appropriately reduced form" for tracer diffusivity of a given system from knowledge of the intermolecular potential, temperature, and composition?

To understand the context of these questions, it is helpful to first consider some background. It has long been appreciated that the following reduced

form of self-diffusivity, $D^R \equiv D\rho^{1/3}(k_\mathrm{B}T/m)^{-1/2}$, can be formally represented as a single-valued function of excess entropy, s^ex, for any model fluid of identical particles which interact via an inverse-power-law (IPL) pair potential of the form $v(r) = \epsilon(\sigma/r)^n$ (see, e.g., [130]). Here, D is self-diffusivity, ρ is number density, T is temperature, k_B is the Boltzmann constant, m is the particle mass, and the combination $\epsilon\sigma^n$ is the single parameter of the IPL potential. The function relating D^R and s^ex strictly depends on the exponent n, but the dependence is weak. In fact, Rosenfeld [6] first pointed out that the relationship is "quasi-universal" in the sense that, for a given value of excess entropy, there is less than 30% variation in the predicted self-diffusivities for different equilibrium IPL fluids with $4 \leq n \leq \infty$. Because of this observation, we refer to D^R in this work as the Rosenfeld form of reduced diffusivity. Recently, Mittal et al. [55] demonstrated that the same quasi-universal relationship also adequately describes the correlation between D^R and s^ex for both bulk (isotropic) and confined (inhomogeneous) equilibrium Lennard-Jones fluids. An important point of the Rosenfeld [6] and Mittal et al. [55] investigations, discussed from a different angle in a more recent study by Dyre and co-workers [131], is that since both the static and dynamic properties of many dense, simple liquids are dominated by their repulsive interactions, they closely mimic the behaviors of "equivalent" IPL fluids. Thus, one can expect D^R of these monatomic simple-liquid systems to scale with s^ex in a way that is consistent with the trend originally identified by Rosenfeld.

Yet there are many fluids that cannot be expected to mimic the be-

havior of monatomic IPL systems. Will excess entropy also prove useful for predicting the dynamics of these more complex fluids? For example, can excess entropy be used to reliably predict the effects of temperature and density on the self-diffusivity of model fluids with soft (or even bounded) pair potentials, like those that characterize the effective interactions between macromolecules or micelles in solution [46, 47, 14]? At present the answer is unclear. A recent molecular dynamics simulation study by Krekelberg et al. [2] demonstrated that D^R of the Gaussian-core fluid is not (even approximately) a single-valued function of s^{ex}, and the same is true for the Rosenfeld-scaled thermal conductivity and viscosity [132]. Is there a systematic way to construct, based on knowledge of the pair potentials and temperature of a system, an alternative reduced form, i.e. a generalized Rosenfeld diffusivity D^{GR}, that (to within acceptable tolerances) is a function of excess entropy alone? One of the goals of this study is to address this question for different types of model systems with a variety of interactions, [e.g., continuous or discontinuous, steeply repulsive (diverging) or soft (bounded)].

A related question is whether excess entropy can be used to predict the effects of temperature, density, and composition on the tracer diffusivities of the components of a fluid mixture? This question has been recently studied in a limited context. Specifically, following initial work on monatomic systems by Dzugutov [7], a scaling for the tracer diffusivities of mixtures based on two-body contributions to the excess entropy has been introduced [22]. Although it appears that this mixture version of the Dzugutov scaling can capture some

of the behaviors exhibited by simple fluid systems, it also has some significant limitations. For example, the reduced diffusivity for the Dzugutov scaling, D_Z, relies on defining an effective "hard-core diameter" for each interparticle potential, which is not convenient for the study of soft or penetrable particles with bounded interactions. Moreover, the Dzugutov scaling fails to describe the behavior of systems in the limit of vanishing number density. Finally, computing the two-body excess entropy requires knowledge of the radial distribution functions between all components in the mixture for each thermodynamic state of interest, which is particularly cumbersome when studying inhomogeneous fluids. This should be contrasted with the excess entropy used in the Rosenfeld scaling, which can be readily calculated from knowledge of the fluid's equation of state. For all of these reasons, we examine in this study whether one can, based on knowledge of mixture composition, temperature, and pair potentials, construct a generalized Rosenfeld form for the reduced tracer diffusivity for component i, D_i^{GR}, that is approximately a single-valued function of the excess entropy of the fluid mixture.

The organization of the chapter is as follows. In Section 4.2, we introduce the simple idea that underlies the generalized Rosenfeld scaling for predicting tracer diffusivity from excess entropy. Section 4.3 provides details on the model fluid systems and the simulation techniques that we use here to put the predictions of this scaling to quantitative tests. In Section 4.4, we analyze the generalized Rosenfeld scaling for a wide variety of binary mixtures of hard spheres, Widom-Rowlinson particles, and Gaussian-core particles. In

Section 4.5, we discuss how this data helps to understand the strengths and limitations of using excess entropy for predicting the effects that macroscopic parameters (temperature, density, composition) and microscopic details (particle diameter, particle mass, softness of the interparticle potential) have on single-particle dynamics.

4.2 Generalized Rosenfeld form for Reduced Tracer Diffusivity

In order to ensure that D_i^{GR}, the generalized Rosenfeld form of the reduced tracer diffusivity of component i, is defined in a way that is useful for making excess-entropy based predictions, we aim to have it satisfy the following three criteria for a given system. (i) It should be proportional to the bare tracer diffusivity, i.e., $D_i^{\mathrm{GR}} = \alpha D_i$. (ii) The prefactor α, which has units of reciprocal diffusivity, should be readily calculable based on knowledge of the parameters that define the fluid system, i.e., macroscopic variables like temperature T, density ρ, and the mole fractions of the species, as well as microscopic parameters like particle masses and the pair potentials $V_{ij}(r)$ describing the effective interactions. (iii) The dimensionless quantity D_i^{GR} should be approximately a single-valued function of s^{ex}.

For the case of a monatomic IPL fluid, the aforementioned criteria are rigorously satisfied at all state points if one adopts the Rosenfeld form of the reduced self-diffusivity D^R discussed in the introduction. In fact, Rosenfeld [6] previously illustrated that, at low number density, an analytical relationship

between D^R and s^{ex} can be obtained for an IPL fluid by using two equations: an Enskog theory expression for D and a truncated second-virial expansion for s^{ex}. Our approach here is to similarly examine the low-density limit of more complex model fluids and mixtures, taking advantage of known theoretical results for the tracer diffusivity and excess entropy to seek out a potentially useful definition for D_i^{GR}. As we show below, these low-density theoretical results do suggest a simple expression for D_i^{GR} that, in the dilute limit, satisfies the three criteria mentioned above. Of course, unlike for an IPL fluid, choosing D_i^{GR} of a complex fluid so that it is a single-valued function of s^{ex} at low density does not guarantee that it will also behave that way at high particle density. In fact, one can view the extent to which the D_i^{GR} versus s^{ex} scaling holds at higher particle density as a measure of the utility of excess entropy for predicting tracer diffusivity of a given fluid system. Section 4.4 focuses on quantitatively examining this point for a variety of model fluids.

To make the above discussion more concrete, first consider that kinetic theory indicates that D_i is inversely proportional to number density ρ in a fluid mixture at low density

$$D_i = \frac{[\rho D_i]_0}{\rho}, \tag{4.1}$$

where the quantity $[\rho D_i]_0 \equiv \lim_{\rho \to 0} \rho D_i$ generally depends on temperature, mixture composition, as well as the masses of the species and their the interparticle interactions. We discuss simple theoretical methods for estimating $[\rho D_i]_0$ for model systems below. The relationship between ρ and s^{ex}, to leading

order in ρ, can be expressed as

$$s^{\mathrm{ex}}/k_{\mathrm{B}} = -\rho\left[B + T\frac{dB}{dT}\right], \tag{4.2}$$

where B is the second virial coefficient, given by

$$B = \sum_{i}^{N_c}\sum_{j}^{N_c} x_i x_j B_{ij}. \tag{4.3a}$$

Here, the sums are over the N_c components of the mixture, x_i is the mole fraction of component i, and B_{ij} can be expressed in terms of the pair potentials $V_{ij}(r)$ as

$$B_{ij} = 2\pi\int_0^\infty \left[1 - e^{-\beta V_{ij}(r)}\right] r^2 dr, \tag{4.3b}$$

where $\beta^{-1} = k_{\mathrm{B}}T$. Using Eq. (4.2) to eliminate ρ from Eq. (4.1) and rearranging leads to

$$\frac{D_i}{\left(B + T\frac{dB}{dT}\right)[\rho D_i]_0} = \frac{1}{-s^{\mathrm{ex}}/k_{\mathrm{B}}}, \tag{4.4}$$

which again is valid only in the the $\rho \to 0$ limit. We identify the dimensionless quantity on the left-hand-side, which is clearly a function of s^{ex} only at low density, as the generalized Rosenfeld reduced form of the tracer diffusivity, D_i^{GR},

$$D_i^{\mathrm{GR}} \equiv \frac{D_i}{\left(B + T\frac{dB}{dT}\right)[\rho D_i]_0}. \tag{4.5}$$

Note that the expression for D^{GR}, the generalized Rosenfeld self-diffusion coefficient for a monatomic fluid, is obtained by replacing D_i with D in Eq. (4.5).

Although the definition for D_i^{GR} given in Eq. (4.5) is compact, it is more convenient for making predictions for model systems if $[\rho D_i]_0$ is further

expressed in terms of the mole fractions of the species, the associated pair potentials, the particle masses, and the temperature. Below, we present simple theoretical expressions for carrying this out for particles with hard-sphere and soft (continuous) interactions, respectively.

4.2.1 Hard-Particle Interactions

For models with hard-sphere interactions, an expression for $[\rho D_i]_0$ is easily obtained within Enskog kinetic theory [133, 9] In particular, the product ρD_i is given by

$$\rho D_i = \frac{3}{8\pi^{1/2}} \frac{\sqrt{k_{\mathrm{B}} T / m_i}}{\sum_{j=1}^{N_c} x_j \sigma_{ij}^2 g(\sigma_{ij}^+) \left[\frac{1}{2}\left(1 + \frac{m_i}{m_j}\right)\right]^{-1/2}}, \tag{4.6}$$

where m_i is the mass of component i, σ_{ij} is the hard-sphere contact diameter between particles of type i and j, and $g_{ij}(\sigma_{ij}^+)$ is the value of the radial distribution function between particles of type i and j at contact. The low density limit $[\rho D_i]_0$ is obtained by substituting $g_{ij}(\sigma_{ij}^+) = 1$ into Eq. (4.6), which gives

$$[\rho D_i]_0 = \frac{3}{8\pi^{1/2}} \frac{\sqrt{k_{\mathrm{B}} T / m_i}}{\sum_{j=1}^{N_c} x_j \sigma_{ij}^2 \left[\frac{1}{2}\left(1 + \frac{m_i}{m_j}\right)\right]^{-1/2}}. \tag{4.7}$$

When computing D_i^{GR} for the hard-sphere and Widom-Rowlinson model mixtures discussed in Section 4.3, we simply substitute Eq. (4.7) into Eq. (4.5).

4.2.2 Soft-Particle Interactions

We also study fluids of soft particles in this work, i.e., particles with continuous and bounded interactions that cannot be treated as hard spheres

with an effective temperature-dependent diameter. In order to predict $[\rho D_i]_0$ for these models, we use an approximate theory due to Tankeshwar and coworkers [134, 135], which we refer to as the Tankeshwar diffusion model (TDM). We have found that this basic theoretical approach strikes a reasonable balance between simplicity and accuracy. It has been shown to semi-quantitatively describe how temperature, composition, and density affect the tracer diffusivity of Lennard-Jones fluids, the one-component plasma, and Yukawa fluids [136]. We have also found that it approximately captures how temperature and density affect the diffusion coefficient of the Gaussian-core fluid.

The details of the TDM are discussed extensively elsewhere [136, 134, 135]. In short, it is based on an approximate expression for the velocity autocorrelation function, and hence the tracer diffusivity D_i via the Green-Kubo relation, for each component i of the fluid in terms of two parameters: the Einstein frequency ω_i and a "jumping" frequency τ_i. The values of these parameters are obtained by ensuring that the velocity autocorrelation functions satisfy some exact microscopic sum rules.

Within this model, the product ρD_i is given by

$$\rho D_i = \rho \frac{k_\mathrm{B} T}{m_i} \frac{\pi}{2} \tau_i \sec\left(\frac{\pi}{2}\omega_i \tau_i\right), \tag{4.8}$$

where

$$\begin{aligned} \tau_i^{-2} &= \frac{\rho A_i^{(4)} - \left[\rho A_i^{(2)}\right]^2}{4\rho A_i^{(2)}}, \\ \omega_i^2 &= -\frac{5\left[\rho A_i^{(2)}\right]^2 - \rho A_i^{(4)}}{4\rho A_i^{(2)}}, \end{aligned} \tag{4.9}$$

and

$$A_i^{(2)} = \frac{4\pi}{3} \sum_{j=1}^{N_c} \frac{x_j}{m_j} \int_0^\infty dr\, r^2 g_{ij}(r) \left(\frac{2}{r} \frac{dV_{ij}}{dr} + \frac{d^2 V_{ij}}{dr^2} \right), \tag{4.10a}$$

$$A_i^{(4)} = \frac{4\pi}{3} \sum_{j=1}^{N_c} \frac{x_j}{m_i} \left(\frac{1}{m_i} + \frac{1}{m_j} \right) \int_0^\infty dr\, r^2 g_{ij}(r) \times \left\{ \frac{2}{r^2} \left(\frac{dV_{ij}}{dr} \right)^2 + \left(\frac{d^2 V_{ij}}{dr^2} \right)^2 \right\}. \tag{4.10b}$$

In Eq. (4.10), V_{ij} is the pair potential between particles of species i and j, and terms involving three-body static correlations have been omitted. In order to evaluate $[\rho D_i]_0$, we take the $\rho \to 0$ limit of Eqs. (4.8)–(4.10), which leads to

$$[\rho D_i]_0 = \frac{k_\mathrm{B} T}{m_i} \left(\frac{A_{i,0}^{(4)}}{[A_{i,0}^{(2)}]^3} \right)^{1/2}. \tag{4.11}$$

Here $A_{i,0}^{(2)} \equiv \lim_{\rho \to 0} A_i^{(2)}$ and $A_{i,0}^{(4)} \equiv \lim_{\rho \to 0} A_i^{(4)}$, each of which follow by replacing $g_{ij}(r)$ in Eq. (4.10), with the Boltzmann factor of the pair potential,

$$\lim_{\rho \to 0} g_{ij}(r) = \exp[-\beta V_{ij}(r)]. \tag{4.12}$$

When computing D_i^{GR} for the Gaussian-core mixtures discussed in Section 4.3, we substitute Eq. (4.11) into Eq. (4.5).

4.3 Model Systems and Simulation Methods

As discussed in Section 4.1, a key aim of this study is to investigate whether it is possible to construct an excess-entropy based strategy for predicting tracer diffusivity generic enough to be successfully applied to fluid mixtures

with either hard (impenetrable) or soft (penetrable) interparticle interactions. For our model systems, we choose familiar representations for both: the hard-sphere (HS) pair potential for the former and the Gaussian-core pair potential for the latter.

The HS pair potential is discontinuous and athermal, assigning infinite energy to configurations that have particle overlaps and zero energy to all others. It is thus represented as

$$V_{ij}^{\mathrm{HS}}(r) = \begin{cases} \infty & r < \sigma_{ij}, \\ 0 & r \geq \sigma_{ij}. \end{cases} \tag{4.13}$$

Here, σ_{ij} is the contact diameter between particles of type i and j. We investigate several binary HS mixtures with additive diameters, i.e., $\sigma_{ij} = (\sigma_i + \sigma_j)/2$. In particular, we first study compositional effects on tracer diffusivity and excess entropy using a system composed of equimass ($m_1/m_2 = 1$) particles with diameter ratio $\sigma_1/\sigma_2 = 1.3$. For this system, we examine mole fractions of component one in the range $0.1 \leq x_1 \leq 0.9$. We also investigate the effects of diameter ratio by considering particles with $\sigma_1/\sigma_2 = 1.3, 2.0, 3.0, 5.0$. These latter studies are carried out at fixed composition $x_1 = 0.1$. All of the above systems are studied across a wide range of packing fractions $\phi_{\mathrm{c}} = \pi(x_1\sigma_1^3 + x_2\sigma_2^3)/6$ spanning between 0.05 (dilute gas) and 0.5 (near the single-component HS freezing transition).

We also consider a highly non-additive version of the binary HS mixture: the Widom-Rowlinson (WR) model [137]. In this system, the contact diameter between particles of the same type is zero ($\sigma_{11} = \sigma_{22} = 0$), but the

cross-diameter is finite $\sigma_{12} = \sigma_{21} = \sigma$ and $m_1 = m_2$. As might be imagined, this system exhibits entropically driven phase separation at sufficiently high density, which we avoid here by studying $0 < \rho\sigma^3 < 0.7$. Since the model is symmetric with respect to the interactions, we can deduce global behavior by studying mole fractions in the range $0 < x_1 \leq 0.5$.

Finally, we study fluids composed of soft particles that interact via the bounded Gaussian-core pair potential [54], given by

$$V_{ij}^{\mathrm{GC}}(r) = \epsilon_{ij} \exp[-(r/\sigma_{ij})^2], \tag{4.14}$$

where ϵ_{ij} and σ_{ij} are parameters that characterize the energy and length scale, respectively, of the interaction between particles of type i and j. For the simulations in this work, we truncate the interparticle interactions at a separation of $3.2\sigma_{ij}$. We examine both single-component and two-component Gaussian-core fluids. For the latter, we adopt the same parameters used in a previous investigation of the static structure and thermodynamics of that system [24]. Specifically, we assign $\sigma_{22} = 0.665\sigma_{11}$ and $\sigma_{12} = \sqrt{(\sigma_{11}^2 + \sigma_{22}^2)/2}$, $\epsilon_{11} = \epsilon_{22}$ and $\epsilon_{12} = 0.944\epsilon_{11}$ (which encourages mixing), and $m_1 = m_2$. We investigate the binary Gaussian-core fluid at compositions $0.1 \leq x_1 \leq 0.9$, temperatures $0.05 \leq k_{\mathrm{B}}T/\epsilon_{11} \leq 0.4$, and densities $0.05 \leq \rho\sigma_{11}^3 \leq 1.0$. At some temperatures, the maximum density in this range is not an isotropic fluid due to propensity of the system to phase separate. We excluded from our analysis any state points that showed thermodynamic or structural indications of phase separation.

To explore the dynamic properties of the above systems, we perform

molecular dynamics (MD) simulations. For the HS and WR mixtures, we use a standard event-driven algorithm [138]. For the binary Gaussian-core fluid, the equations of motion are integrated using the velocity-Verlet method [17] with time step $\delta t = 0.05\sqrt{m_1\sigma_{11}^2/\epsilon_{11}}$. All MD simulations are carried out in the microcanonical ensemble with $N = 3000$–5000 particle using a periodically-replicated cubic simulation cell with volume V, chosen in accord with the desired fluid density. Tracer diffusion coefficients D_i are calculated by fitting the long time average mean squared displacement of the i type particles $\langle \delta r_i^2 \rangle$ to the Einstein relation $6D_i t = \langle \delta r_i^2 \rangle$. Note that, for the case of the monatomic fluid, this definition of the tracer diffusivity reduces to the self diffusivity. We perform multiple independent simulations at several state points for each model, and we find the relative standard error in tracer diffusivities to be less than 1%.

Thermodynamic properties of the Gaussian-core fluid mixtures are computed using grand-canonical transition-matrix Monte Carlo (GC-TMMC) simulations. These simulations are conceptually equivalent to a series of semi-grand simulations performed over a range of fluid densities stitched together using ghost insertion/deletion moves. Details of this method can be found elsewhere [139, 140]. These simulations require fixed values of the activity, $\{\xi_1, \xi_2\}$, volume, V, and temperature, T, as inputs. The activity is defined as $\xi_i = \Lambda_i^{-3} \exp(\mu_i/k_{\rm B}T)$, where μ_i and Λ_i are the chemical potential and the thermal de Broglie wavelength of component i, respectively. All GC-TMMC simulations for the Gaussian-core fluid mixtures reported here use a system

volume of $V = 343$. For the activities, the values of $\ln \xi_i$ that we use span from 32.63 at the lowest temperature to 12.24 at the highest temperature investigated. Thermodynamic properties at other values of activity are obtained via the histogram re-weighting technique. The primary quantity obtained from GC-TMMC is the particle number probability distribution $\Pi(N; \{\mu_i\}, V, T)$. From this, excess entropies are trivially calculated (see [113]). System size effects in excess entropy for the Gaussian-core mixtures are found to be negligle by comparing results to a series of simulations using a smaller volume of $V = 216$. We confirmed that the equation of state (and hence excess entropy) of Gaussian-core fluid mixtures produced from the GC-TMMC simulations is statistically indistinguishable with that produced from molecular dynamics simulations.

GC-TMMC calculations for the WR mixtures are performed using a system volume of $V = 343$. For this fluid, simulations are completed with activity values of $\xi_1 = \xi_2 = 1$, and histogram re-weighting is applied to obtain thermodynamic quantities at other values of activity. System size effects are examined by performing simulations over a limited density and composition range with a volume of $V = 1000$, and are also found to be negligible.

The excess entropy data we present for the binary HS mixtures is calculated from the accurate Boublik-Mansoori-Carnahan-Starling-Leland (BMCSL) equation of state [141, 142]. As a check, we compared the BMCSL values for compressibility factor and excess entropy against those obtained via molecular dynamics simulations for selected state points as a function of par-

ticle diameter ratio and packing fraction, and we found the agreement to be excellent.

Finally, we also compare the results for the binary systems to corresponding single-component systems. For the single-component HS system we use the data of [114] and for the single-component Gaussian-core fluid we use the data of [2].

4.4 Results and discussion

4.4.1 Hard-sphere mixtures

4.4.1.1 Compositional effects

We begin by investigating the effects of composition on mixtures of HS particles with size ratio $\sigma_1/\sigma_2 = 1.3$. Figure 4.1a displays the tracer diffusion coefficients D_i of the two components as a function of total packing fraction ϕ_c for several different compositions, indicated by the mole fraction of large particles, x_1. As must be the case, when one of the species is present in high concentration, its tracer diffusivity approaches the value of the self-diffusion coefficient D of the single-component HS fluid at the same packing fraction ϕ_c. However, the tracer diffusivity of the dilute component is generally different than D. In particular, when component 1 (the larger particles) is dilute, one should expect $D_1 < D$. This logic can be qualitatively rationalized by the fact that, on average, motion of the larger solute would require larger local structural rearrangements (i.e., fluctuations) than for the motion of the smaller solvent particles. Conversely, by an analogous argument, one expects $D_2 > D$

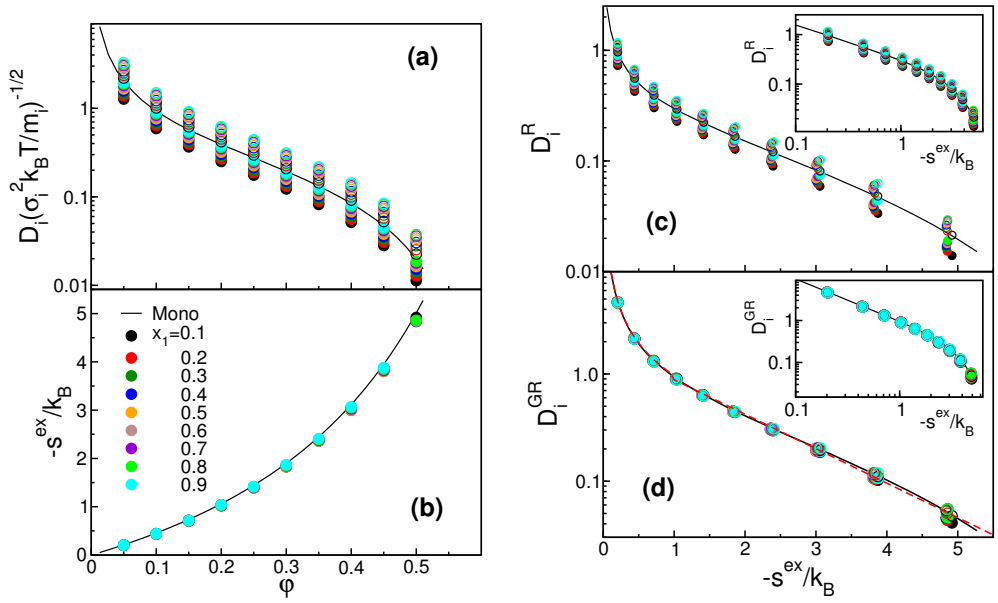

Figure 4.1: Properties of the binary HS mixture with particle diameter ratio $(\sigma_1/\sigma_2) = 1.3$, equal mass, and a variety of compositions. (a) Tracer diffusion coefficients D_i and (b) (negative) excess entropy $-s^{\rm ex}$ as a function of packing fraction $\phi_{\rm c}$. (c) Rosenfeld D_i^R and (d) generalized Rosenfeld $D_i^{\rm GR}$ tracer diffusivities as a function of $-s^{\rm ex}$. Filled and open symbols denote component 1 (large) and 2 (small), respectively. The color of symbols denotes the mole fraction of component 1, x_1, specified in the legend of (a). The solid line in each figure is the result for the single-component HS system. The dashed red line in (d) represents a least-squares fit of the data to Eq. (4.15), which results in $\alpha = 0.95$, $A = 1.85$, and $\beta = 0.74$. In (c) and (d), the insets are the same as the main plots, but on a log-log scale.

if component 2 (the smaller particles) is dilute. The data in Figure 4.1a is consistent with these expectations.

It is interesting to note that the compositional variation in $\ln D_i$ is fairly insensitive to the value of ϕ_c. Moreover, the excess entropy [Figure 4.1b] exhibits almost no compositional dependence whatsoever, and its packing fraction dependence for any particular composition is nearly identical to that of the single-component HS fluid. All of this suggests that an appropriate composition dependent rescaling of the tracer diffusivity data might (approximately) make it a single-valued function of excess entropy. Indeed, Figures 4.1c and 4.1d show that the generalized Rosenfeld tracer diffusivities D_i^{GR} of Eq. 4.5 for both species collapse onto a single curve [that describing the single-component (SC) fluid data, $D_{\mathrm{SC}}^{\mathrm{GR}}$] when plotted versus excess entropy, while no data collapse occurs if the tracer diffusivities are naïvely represented in the original Rosenfeld reduced form D_i^R.

The single-component relationship $D_{\mathrm{SC}}^{\mathrm{GR}}(s^{\mathrm{ex}})$ can be described by a piece-wise function. The form of its low-density (low $-s^{\mathrm{ex}}$) scaling is an inverse power law, given by Equation (4.4). From Figure 4.1d, we infer that when $-s^{\mathrm{ex}}/k_{\mathrm{B}} \gtrsim 1$, the relationship becomes approximately exponential. A least squares fit assuming these generic function forms, i.e.,

$$D_{\mathrm{SC}}^{\mathrm{GR}}(s^{\mathrm{ex}}) = \begin{cases} \alpha[-s^{\mathrm{ex}}/k_{\mathrm{B}}]^{-1} & -s^{\mathrm{ex}}/k_{\mathrm{B}} < 1, \\ A\exp[-Bs^{\mathrm{ex}}/k_{\mathrm{B}}] & -s^{\mathrm{ex}}/k_{\mathrm{B}} > 1, \end{cases} \tag{4.15}$$

yields $\alpha = 0.95$, $A = 1.85$, and $\beta = 0.74$, and describes the simulation data very well (see red dashed line in Fig. 4.1d).

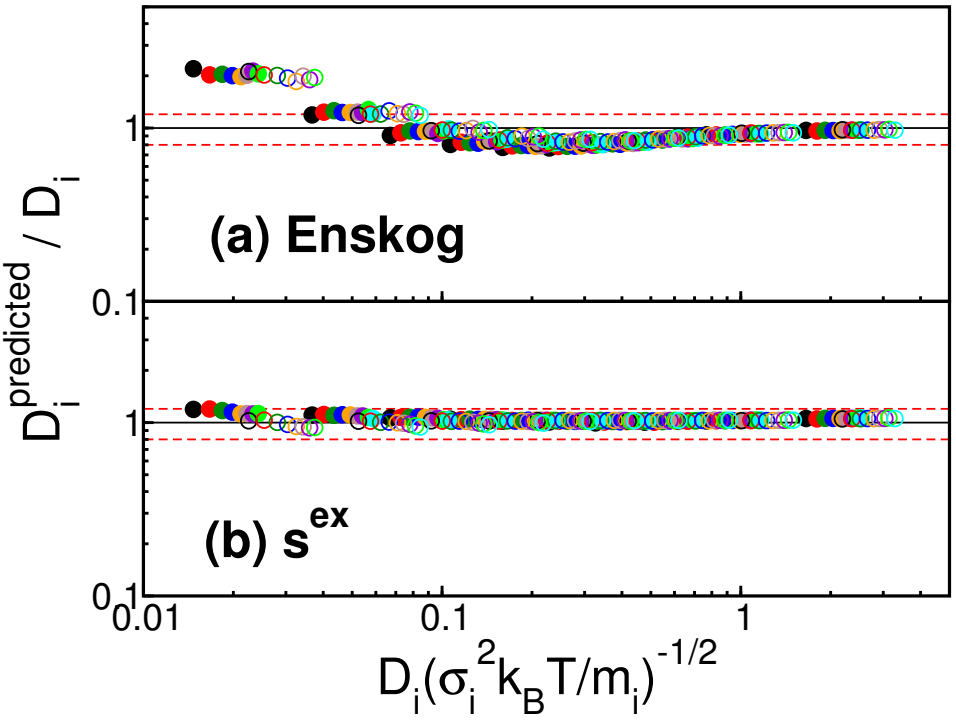

Figure 4.2: Ratio of tracer diffusivity predicted from (a) Enskog theory [Eq. (4.6)] and (b) from excess entropy and the single-component HS result (generalized Rosenfeld scaling) [Eq. (4.16)], for a HS mixture with $(\sigma_1/\sigma_2) = 1.3$, equal mass, and a variety of compositions. Red dashed lines represent 20% relative error of prediction. Symbols have the same meaning as in Figure 4.1.

The data collapse of Figure 4.1d suggests that tracer diffusivities, D_1 and D_2, of this mixture might also be adequately predicted using Eq. (4.15) together with knowledge of the pair potentials, composition, and excess entropy of the mixture. Specifically, the generalized Rosenfeld scaling prediction for tracer diffusivity of component i is given by

$$D_i^{\text{predicted}}(s^{\text{ex}}) = \left\{ [\rho D_i]_0 \left[B + T\frac{dB}{dT} \right] \right\} D_{\text{SC}}^{\text{GR}}(s^{\text{ex}}) \tag{4.16}$$

with B from Eq. (4.3), $[\rho D_i]_0$ from Eq. (4.7), and $D_{\text{SC}}^{\text{GR}}(s^{\text{ex}})$ from the fit of the single-component data to Eq. (4.15).

One way to quantitatively assess the relative predictive ability of Eq. (4.16) is to compare it to the results of, e.g., the basic Enskog theory given by Eq. (4.6). Both equations require as inputs several pieces of information, including the form of the pair potentials and the mixture composition. While predictions based on the generalized Rosenfeld scaling also require knowledge of s^{ex} for the mixture and properties of the single-component system, Enskog theory requires knowledge of the state dependent contact values of the three partial radial distribution functions of the mixture.

Figure 4.2 displays the relative error in the predicted tracer diffusivity to the simulated diffusivity $D_i^{\text{predicted}}/D_i$. Enskog theory [Figure 4.2a] provides good predictions at high values of tracer diffusivity (i.e., low ϕ_{c}). However, as the value of D_i decreases (i.e. , ϕ_{c} increases) Enskog theory first underpredicts, then ultimately significantly overpredicts D_i. When looking at the entire range of ϕ_{c} studied here, 80% of the Enskog theory predictions lie within 20% of

the molecular simulation data. On the other hand, the excess entropy based expression of Eq. (4.16) [Figure 4.2b] predicts the tracer diffusivities semi-quantitatively for all state points investigated here (100% of predictions within 20% of the simulation data).

4.4.1.2 Particle-size asymmetry effects

We also study the effects of particle-size asymmetry on the relationship between excess entropy and tracer diffusivity by examining a series of binary HS mixtures at composition $x_1 = 0.1$ and packing fractions in the range $0 < \phi_c \leq 0.5$. Particles of types 1 and 2 were taken to have identical masses, but we investigated several systems with different diameter ratios [$\sigma_1/\sigma_2 = 1.3$, 2.0, 3.0 and 5.0]. Figure 4.3a displays the tracer diffusivities, D_1 and D_2, for these systems. Increasing the magnitude of the diameter ratio leads to progressively larger deviation of the tracer diffusivities from the self-diffusion coefficient D of the HS fluid at the same ϕ_c. As expected, larger particles diffuse slower than smaller particles [$D_1 < D < D_2$]. How is the excess entropy affected by increasing the ratio of particle diameters? Figure 4.3b shows that increasing σ_1/σ_2 at fixed ϕ_c and x_1 systematically decreases $-s^{ex}$ (i.e., weakens the static interparticle correlations). This effect is qualitatively connected to the more efficient packing arrangements that spheres can sample when significant polydispersity is present [143, 144].

Given that increasing size ratio uniformly reduces structural correlations, but impacts the dynamics of large and small particles in different ways,

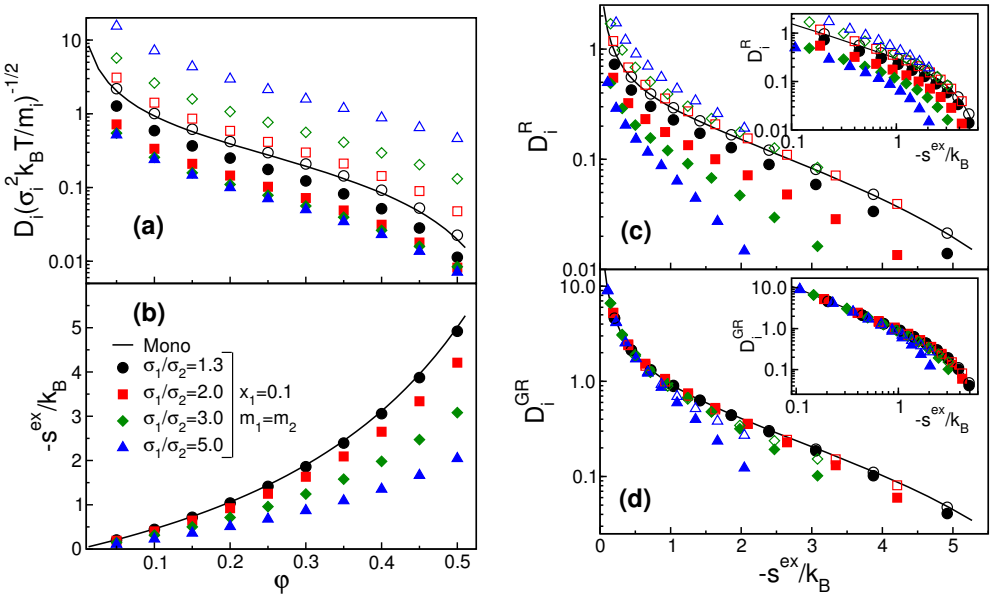

Figure 4.3: Properties of the binary HS mixture at composition $x_1 = 0.1$, equal mass, and several size ratios (σ_1/σ_2) [see legend in (a)]. (a) Tracer diffusion coefficient D_i and (b) (negative) excess entropy $-s^{\rm ex}$ versus packing fraction $\phi_{\rm c}$. (c) Tracer diffusivity reduced in the original Rosenfeld D_i^R and (d) generalized Rosenfeld $D_i^{\rm GR}$ forms as a function of $-s^{\rm ex}$. Filled and open symbols represent large (component 1) and small (component 2) spheres. Symbol shapes denote different particle diameter ratios, as described in the legend of (a). The solid line in each figure is the result for the single-component HS system. In (c) and (d) the insets are the same as the main plots, but on a log-log scale.

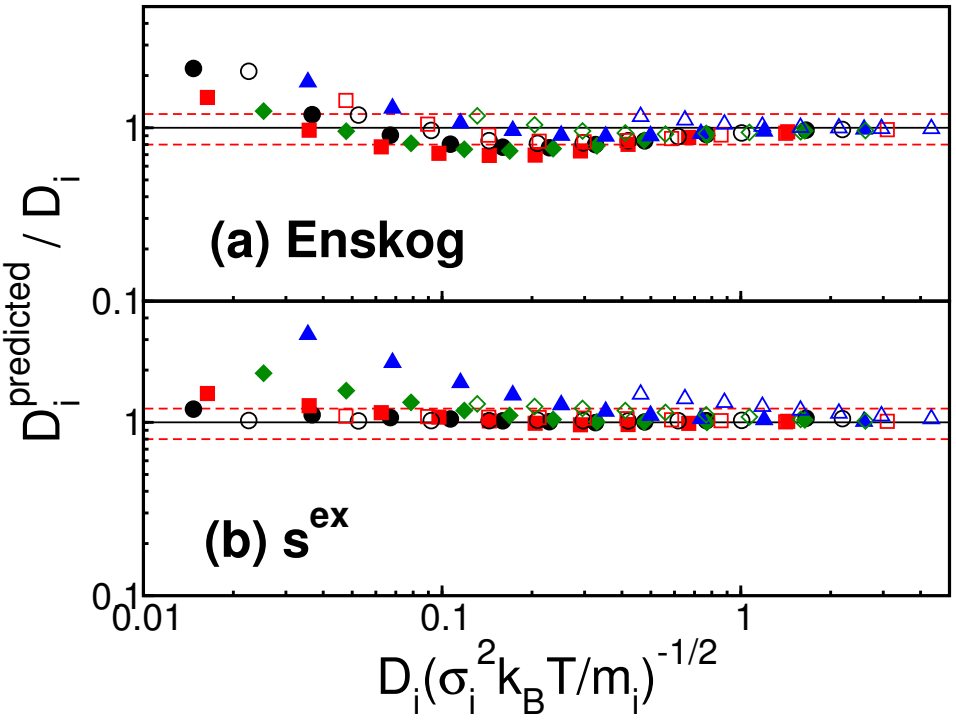

Figure 4.4: Ratio of tracer diffusivity predicted from (a) Enskog theory [Eq. (4.6)] and (b) from excess entropy and the single-component HS data (i.e., generalized Rosenfeld scaling) [Eq. (4.16)], for a HS mixture with equal mass, composition $x_1 = 0.1$, and a variety of size ratios (σ_1/σ_2). Red dashed lines represent 20% relative error of prediction. Symbols have the same meaning as in Figure 4.3.

it might not be surprising that tracer diffusivity data represented in the original Rosenfeld form, D_i^R, does not collapse when plotted versus excess entropy [Fig. 4.3c]. The D_i^R data for the smallest size ratio $\sigma_1/\sigma_2 = 1.3$ is qualitatively similar to the single-component result. However, there is significant deviation for larger diameter ratios, with excess entropy underpredicting the mobility of smaller particles and overpredicting that of larger particles. Figure 4.3d shows, however, that tracer diffusivity reduced in the generalized Rosenfeld form, D_i^{GR}, mostly collapses to the single-component curve when plotted versus $-s^{\mathrm{ex}}$. The most pronounced deviations are for the largest size ratio ($\sigma_1/\sigma_2 = 3$, 5) at the highest packing fractions ($\phi \geq 0.45$).

Figure 4.4 quantitatively compares the predictions of Enskog theory [Eq. (4.6)] with those based on the generalized Rosenfeld scaling [Eq. (4.16)]. At high values of D_i (low ϕ_{c}), both methods provide accurate predictions. As before, for decreasing D_i (increasing ϕ_{c}), Enskog theory first underpredicts and then ultimately overpredicts the tracer diffusivities. The excess entropy based predictions never underpredict, but eventually overpredict the mobility at high values of ϕ_{c}. As an overall measure, the Enskog and the excess entropy expressions predict 70% and 80% of the tracer diffusivities within 20% of the simulated values, respectively. Moreover, we note that while the excess entropy method predicts the tracer diffusivities of the two components with similar reliability, the Enskog expression does well for the small particles (90% within 20%), but poorly for the large particles (50% within 20%).

4.4.1.3 Two-body excess entropy scaling

As noted in Section 4.1, an alternative excess entropy based scaling for diffusion was introduced by Dzugutov [7], who found that an appropriately reduced form of the self-diffusion coefficient D_Z for atomic fluids at moderate densities is nearly a universal function of the two-body contribution to the excess entropy $s^{(2)}$. Subsequently, others have suggested a generalization of this scaling [22] to predict tracer diffusivities of fluid mixtures. In the generalization, the reduced tracer-diffusion coefficient, defined as $D_{Z,i} \equiv D_i/\chi_i$, where

$$\chi_i \equiv 4(\pi k_{\mathrm{B}} T)^{1/2} \sum_{j=1}^{N_{\mathrm{c}}} x_i \rho \sigma_{ij}^4 g_{ij}(\sigma_{ij}^+) \left(\frac{m_i + m_j}{2 m_i m_j} \right)^{1/2}, \tag{4.17}$$

is thought to approximately scale with the i-component contribution to the two-body excess entropy, defined as [22]

$$s_i^{(2)}/k_{\mathrm{B}} \equiv -\frac{1}{2}\rho \sum_{j=1}^{N_{\mathrm{c}}} x_j \int d\mathbf{r} \{g_{ij}(\mathbf{r}) \ln g_{ij}(\mathbf{r}) - [g_{ij}(\mathbf{r}) - 1]\}. \tag{4.18}$$

Note that the two-body excess entropy per particle is given by $s^{(2)} = \sum_i x_i s_i^{(2)}$ [59].

In Figure 4.5a and b we examine the mixture generalization of the Dzugutov scaling for the HS systems discussed above. Specifically, we show data with fixed diameter ratio and varying composition in panel (a) and fixed composition and varying diameter ratio in panel (b). Both sets of data more or less track the scaling. However, deviations from the single component curve

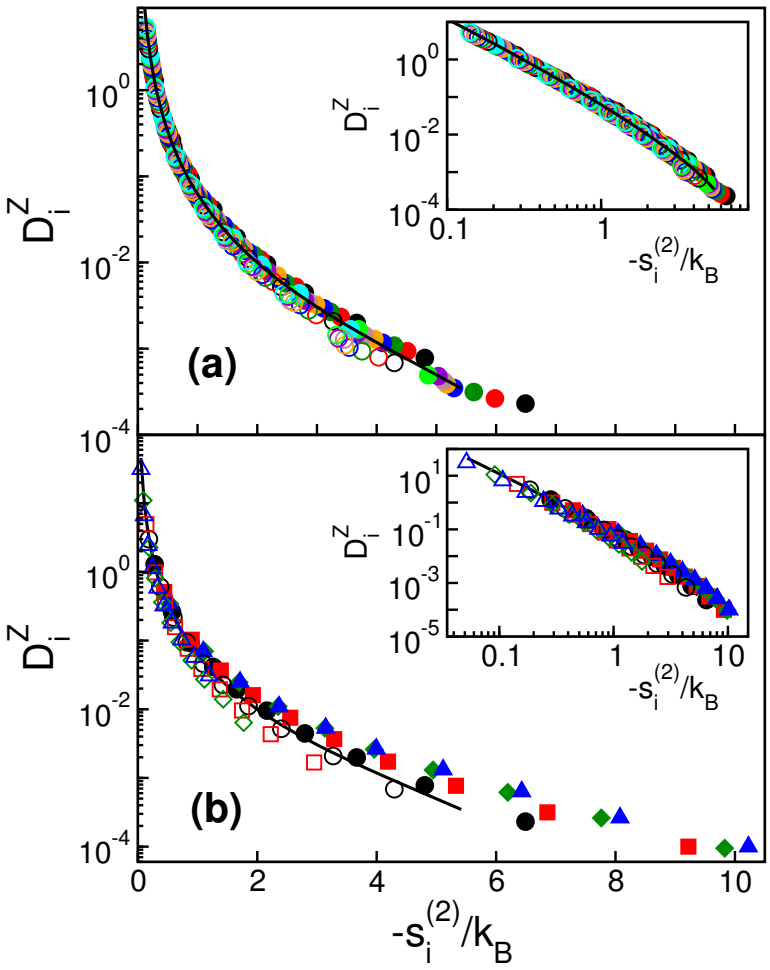

Figure 4.5: Tracer diffusivity reduced in generalized Dzugutov form $D_{Z,i}$ discussed in text versus (negative) i-component contribution to two-body excess entropy $-s_i^{(2)}$ of binary HS mixtures. (a) Particle diameter ratio $\sigma_1/\sigma_2 = 1.3$, equal mass, and a variety of compositions. Symbols have same meaning as Figure 4.1. (b) Composition $x_1 = 0.1$, equal mass, and a variety of size ratios. Symbols have same meaning as Figure 4.3. Insets are the same as the main plots, but with a log-log scale.

appear systematic. The single-component relation with $s_i^{(2)}$ overpredict the small sphere mobility and underpredict the large sphere mobility.

Unfortunately, the predictive value of this type of scaling is inherently limited by the fact that the single-component data cannot access the large values of $-s_i^{(2)}$ realized by the large spheres in a mixture. The former reach a value of $5.5k_{\mathrm{B}}$ at $\phi_{\mathrm{c}} = 0.5$, while the latter are greater than $10k_{\mathrm{B}}$ for the largest size ratios examined here. As a result, "predicting" tracer diffusivities of a mixture would require some systematic way of extrapolating the single-component curve by a substantial amount. As discussed in Section 4.1, the scaling is also limited to systems, like the HS fluid, for which the interparticle repulsions are steep enough to define an effective hard-core diameter to each interaction. Thus, it will be of little use for studying systems with bounded interactions like the Gaussian-core potential or a other models that characterize the soft effective interactions between macro- or supramolecular species in solution [14].

4.4.2 Widom-Rowlinson mixtures

Here we examine the behavior of the Widom-Rowlinson (WR) model fluid introduced in Section 4.3. Recall that it is defined as a mixture of non-additive hard spheres with $\sigma_{11} = \sigma_{22} = 0$ but $\sigma_{12} = \sigma$. Figure 4.6a displays the tracer diffusivity D_i as a function of density for a several compositions x_1. Note that the D_i is always greater then the self-diffusion of the single-component HS fluid, since the number of collisions per unit time will clearly

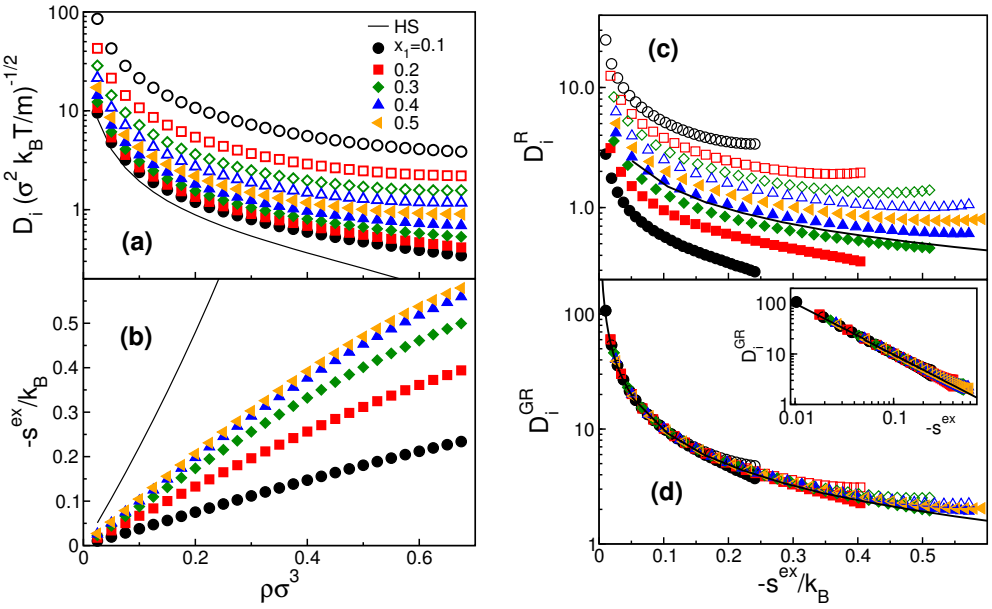

Figure 4.6: Properties of the Widom-Rowlinson mixture. (a) Tracer diffusivities D_i ($i = 1, 2$) and (b) (negative) excess entropy $-s^{\rm ex}$ as function of density $\rho\sigma^3$. (c) Tracer diffusivity reduced in original Rosenfeld form D_i^R and (d) generalized Rosenfeld form $D_i^{\rm GR}$ as a function of $-s^{\rm ex}$. Filled and open symbols denote component 1 and 2, respectively. The symbol type denotes the mole fraction of component 1, x_1, indicated in the legend of (a). The solid line in each figure is the result for the single-component HS fluid. In (d) the insets are the same as the main plots, but on a log-log scale.

be less in the WR fluid than in the HS fluid at the same density. At $x_1 = 0.5$, $D_1 = D_2$, since the fluid is symmetric. At fixed density, as x_1 decreases, D_1 decreases while D_2 increases. This is because the dilute species will experience many more collisions per unit time (it has more neighbors of the opposite type) than the concentrated species. Likewise, Figure 4.6b shows $-s^{\mathrm{ex}}$ for the WR fluids is always less than that of a single-component HS fluid of the same density. This is expected since particles of the same type do not directly exclude volume from one another, which in turn reduces the entropic driving force for forming strong interparticle correlations. Decreasing x_1 from 0.5 toward zero at fixed density decreases $-s^{\mathrm{ex}}$ because it increases the number of particles in the system that do not interact.

As was the case for the HS fluid mixtures, Figure 4.6c shows that the tracer diffusivity reduced in the original Rosenfeld form, D_i^R, is not even approximately a single-valued function of s^{ex}. On the other hand, Figure 4.6d shows that the tracer diffusivity data cast in the generalized Rosenfeld form, D_i^{GR}, largely collapses when plotted versus excess entropy. Interestingly, D_i^{GR} of the WR fluid is well described by the mathematical form of the single-component HS data. The quality of the collapse is more easily seen on a log-log scale (inset to Figure 4.6d).

Figure 4.7a and b compare the accuracy of predicting tracer diffusivity of the components of the WR fluid based on Enskog theory [Eq. (4.6)] versus excess entropy of the WR mixture and the single-component relation for the HS fluid [Eq. (4.16)]. As for the HS fluid, Enskog theory predicts 80% of

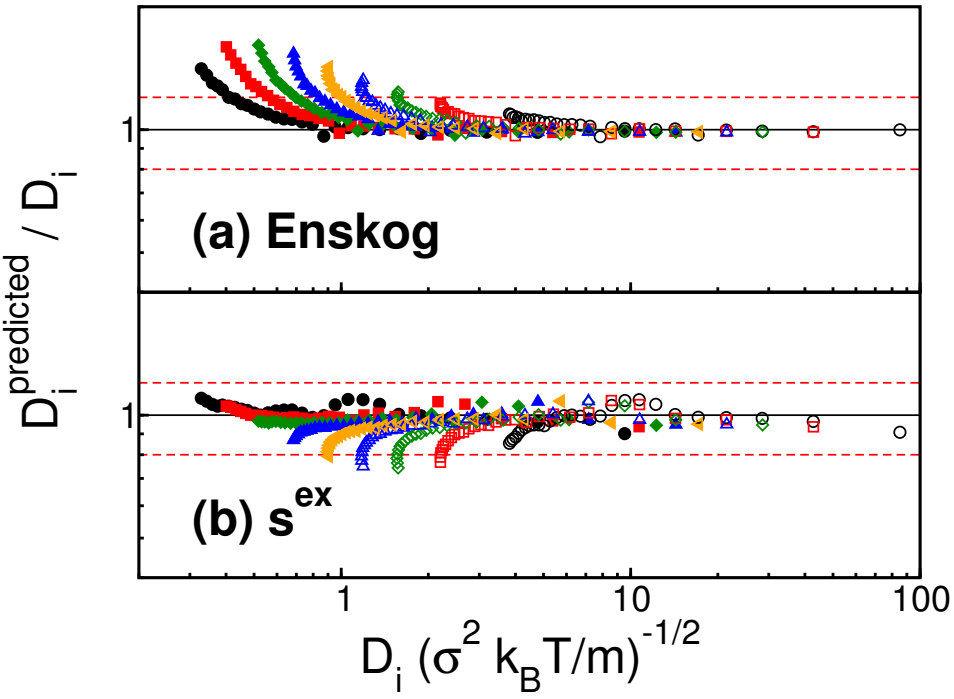

Figure 4.7: Ratio of tracer diffusivity predicted from (a) Enskog theory [Eq. (4.6)] and (b) from excess entropy and the single-component HS result (generalized Rosenfeld scaling) [Eq. (4.16)], for the Widom-Rowlinson mixture. Red dashed lines indicate 20% relative error of prediction. Symbols have the same meaning as in Figure 4.6.

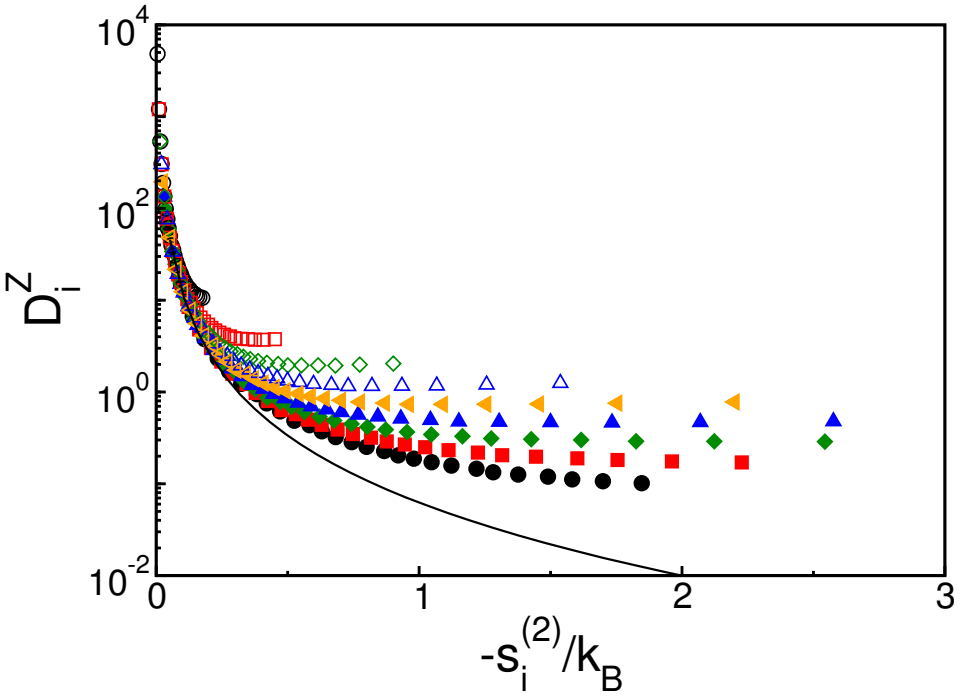

Figure 4.8: Tracer diffusivity reduced in the mixture generalized Dzugutov form discussed in text $D_{Z,i}$ versus the (negative) i-component of the two-body excess entropy $s_i^{(2)}$ for the Widom-Rowlinson model. Symbols have same the meaning as Figure 4.6.

the WR data within 20% of the simulation values. In contrast, the excess entropy method predicts 97% of the data within 20% of the simulated tracer diffusivities.

Lastly, since the WR model is composed of (non-additive) hard particles, it represents another good test case for the mixture generalization of the Dzugutov scaling. Figure 4.8, however, clearly shows that this two-body scaling does not collapse the WR data. In general, particles of type i diffuse considerably faster than would be predicted based on the single-component HS fluid behavior and the i-component of the two-body excess entropy in the WR mixture. Moreover, the magnitude of the under prediction depends sensitively on composition. This breakdown of the mixture version of the Dzugutov relation for non-additive HS fluids indicates that it is not as widely applicable, even within the limited class of HS model fluids, as the generalized Rosenfeld scaling introduced here.

4.4.3 Single-component Gaussian-core fluid

As discussed in Section 4.1, and much more extensively in [50, 52, 2, 40], the properties of the single-component Gaussian-core fluid are anomalous compared to those of simple atomic liquids. For example, as shown in Figure 4.9a, the self diffusivity D of the Gaussian-core fluid first decreases, and then anomalously increases as a function of particle density along an isotherm. Likewise, $-s^{\text{ex}}$ at constant temperature first increases (the fluid becomes more structured), and then anomalously decreases (the fluid becomes less structured) as

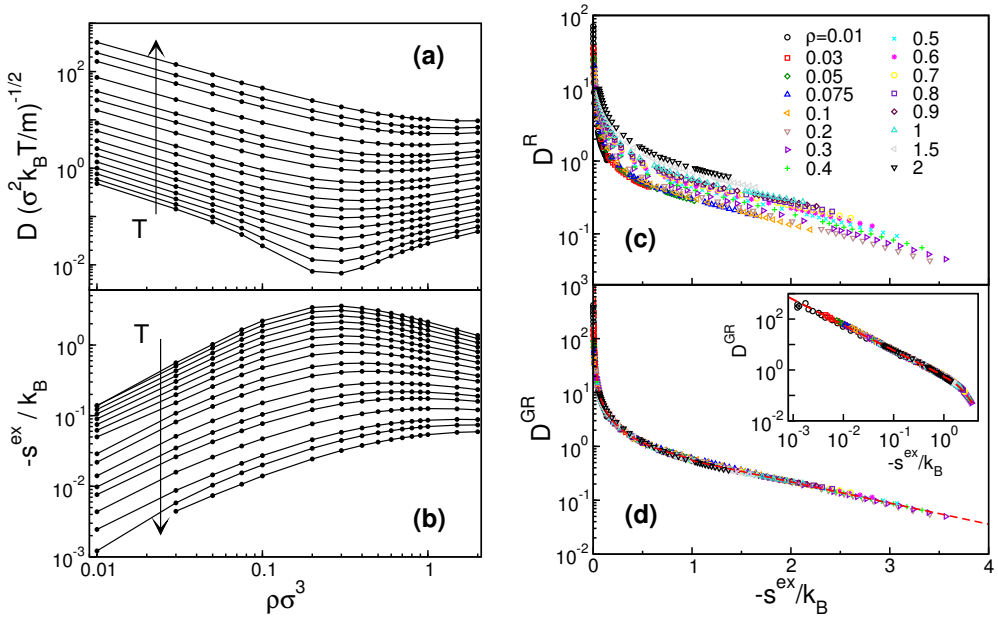

Figure 4.9: Properties of the single-component Gaussian-core fluid. (a) Self diffusivity D and (b) (negative) excess entropy $-s^{\mathrm{ex}}$ versus density ρ. (c) Self diffusivity reduced in the Rosenfeld form D^R and (d) the generalized Rosenfeld form D^{GR} as a function of $-s^{\mathrm{ex}}$. In (a) and (b), arrows indicate increasing temperature T. In (c) and (d), symbol type corresponds to density, indicated in the legend of (c). In (d), inset is the same as the main plot but on log-log scale. In (d), the red dashed line represents a least-square fit of the data to Eq. (4.15).

a function of density.

In brief, these unusual trends can be qualitatively rationalized based on the Gaussian form of the repulsion. When the density and temperature are sufficiently low, the distance between particles is larger than the range of the potential. Under these conditions, the part of the interaction that the particles sample when they "collide" appears steeply repulsive, and thus the effects of density on structure and dynamics are similar to those of HS fluid. However, at high particle densities, particles in the Gaussian-core fluid effectively overlap one another due to the bounded form of the interaction. The effect is that each particle constantly experiences largely canceling soft repulsive forces of many neighbors. Increasing the particle density under these conditions enhances this effect, paradoxically weakening the structural correlations and increasing the self diffusivity of the fluid.

It is clear from Figure 4.9a and b that both D and s^{ex} are strongly correlated for the Gaussian-core fluid. In Figure 4.9c, we show the self-diffusion coefficient expressed in the original Rosenfeld form, D^R, as a function of $-s^{\mathrm{ex}}$. As noted previously [2], this basic scaling is not even approximately a single-valued function of excess entropy. However, similar to the behavior of the HS and WR mixtures discussed previously, Figure 4.9d shows that the generalized-Rosenfeld-scaled self diffusivity D_i^{GR} collapses to a single curve when plotted versus excess entropy. The quality of the collapse at even low density is apparent in the log-log plot shown in the inset to Figure 4.9d. We also observe that the same functional form that was used to fit the single-component HS

data can also be applied to the Gaussian-core system. In particular, fitting the data to Eq. (4.15) yields $\alpha = 0.59$, $A = 1.33$, and $B = 0.90$. As shown in Figure 4.9d, Eq. (4.15) with these parameters (red dashed line) describes the simulation data very well.

4.4.4 Binary Gaussian-core mixtures

As a final test of the relationship between single-particle dynamics and excess entropy in soft-particle fluids, we examine the binary mixture of Gaussian-core particles described in Section 4.3. In particular, Figures 4.10a–b display the tracer diffusivities of the large and small Gaussian-core particles as a function of density for a variety of mixture compositions ($x_1 = 0.1$, 0.3, 0.5, 0.7, and 0.9) and reduced temperatures $k_{\mathrm{B}}T/\epsilon = 0.05$, 0.1, and 0.2. The first point of interest in the data, evident in Figure 4.10a, is that the tracer diffusivity of the larger type 1 particles displays the same anomalous trend as a function of density as the single component Gaussian-core fluid. That is, increasing the density eventually leads to an anomalous increase in D_1. However, over the density range considered here, the tracer diffusivity of the small type 2 particles does not show this anomalous trend (see Figure 4.10b). From a qualitative perspective, these different behaviors perhaps might be expected, since the larger particles begin to overlap more (and hence transition into anomalous, mean-field behavior) at lower densities than the smaller particles. This aspect of binary Gaussian-core mixtures in discussed in detail elsewhere [40].

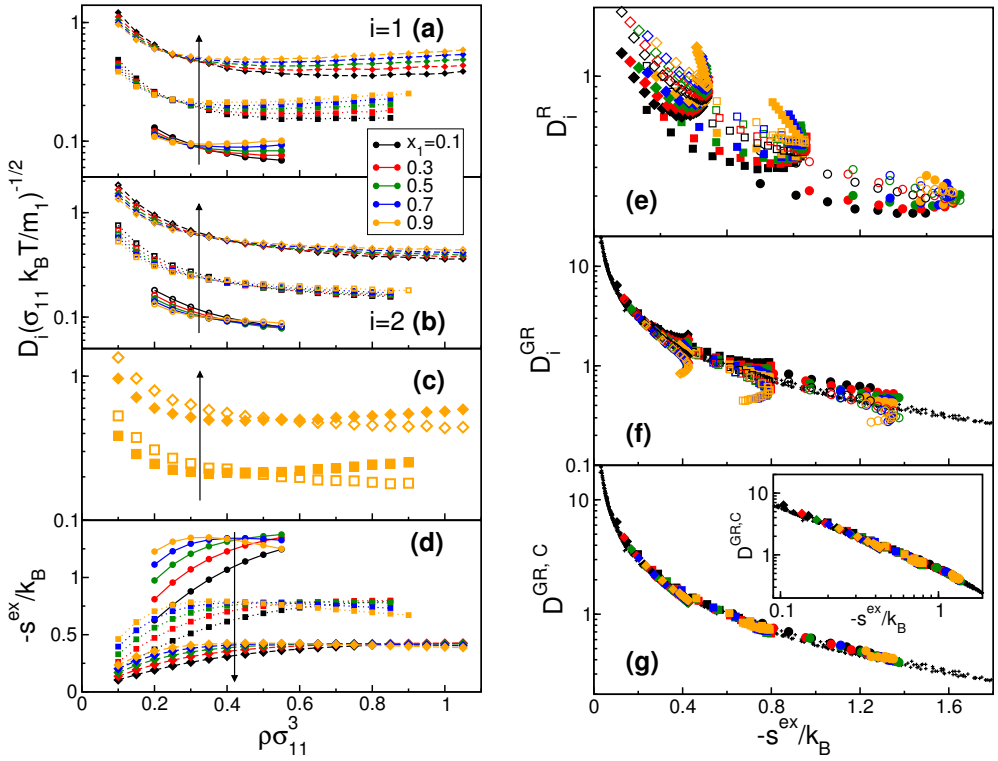

Figure 4.10: (color online) Properties of the binary Gaussian-core fluid described in the text. Tracer-diffusion coefficient of (a) component 1 and (b) component 2 versus density. (c) Illustration of the crossover in tracer diffusivity for components 1 and 2 as a function of density. (d) Excess-entropy $-s^{\rm ex}$ versus density. (e) Rosenfeld scaled tracer-diffusivity D_i^R, (f) generalized Rosenfeld tracer diffusivity $D_i^{\rm GR}$, and "collective" generalized Rosenfeld tracer diffusivity $D^{\rm GR,C} = (D_1^{\rm GR})^{x_1}(D_2^{\rm GR})^{x_2}$ versus $-s^{\rm ex}$. Symbol type corresponds to reduced temperature $k_{\rm B}T/\epsilon_{11}$: 0.05 (circles), 0.1 (squares), and 0.2 (diamonds). For clarity in (a)-(d), increasing temperature is given by the direction of the arrow.. In (a)-(f), closed and open symbols denote components 1 and 2, respectively. Panel (c) displays the crossover behavior of the tracer diffusivities for $x_1 = 0.9$ and $k_{\rm B}T/\epsilon_{11} = 0.05$ and 0.1. In panels (f) and (g), small black crosses represent the single-component Gaussian-core data. Inset to (g) is the same as the main plot but on a log-log scale.

One consequence of the dynamic decoupling of small and large particles described above is a crossover density for tracer diffusivity. Specifically, large particles have lower tracer diffusivity than small particles at low density, but they attain higher values of tracer diffusivity than small particles at sufficiently high density [see Figure 4.10c]. Because of this crossover, the Gaussian-core fluid mixture is an interesting counterexample to the fluids discussed thus far. It appears that both components cannot scale in a simple way with a single static measure like $-s^{\mathrm{ex}}$ [Figure 4.10d]. This is evident, when one considers how the reduced Rosenfeld [Figure 4.10d] and generalized Rosenfeld [Figure 4.10e] forms of tracer diffusivity behave as a function of $-s^{\mathrm{ex}}$. As before, the original Rosenfeld form, D_i^R, fails to collapse any of the data. The generalized Rosenfeld form, D_i^{GR}, does an excellent job of collapsing the low-density data, but necessarily breaks down at higher densities, where the anomalous behavior emerges.

We close our discussion of the binary Gaussian-core mixture with an interesting empirical observation. In the spirit of [21], we find that a collective tracer diffusivity of the mixture, which we define here as $D^{\mathrm{GR,C}} \equiv (D_1^{\mathrm{GR}})^{x_1}(D_2^{\mathrm{GR}})^{x_2}$, is still a single-valued of excess entropy over the wide range of temperature, density, and compositions investigated here [see Figure 4.10g]. As can be seen, it also quantitatively tracks the relationship between D^R and $-s^{\mathrm{ex}}$ for the single-component Gaussian-core fluid. What this implies is that tracer diffusivity of one component can be predicted based on knowledge of tracer diffusivity of the other component, the excess entropy of the mixture,

and the behavior of the one-component fluid. Of course, this observation also holds true (trivially) for the other mixtures we discussed earlier because the generalized Rosenfeld tracer diffusivities themselves are single-valued functions of s^{ex} of those systems.

4.5 Conclusions

In this work, we present a new dimensionless form of the tracer diffusion coefficient of a species which we call the generalized Rosenfeld tracer diffusivity. We show, via molecular simulation, that this quantity is approximately a single-valued function of excess entropy for a range of model one- and two-component fluid mixtures. The empirical excess entropy scaling is consistent with the various effects that composition, temperature, density, and microscopic interactions have on the equilibrium single-particle dynamics of these systems. Generalizing an earlier argument of Rosenfeld [6], we show that the functional form of the reduced tracer diffusivity can be obtained by examining the theoretical behavior of excess entropy and tracer diffusivity in the low-particle-density limit.

We demonstrate that the aforementioned "generalized Rosenfeld" scaling applies more broadly than other simple approaches such as Enksog theory or empirical scalings based on the pair-correlation contribution to the excess entropy. However, we also identify some important limitations of the approach. For example, the scaling breaks down for highly asymmetric hard-sphere mixtures (diameter ratios of 5 or larger) for packing fractions near the freezing

transition. It also breaks down for Gaussian-core mixtures, where the softness of the interactions combined with the size asymmetry gives rise to significant decoupling of the single-particle dynamics of the species. Interestingly, even in this latter case, we show that a single, collective measure of the tracer diffusivities obeys an excess entropy scaling, which provides a quantitative link between structure and the tracer diffusivities of the two components.

It may also be fruitful in future work to develop generalized Rosenfeld scalings for other transport coefficients, like thermal conductivity and shear viscosity. We plan to focus on extending the ideas of the present study to systems with other types of dynamics (e.g., including effects of dissipation, hydrodynamic interactions, etc.). We also are studying what aspects of interparticle interactions can give rise to decoupling of species-specific structural and dynamic quantities.

4.6 Author Contributions

The work in this chapter was originally published in 2009 [2]. Thomas M. Truskett designed the research, developed the virial scalings and helped write the document. William P. Krekelberg provided MD simulations of the Widom-Rowlinson fluid, analyzed data and wrote the core of the document. Gaurav Goel analyzed data and provided the calculation of the hard-sphere excess entropy through the BMCSL equation of state. Jeffrey R. Errington and Vincent K. Shen provided GC-TMMC simulations. Mark J. Pond provided MD simulations of the binary hard-sphere fluid and the binary Gaussian-core

fluid, analyzed data and contributed to writing the document.

Chapter 5

Generalizing Rosenfeld's excess-entropy scaling to predict long-time diffusivity in dense fluids of Brownian particles: From hard to ultrasoft interactions

5.1 Introduction

Dense suspensions of hard-sphere colloids have long served as useful experimental models for exploring how constraints of particle packing affect the properties of condensed phases.[145, 146, 147] Nonetheless, many technologically relevant suspensions contain high concentrations of "particles" (e.g., micelles, microgel colloids, dendrimers, or star polymers) which interact with one another through considerably softer *effective* potentials.[14, 47, 24] Such systems are of fundamental interest because they exhibit novel properties that cannot be readily understood in terms of concepts derived from idealized hard-particle systems like "excluded volume", "crowding", "collision rate", etc. Examples highlighted in theoretical and computer simulation studies include reentrant and cluster crystalline phases, [53, 148, 46, 149, 35, 150, 151, 152, 51, 153, 154] as well as anomalous dependencies of fluid-phase thermodynamic, [50, 155, 2, 42] structural, [156, 52, 2, 40, 157, 158, 159, 160] and dynamic [156, 50, 152, 52, 2, 40, 42, 158, 157, 160] properties on particle con-

centration.

To date, much of the theoretical work on these systems has been devoted to developing and testing statistical mechanical approaches for predicting their structural and thermodynamic behavior.[14, 161, 15, 162] However, some of the focus is beginning to shift toward predicting dynamics. For example, it has recently been shown that generalized Langevin theories[52, 163, 164] can qualitatively (but not yet quantitatively) predict the anomalous density dependence of the long-time self-diffusivity observed in Brownian dynamics simulations of the Gaussian-core model. Likewise, mode-coupling theory has been able to capture some of the non-monotonic dynamic trends displayed by fluids of particles that interact via star-polymer-like,[156] harmonic,[165] Hertzian,[160] or Gaussian-core [158, 166] pair potentials. Kinetic theory has also been used to gain insights into the nontrivial temperature- and density-dependent trends in the long-time molecular dynamics of particles with bounded, penetrable-sphere interactions.[167]

Another promising, albeit more heuristic, approach for predicting the dynamic properties of soft-particle fluids is a recently proposed generalization[42] of the excess-entropy scaling method of Rosenfeld.[5, 6] Here, excess entropy s^{ex} refers to the difference between the entropy per particle of the fluid and that of an ideal gas of particles with the same number density ρ. Excess entropy is a negative quantity, and its magnitude characterizes the extent to which static interparticle correlations – present due to interparticle interactions – reduce the number of microstates accessible to the fluid. The qualitative expectation,

corroborated by data from both computer simulations and experiments (see, e.g., refs. [6, 7, 122, 55, 10, 1, 11, 131]), is that changes to a fluid that strengthen its interparticle correlations also result in slower dynamic relaxation processes.

In the *generalized* Rosenfeld (GR) scaling approach,[42] information about interparticle interactions is used to recast the species' long-time tracer diffusivities as dimensionless (GR-reduced) combinations that are, by construction, single-valued functions of s^{ex} in the low ρ limit. For fluids of particles that interact solely via an inverse-power-law pair (IPL) repulsion, one can easily show that GR-reduced diffusivities remain single-valued functions of s^{ex} for all values of ρ and temperature T. Interestingly, Krekelberg et al. have further discovered that GR-reduced tracer diffusivities obtained from *molecular dynamics* simulations of more complex model systems – equilibrium fluid mixtures of (additive or non-additive) hard-sphere or Gaussian-core particles at different values of ρ, T, and composition – approximately follow a similar excess-entropy based scaling relation.[42] From a practical viewpoint, this means that knowledge of the interparticle interactions and the thermodynamic excess entropy for these model fluids allows one to predict key aspects of their long-time dynamic behavior.

Can the GR scaling method be extended to treat systems with different types of dynamics (e.g., with equations of motion that incorporate dynamic effects of "solvent" surrounding the particles)? In this work, we take a step toward addressing this question. Specifically, we present simulation data that tests whether the GR scaling method can be recast in a manner useful

for predicting long-time tracer diffusivities of suspended particles undergoing Brownian (i.e., overdamped Langevin) dynamics in the absence of interparticle hydrodynamic forces.

5.2 Methods and Definitions

The model fluids considered here comprise particles that interact via pair potentials $\mathcal{V}(r)$ of the IPL [$\mathcal{V}(r) = \epsilon(\sigma/r)^{\mu}$], Gaussian-core [$\mathcal{V}(r) = \epsilon \exp\{-(r/\sigma)^2\}$], and Hertzian [$\mathcal{V}(r) = \epsilon(1 - r/\sigma)^{5/2}$] forms. Here ϵ and σ represent characteristic energy and length scales of these interactions, respectively, and μ determines the "softness" of the IPL repulsion. As we discuss below, a key result from our study is that GR-reduced tracer diffusivities, sampled across a wide range of T and ρ for these models, approximately collapse onto a single curve when plotted versus s^{ex}. A consequence is that the tracer diffusivities of the ultrasoft Gaussian-core and Hertzian particle fluids, which display anomalous trends with increasing ρ,[52, 157] can be estimated (to within 20% relative error) – with no adjustable parameters– from knowledge of (1) the interparticle interactions, (2) the value of s^{ex} at the state point of interest, and (3) the GR scaling behavior of simpler IPL fluids.

For the case of Brownian dynamics considered here, it is convenient to express the GR-reduced long-time diffusivity as[42]

$$(1 - D/D_0)^{GR} \equiv (1 - D/D_0)\frac{B[1 - d\ln B/d\ln\beta]}{D_2}, \tag{5.1}$$

where B is the second virial coefficient, $\beta \equiv 1/k_{\mathrm{B}}T$, k_{B} is Boltzmann's con-

stant, and $D_2 = -(\partial[D/D_0]/\partial\rho)_T|_{\rho=0}$ quantifies how pair interactions at low particle concentration modify the tracer diffusivity D relative to the infinite dilution value D_0. As has been shown elsewhere,[42] $(1 - D/D_0)^{GR} = -s^{\mathrm{ex}}/k_{\mathrm{B}}$ for densities low enough that $\mathcal{O}(\rho^2)$ quantities can be neglected.

Based on eq. 5.1, it is evident that four quantities must be computed to test the GR excess-entropy scaling relation for state points across the T-ρ plane: B, D_2, D/D_0, and s^{ex}. The first two depend solely on β and $\mathcal{V}(r)$ and can be calculated from simple theoretical considerations. Specifically, B can be obtained by integrating the following expression numerically: $B = -(1/2)\int d\mathbf{r}\{\exp[-\beta\mathcal{V}(r)] - 1\}$. Likewise, D_2 can be computed via a one-dimensional numerical integration,

$$D_2 = \frac{2\pi}{3}\int_0^\infty \frac{d[\exp(-\beta\mathcal{V}(r))]}{dr} Q(r) r^2 \, dr \tag{5.2}$$

Eq. 5.2 is derived by the relaxation method, an approach outlined in detail elsewhere.[168, 169, 170, 171] The function $Q(r)$ is calculable from knowledge of $\mathcal{V}(r)$ via[1]

$$r^2\frac{d^2Q}{dr^2} + r\frac{dQ}{dr}\left[2 - r\frac{d(\beta\mathcal{V})}{dr}\right] - 2Q = r^2\frac{d(\beta\mathcal{V})}{dr} \tag{5.3}$$

The physical significance of $Q(r)$ is that it characterizes the extent to which application of a small external force $\mathbf{f}$ to a particle in the low-ρ fluid would distort its pair correlation function with its neighbors, $g(\mathbf{r}) = \exp[-\beta\mathcal{V}(r)]\{1+$

[1] In this work, we used the MATLAB function bvp4c to solve eq. 5.3

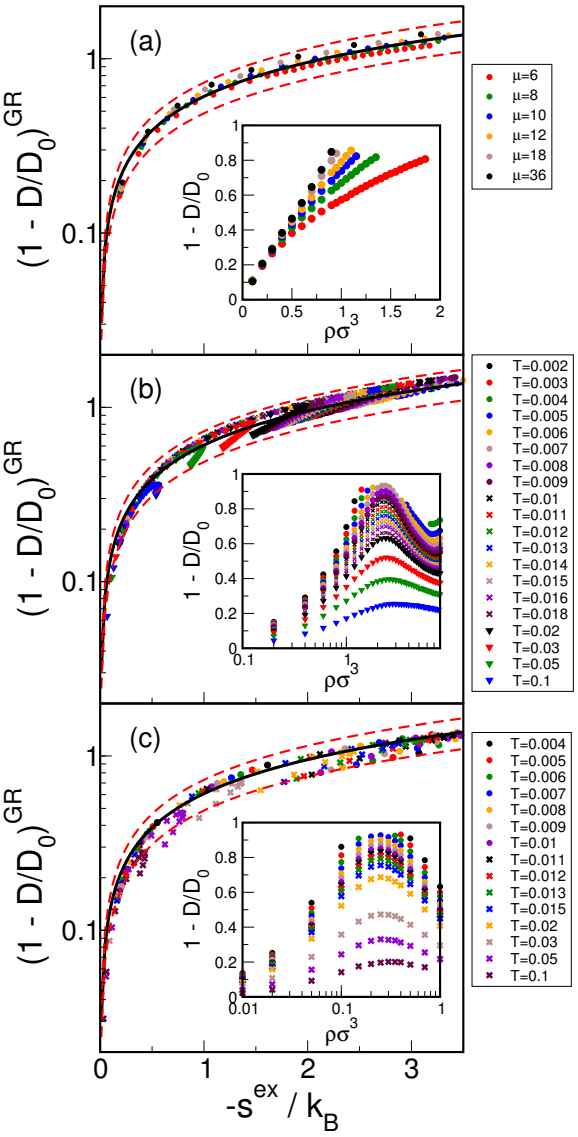

Figure 5.1: GR-reduced long-time diffusivity, $(1 - D/D_0)^{GR}$, versus negative excess entropy $-s^{\text{ex}}/k_B$ for (a) IPL, (b) Hertzian and (c) Gaussian-core fluids. The IPL fluids have exponents μ discussed in the text. The solid black curve is a least-squares fit to the IPL data from Figure 5.1a. The dashed red lines indicate a difference of 20% from the IPL fit. The insets show the reduced diffusivity change, $1 - D/D_0$, as a function of density, $\rho\sigma^3$.

$\beta Q(r)\mathbf{r}\cdot\mathbf{f}/2r\}$, and hence modify its effective mobility. One boundary condition on $Q(r)-$ valid for all $\mathcal{V}(r)$ considered here – is that the force-induced distortion of the pair correlation function must decay at large distances from the central particle, $Q(\infty) = 0$. The second boundary condition depends on the form of the short-range interparticle repulsion. For interactions studied previously with a hard-sphere repulsion at a separation $r = \sigma$,[168, 169, 170, 171] the following condition holds: $(dQ/dr)|_{r=\sigma} = -1$. We have verified that this condition also accurately describes the behavior of particles with softer IPL repulsions if it is applied at an effective hard-sphere "Boltzmann"[172] diameter $r = \sigma_{\mathrm{B}}$ defined by $\mathcal{V}(\sigma_{\mathrm{B}}) = 10k_{\mathrm{B}}T$. To our knowledge, this work is the first to consider D_2 for ultrasoft potentials like the Gaussian-core or Hertzian models that are bounded at zero interparticle separation. From eq. 5.3, it is apparent that the condition $Q(0) = 0$ applies for such models.

To compute D/D_0, we use Brownian dynamics simulations, where particle translations are governed by the Langevin equation, solved in the overdamped limit. The algorithm we employ, wherein the position $\mathbf{r}_i$ of each particle $i \in [1, N]$ updates at each time step according to $\mathbf{r}_i(t + \Delta t) = \mathbf{r}_i(t) - D_0\Delta t\nabla\sum_{j\neq i}^{N}\beta\mathcal{V}(r_{ij}(t)) + \Delta\mathbf{r}_i$, is detailed elsewhere. [36, 17] The quantity $\Delta\mathbf{r}_i$ denotes a random displacement due to solvent collisions; its magnitude is taken to be Gaussian-distributed with a mean of zero and a variance of $6D_0\Delta t$.

The Brownian dynamics simulations track N particles in a periodically-replicated cubic simulation cell whose volume V sets $\rho = N/V$. We use $N =$

1000, 2000, and 3000 particles for the IPL, Hertzian, and Gaussian-core fluids, respectively. Interparticle potentials were truncated at $r = 1.4\sigma$ - 3.9σ,[2] σ, and 3.71σ, respectively, for these systems. For simulations of the IPL fluids, we set $D_0 = 0.001(\sigma^2\epsilon/m)^{1/2}$ and the $\Delta t = 0.025\tau_B$, where $\tau_B \equiv mD_0/k_BT$ is a characteristic Brownian time scale. For simulations of Gaussian-core and Hertzian particle systems, we set $D_0 = 0.0001(\sigma^2\epsilon/m)^{1/2}$ and $\Delta t = 0.1\tau_B$. Long-time tracer diffusivities are computed from the mean-squared displacements via the Einstein relation, $D = \langle \Delta r^2 \rangle / 6t$ as $t \to \infty$.

We employ free-energy-based simulation techniques to evaluate s^{ex}. In the first step, we obtain the ρ dependence of the Helmholtz free energy at high T using grand canonical transition matrix Monte Carlo simulation. [103] In the second step, we perform a canonical temperature expanded ensemble simulation [105] with a transition matrix Monte Carlo algorithm [173] to evaluate the change in Helmholtz free energy with T at constant ρ. Collectively, these simulations provide values for excess Helmholtz free energy and excess energy, and hence s^{ex}, at a state point of interest. Interested readers can find additional details in our earlier papers. [111, 174]

5.3 Results and Discussion

We now examine the simulated behavior of six IPL fluids with exponents of μ = 6, 8, 10, 12, 18, and 36. Specifically, Figure 5.1a shows how

[2]The cutoff radius r_{cut} was determined by $\int_0^{r_{cut}} d\mathbf{r}\{\exp[-\mathcal{V}(r)/k_{\mathrm{B}}T] - 1\} = 0.99 \int_0^{\infty} d\mathbf{r}\{\exp[-\mathcal{V}(r)/k_{\mathrm{B}}T] - 1\}$

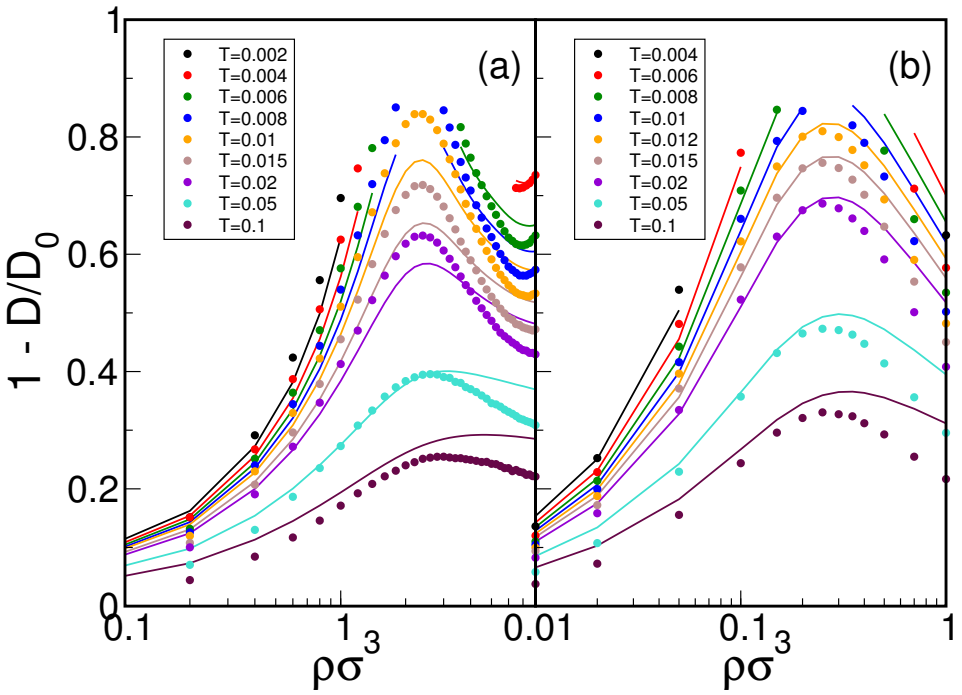

Figure 5.2: GR predictions (curves, discussed in text) and Brownian dynamics simulation data (symbols) for long-time diffusivity of the (a)Hertzian and (b) Gaussian-core fluids as a function of density $\rho\sigma^3$.

$(1 - D/D_0)$ and its GR-reduced counterpart $(1 - D/D_0)^{GR}$ vary with density $\rho\sigma^3$ and $-s^{\mathrm{ex}}/k_{\mathrm{B}}$, respectively, for these fluids at $T = \epsilon/k_{\mathrm{B}}$. As should be expected, systems with softer interparticle repulsions (i.e., lower μ) display considerably faster single-particle dynamics at a given $\rho\sigma^3$. For example, the $\mu = 6$ fluid must realize a density twice that of the $\mu = 36$ fluid for both systems to exhibit $D/D_0 = 0.2$. In contrast, $(1 - D/D_0)^{GR}$ for these fluids shows only minor systematic variation when plotted versus $-s^{\mathrm{ex}}/k_{\mathrm{B}}$, with less than 20% difference between the $\mu = 6$ and $\mu = 36$ values.

To put to the GR scaling relationship for Brownian dynamics to a more stringent test, we further analyze the behaviors of model fluids with ultrasoft Hertzian and Gaussian-core interactions (see Figures 5.1b and 5.1c, respectively). In particular, we explore a broad range of $\rho\sigma^3$ for these two systems along isotherms spanning from the moderately supercooled liquid ($T \leq 0.004\epsilon/k_{\mathrm{B}}$) to temperatures high enough ($T \geq 0.01\epsilon/k_{\mathrm{B}}$) for the models to exhibit mean-field-like behavior.[157, 53, 47, 14] Note that this data set includes state points for which D/D_0 increases with increasing $\rho\sigma^3$ in both systems, behavior that is anomalous when compared to the trends exhibited by simpler atomic and colloidal fluids. The main conclusion to be drawn from Figures 5.1b and 5.1c is that, despite the anomalous relationship between single-particle dynamics and ρ in these systems, the GR excess entropy scaling relation looks strikingly similar to the quasi-universal form of the IPL fluids. In fact, the Hertzian and Gaussian-core data deviate by less than 20% from the least-squares fit to the $(1 - D/D_0)^{GR}$ versus s^{ex} data from Figure 5.1a.

5.4 Conculusions

One consequence of this quasi-universal scaling behavior is that one can estimate Brownian dynamics D/D_0 data, *even for nontrivial systems with ultrasoft potentials*, simply from knowledge of their interparticle interactions, the excess entropy, and, e.g., a least-squares fit of the IPL data of Figure 5.1a. Figure 5.2 illustrates the quality of the predictions made by this approach for the Hertzian and Gaussian-core model fluids. As can be seen – with no adjustable parameters – the estimated values of diffusivity are accurate for low-to-moderate ρ, and remain qualitatively reliable for higher ρ where the anomalous trends emerge. Collectively, these results illustrate a strong apparent link between static interparticle correlations and long-time dynamics for model fluids with either hard or ultrasoft interactions.

Finally, whether the approach outlined here can provide an accurate estimate to the "thermodynamic" component of diffusivity for systems which also have strong hydrodynamic interparticle contributions to dynamics is an open question which deserves attention in future studies. Furthermore, it will be interesting to test whether the GR scaling for diffusivity in Brownian dynamics also holds for systems with more complex interparticle interactions (e.g., with more than one characteristic length scale).

5.5 Author Contributions

The work in this chapter was originally published in 2011 [43]. Thomas M. Truskett designed the research and helped write the document. Jeffrey R.

Errington provided Monte Carlo simulations to determine the excess entropy. Mark J. Pond provided Brownian dynamics simulations, analyzed data and wrote the core of the document.

Chapter 6

Mapping between long-time molecular and Brownian dynamics

6.1 Introduction

Computer simulations and statistical mechanical theories have long served as invaluable tools for understanding relaxation processes that occur in fluid systems that range from molecular liquids to complex suspensions of Brownian particles. [14] Depending on the resolution of the interparticle interactions used to model these systems, some descriptions of the microscopic dynamics are more appropriate to adopt than others. Simplistically, Newtonian (i.e., classical molecular) dynamics (MD) is suitable when the particles of interest are described by force fields with molecular-scale resolution. Modeling the motion of suspended Brownian particles, on the other hand, typically calls for coarser interparticle forces and dynamics that approximately account for the effects of the solvent. [13, 36, 37, 38, 39]

Although the short-time behavior of a given model depends sensitively on its microscopic dynamics,[175] there is evidence that under certain conditions–e.g., dense fluids near the glass transition–the qualitative long-time behavior is largely independent of those details.[176, 177] With this in mind, it

is perhaps not surprising that researchers often select the type of microscopic dynamics to use in simulations based on other considerations, such as computational efficiency. A common example is adopting classical MD to explore the long-time dynamic behavior of model complex fluids with coarse, effective interactions, ignoring the kinetic role of the implicit "fast" degrees of freedom, e.g, solvent.[54, 178, 31, 50, 153, 2, 157, 40, 160] Although the qualitative trends provided by these MD simulations have been valuable, there is still the question of how to map between the long-time MD data of such simulations and that which would have been produced assuming a different type of microscopic dynamics.

Here, we take a first step toward addressing this issue. Specifically, we present computer simulation results that test a simple heuristic approach for mapping between long-time self-diffusion coefficients obtained from Newtonian and Brownian (i.e., overdamped Langevin) dynamics (BD). The method follows from a seemingly naive hypothesis that "what matters" in such a mapping can be deduced from the behavior of a fluid of particles that interact via an inverse-power-law (IPL) pair potential [$\mathcal{V}(x) = \epsilon x^{-\mu}$], where $x = r/\sigma$, r is the interparticle separation, ϵ and σ represent characteristic energy and length scales of the interaction, and μ determines the steepness of the IPL repulsion. The IPL model is a natural reference system for dense atomic or colloidal fluids, whose static and dynamic properties are dominated by the repulsive part of their interactions. Furthermore, one can show[5, 130, 131] that a one-to-one relation must exist between the following dimensionless representations of the

long-time diffusivities of an IPL fluid associated with the two types of dynamics: $D_{\rm MD}\rho^{1/3}\sqrt{m/k_{\rm B}T}$ and $D_{\rm BD}/D_0$. Here, ρ is the number density, m is the particle mass, $k_{\rm B}$ is the Boltzmann constant, and T is temperature. $D_{\rm MD}$ ($D_{\rm BD}$) represents the long-time self diffusivity obtained from MD (BD) trajectories, respectively, and D_0 is the value of $D_{\rm BD}$ in the dilute ($\rho \to 0$) limit. Based on previous work,[6, 179, 43] it is clear that the relationship between $D_{\rm MD}\rho^{1/3}\sqrt{m/k_{\rm B}T}$ and $D_{\rm BD}/D_0$ for IPL fluids is approximately independent of μ for $\mu > 4$. Hence, a more precise statement of our aforementioned hypothesis is that the quasi-universal IPL mapping relationship can also be used to estimate $D_{\rm MD}$ from $D_{\rm BD}$ (or vice versa) for other types of fluids, perhaps including those with very different types of interactions and physical properties.

6.2 Methods

To test this hypothesis, we carry out MD and BD simulations that probe the long-time dynamics of fluids of particles that interact via IPL potentials with $\mu = 8$, 10, 12, 18, and 36. We also explore the behavior of fluids with particles interacting via ultrasoft Gaussian-core[53] [$\mathcal{V}(x) = \epsilon \exp\{-x^2\}$], Hertzian[157] [$\mathcal{V}(x) = \epsilon(1-x)^{5/2}$], and effective star-polymer[180] [$\mathcal{V}(x) = A\{-\ln x + B\}$ for $x < 1$, and $\mathcal{V}(x) = ABx^{-1}\exp\{(B^{-1}-1)(1-x)\}$ for $x \geq 1$] potentials. Here, $B = f^{1/2}/2$, $A = (20/9)k_{\rm B}T(B^{-1}-1)^3$, and f is the star polymer arm number. The latter three model systems have received considerable attention recently in the theoretical soft matter literature,[14, 156, 157] and represent stringent test cases for our approach (and others) due to their

distinctive dynamical trends; e.g., each exhibits a wide range of conditions where self diffusivity anomalously increases with *increasing* particle density, as opposed to the behavior of IPL fluids. The MD and BD simulations that we present here cover much of the computationally accessible phase space of these model fluids, including both equilibrium and moderately supercooled conditions ($\sim 10^3$ state points in total). As we show below, a potentially useful outcome of our analysis of this extensive data set is an empirical analytical equation that semi-quantitatively relates D_{MD} and D_{BD} for these systems.

The MD simulations of our study generate dynamic trajectories by solving Newton's equation of motion using the velocity-Verlet algorithm in the microcanonical ensemble.[17] For IPL, Hertzian, and star-polymer fluids, they contain N particles ($N = 1000$, 4000, and 4000, respectively) and use integration time steps of $0.00005\sqrt{m\sigma^2/\epsilon}$, $0.01\sqrt{m\sigma^2/\epsilon}$, and $0.001\ \sqrt{m\sigma^2/k_{\mathrm{B}}T}$, respectively. The BD simulations presented here generate trajectories by solving the Langevin equation in the high-friction limit using the conventional Brownian (Ermak) algorithm.[17, 36] For the star-polymer fluid, they contain $N = 4000$ particles, and use a time step of $\Delta t = 0.1\tau_B$, where $\tau_B = mD_0/k_{\mathrm{B}}T$ and $D_0 = 0.001\sqrt{\sigma^2 k_{\mathrm{B}}T/m}$. All simulations use a periodically replicated cubic cell with reduced volume V/σ^3 determined by the number density $\rho\sigma^3 = N\sigma^3/V$ of interest. For the IPL, Hertzian, and star-polymer systems, the pair potentials are truncated at $r_{cut} = 1.4 - 3.9\sigma$ (depending on μ)[43], 1σ, and 3.6σ respectively. Long-time tracer diffusivities from both MD and BD simulation trajectories are computed from the average mean-squared

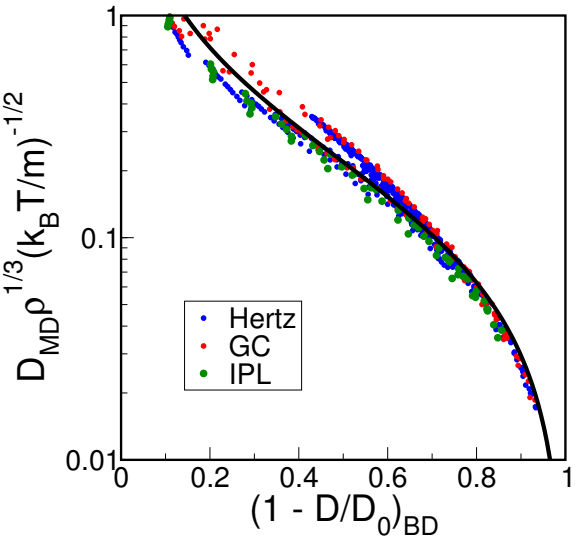

Figure 6.1: Reduced long-time diffusivity from MD simulations $D\rho^{1/3}(k_{\rm B}T/m)^{-1/2}$ versus the fractional reduction in the long-time diffusivity from BD simulations (relative to the dilute value), $(1 - D/D_0)_{\rm BD}$. The blue circles correspond to the Hertzian fluid at temperatures ranging from $0.002 - 0.02\ \epsilon/k_{\rm B}$ and densities that range from $0.2 - 8.0\ \sigma^{-3}$. The red circles correspond to the Gaussian-core fluid at temperatures ranging from $0.004 - 0.2\ \epsilon/k_{\rm B}$ and densities that range from $0.01 - 1.0\ \sigma^{-3}$. The green circles correspond to IPL fluids with exponents, μ, ranging from 8 to 36 and values of the parameter $\rho\sigma^3(\epsilon/k_{\rm B}T)^{3/\mu}$ that span the respective equilibrium fluid phases. The curve is a least-squares fit to the data for the three systems, and is given by eq. 6.1 with $c_1 = 3.3176$ and $c_2 = 2.6645$.

particle displacements via the Einstein relation. For the analysis presented below, we also include some previously reported MD simulation data[2] for the Gaussian-core fluid and BD simulation data[43] for the IPL, Gaussian-core, and Hertzian fluids. The methods used in those studies are the same as those described above, and the required simulation parameters can be found in the original papers.

6.3 Results and Discussion

6.3.1 Constructing and fitting an expression

Before examining the simulation data of the various model fluids discussed above, we first consider what should generally be expected about the relationship between the dimensionless diffusivities, D_{BD}/D_0 and $D_{\mathrm{RMD}} \equiv D_{\mathrm{MD}}\rho^{1/3}\sqrt{m/k_{\mathrm{B}}T}$. For example, to leading order in ρ, we know that $1 - D_{\mathrm{BD}}/D_0 \propto \rho$ and $D_{\mathrm{MD}}^{-1} \propto \rho$, which together imply that $1 - D_{\mathrm{BD}}/D_0 \propto D_{\mathrm{RMD}}^{3/2}$ in this limit. Furthermore, there is also evidence[176, 177] suggesting that $D_{\mathrm{BD}} \propto D_{\mathrm{MD}}$ for supercooled liquids near the glass transition (D_{MD}, $D_{\mathrm{BD}} \to 0$). Since D_{MD} necessarily shows pronounced variations with small changes in ρ or T under these latter conditions, we also have $D_{\mathrm{BD}}/D_0 \propto D_{\mathrm{RMD}}$. The following expression,

$$(1 - D/D_0)_{\mathrm{BD}} = (1 + c_1 D_{\mathrm{RMD}} + c_2 D_{\mathrm{RMD}}^{3/2})^{-1}, \tag{6.1}$$

is an example of a simple heuristic functional form that interpolates between the aforementioned characteristic "fast" and "slow" limiting behaviors. Below, we examine how well eq. 6.1 can describe the simulation data for a variety of fluids comprising hard to ultrasoft particles if c_1 and c_2 are treated as constants.

Computer simulation data of D_{RMD} plotted versus $1 - D_{\mathrm{BD}}/D_0$ for the IPL, Gaussian-core, and Hertzian fluids are presented in Fig. 6.1. The data span the $k_{\mathrm{B}}T/\epsilon - \rho\sigma^3$ plane (details in the caption), characterizing the relationship between MD and BD long-time diffusivities for these fluids in their equilibrium and moderately supercooled states. Also presented in Fig. 6.1 is a least-squares fit of the data using the form provided by eq. 6.1. As can be

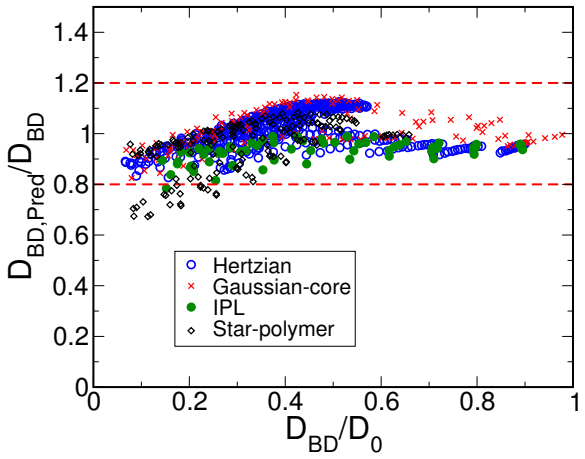

Figure 6.2: Ratio of long-time BD diffusivity estimated from eq. 6.1 in the text, $D_{\mathrm{BD,Pred}}$, to that obtained from simulation, D_{BD}, plotted as a function of D_{BD}/D_0. The Hertzian, Gaussian-core, IPL and star-polymer fluids are represented by open blue circles, red crosses, filled green circles and open black diamonds, respectively. The dashed red lines represent a 20% deviation of the predicted diffusivity from the value measured in simulation.

seen–despite the distinctive non-monotonic dynamic trends of the Gaussian-core and Hertzian fluids as a function of density[50, 52, 2, 52, 157, 42, 43] –the data qualitatively behave as the equation predicts. In fact, as is illustrated in Fig. 6.2, more than 98% of the simulation data for D_{BD} for each of these model fluids are within 20% of the eq. 6.1 estimation based on the simulated D_{MD}. Furthermore, to the extent that the data Fig. 6.1 reflects quasi-universal behavior, it suggests that the well-known, empirical dynamic freezing criterion for colloidal fluids ($D_{\mathrm{BD}}/D_0 \approx 0.1$),[181] has an analog in atomic systems ($D_{\mathrm{RMD}} \approx .03$).

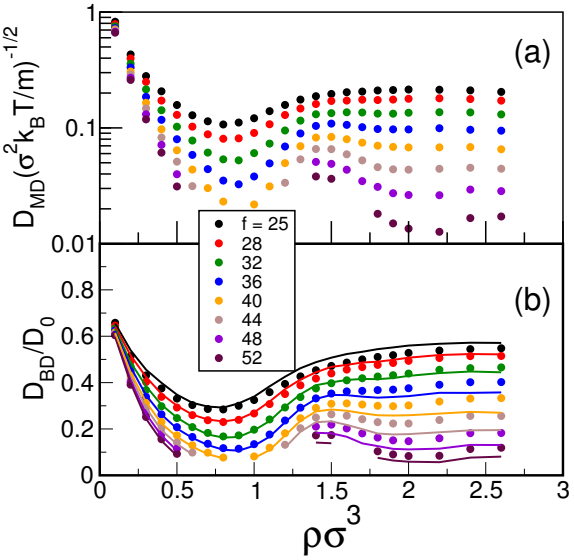

Figure 6.3: Reduced long-time self diffusivity $[D_{\mathrm{MD}}(\sigma^2 k_{\mathrm{B}}T/m)^{-1/2}$ and $D_{\mathrm{BD}}/D_0]$ for the star-polymer fluid plotted versus reduced density $\rho\sigma^3$ from MD and BD simulations, respectively Fluids of stars with different arm numbers ranging from $f = 25 - 52$ (top to bottom) and reduced densities $\rho\sigma^3 = 0 - 2.6$ are shown. (a) Results from MD simulations. (b) Results from BD simulations (symbols) and estimates (curves) based on simply substituting the D_{MD} data of panel (a) into eq. 6.1 with constants given in the caption of Fig 6.1.

6.3.2 Predicting dynamics of the star-polymer fluid

As an illustration of how eq. 6.1 might be further used, we consider the star-polymer fluid[180] mentioned above. The soft, logarithmic repulsive interactions of this model are known to produce highly non-monotonic dynamic trends; e.g., diffusivity show two minima as a function of $\rho\sigma^3$ (see Fig. 6.3 of this paper and Fig. 1 of Foffi et al. [156]). When a model fluid displays such nontrivial behavior with one type of microscopic dynamics (e.g., MD), it is not

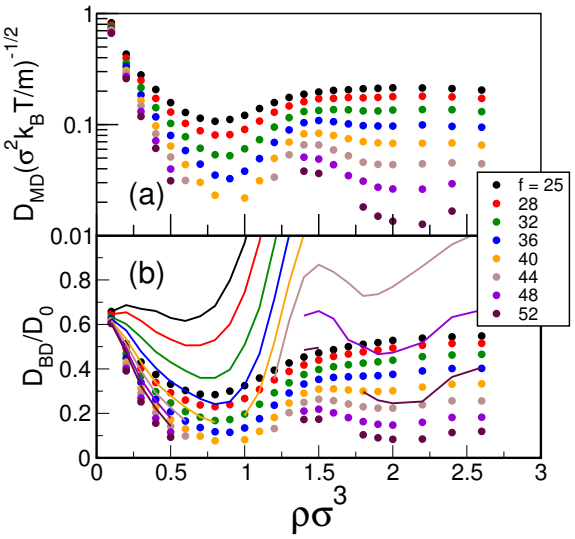

Figure 6.4: Long-time diffusivity of the star-polymer system from MD and BD simulations. Symbols are the same as in Fig. 6.3. Curves in panel (b) show prediction based on $D_{\rm BD}/D_0 = (D_{\rm MD}) / ([\rho D]_0 / \rho)$, where $[\rho D]_0 = \lim_{\rho \to 0} \rho D_{\rm MD}$ [4].

obvious a priori whether the trends will necessarily be reflected when another type (e.g., BD) is employed. In fact, an earlier investigation of this system[156] made a point to report dynamic results from both types of simulations. What Fig. 6.3b illustrates that is that one can, to a very good approximation, predict $D_{\rm BD}/D_0$ for this system by simply substituting its $D_{\rm MD}$ data of panel Fig. 6.3a into eq. 6.1 with no adjustable parameters (i.e., using c_1 and c_2 from data in Fig. 1). As is illustrated in Fig. 6.2, the predicted values for 88% of the state points are within 20% of the simulation results.

We are not aware of another mapping approach that can make predictions of similar accuracy for both hard and ultrasoft particle fluids. One alter-

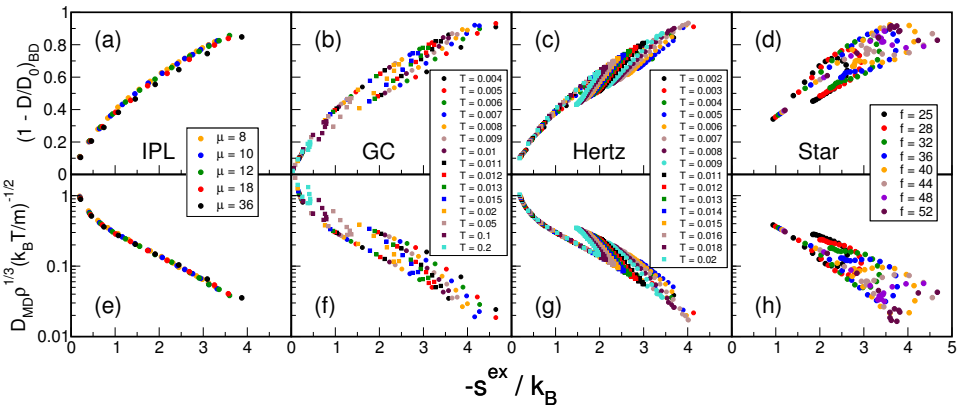

Figure 6.5: Fractional reduction in the long-time diffusivity from BD simulations (relative to the dilute value), $(1 - D/D_0)_{\rm BD}$ [panels (a)-(d)], and reduced long-time diffusivity from MD simulations $D\rho^{1/3}(k_{\rm B}T/m)^{-1/2}$ [panels (e)-(h)], plotted versus negative excess entropy per particle, $-s^{\rm ex}/k_{\rm B}$. Dynamic data corresponds to that of Fig. 6.1 and 6.3, and $-s^{\rm ex}$ data were computed via the free-energy-based simulation techniques discussed in the text.

native strategy,[182, 183, 184, 4] hypothesizes that $\rho D_{\rm MD}/[\rho D]_0 = D_{\rm BD}/D_0$, where $[\rho D]_0 = \lim_{\rho\to 0}\{\rho D_{\rm MD}\}$. Although this relationship approximately holds for simple fluids with steep repulsions (the so-called hard-sphere dynamic universality class),[4] we show that it breaks down qualitatively for fluids with ultrasoft interactions. Specifically, Fig. 6.4 illustrates that predictions based on this hypothesis for the star-polymer system are generally very inaccurate–except for a narrow region of phase space with extremely low $\rho\sigma^3$ and high f–where particle overlaps are avoided.

6.3.3 Implications for structure-dynamics relationships

Note that a quantitative link between D_{RMD} and D_{BD}/D_0 is easy to establish for models where both can be expressed as single-valued functions of the same static quantity. For example, one can show[131] that, for an IPL fluid, D_{RMD} and D_{BD}/D_0 are strictly single-valued functions of excess entropy (relative to ideal gas), s^{ex}. In fact, the same is approximately true for other simple liquids that are "strongly correlating" and mimic a variety of static and dynamic properties of IPL systems.[131]

Do Gaussian-core, Hertzian, and star-polymer fluids show excess-entropy scaling behaviors similar to the IPL fluids? To check this, we compute s^{ex} for these models using free-energy-based simulation methods. Specifically, we determine the density dependence of the Helmholtz free energy at high temperature using grand canonical transition-matrix Monte Carlo simulation.[103] We then carry out canonical temperature-expanded ensemble simulations[105] with a transition-matrix Monte Carlo algorithm[173] to calculate the change in Helmholtz free energy with temperature at constant density. Together, these simulations provide the excess Helmholtz free energy and excess energy, and hence s^{ex}. Additional details on these simulations can be found elsewhere.[111, 41]

The excess entropy scaling behaviors of $1 - D_{\mathrm{BD}}/D_0$ and D_{RMD} are plotted in Fig. 6.5 for all model fluids and state points shown in Fig. 6.1 and 6.3. The main point is that, in stark contrast to the behavior of the IPL fluids, $1 - D_{\mathrm{BD}}/D_0$ and D_{RMD} of the ultrasoft fluids are not (even approximately) single-

valued functions of s^{ex}. Hence, the success of the IPL-motivated mapping strategy between MD and BD diffusivities reported here cannot be explained by appealing to arguments about strongly-correlating fluids.

6.4 Author Contributions

The work in this chapter was in preparation for publication at the time of the submission of the dissertation[44]. Thomas M. Truskett designed the research and helped write the document. Jeffrey R. Errington provided GC-TMMC simulations and offered commentary on the construction of the document. Mark J. Pond provided MD and BD simulations, designed the fitting equation, analyzed data and wrote the core of the document.

Chapter 7

Future work

7.1 Translational order parameter scalings

The research into structure and dynamics relationships in this dissertation have been focused on finding excess-entropy-based correlations. However, there is no definitive reason for excess entropy to be the optimal structural order metric for scaling. One easily approachable alternative to excess-entropy based scalings would be to compare non-dimensionalized dynamics to the translational order parameter, τ. For mixtures, τ is defined as

$$\tau = y_c^{-1} \sum_i \sum_j x_i x_j \int_0^{y_c} |g_{ij}(y) - 1| dy \tag{7.1}$$

where $y = r\rho^{1/3}$ and y_c is a cut-off value (we chose $y_c = 4$).[60, 102]

In our preliminary investigations, τ has similar correlations with non-dimensionalized diffusivity as $s^{(2)}$ does – as seen in Figure 7.1. This is intuitive because they are similar integrals of the radial distribution function. To compare how well the different structural order metrics correlate with dynamics, we can fit a one-to-one function between a structural order metric and non-dimensionalized dynamics. From this fit, we can evaluate the function at a value of the structural order metric and see how well it correlates with dynamics measured in simulations. To the eye, an evaluation of a single-valued

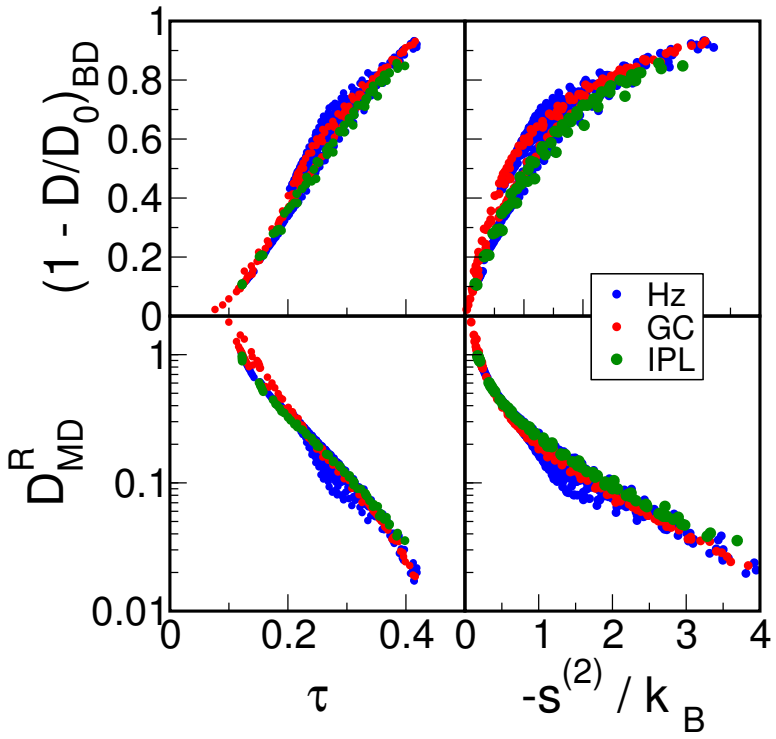

Figure 7.1: Brownian dynamics diffusivity, $(1 - D/D_0)_{\mathrm{BD}}$ (top), and Rosenfeld-scaled molecular dynamics diffusivity, $D^R = D\rho^{1/3}(k_{\mathrm{B}}T/m)^{-1/2}$ (bottom), as a function of the translational order parameter, τ (left), and two-body excess entropy, $s^{(2)}$ (right). The blue circles correspond to the Hertzian sphere fluid at temperatures ranging from 0.002 $k_{\mathrm{B}}T/\epsilon$ to 0.02 $k_{\mathrm{B}}T/\epsilon$ and densities that range from 0.2 to 8.0 particles per σ^3. The red circles correspond to the Gaussian-core fluid at temperatures ranging from 0.004 $k_{\mathrm{B}}T/\epsilon$ to 0.2 $k_{\mathrm{B}}T/\epsilon$ and densities that range from 0.01 to 1.0 particles per σ^3. The green circles correspond to inverse power law fluids with exponents, μ, ranging from 8 to 36 and densities that approach the freezing transition for each individual exponent.

scaling fit of τ to the dynamic data would be closer to the behavior measured in the simulations than a function based on $s^{(2)}$ would. The preliminary investigations show promise as a fertile research ground to start a study on new structural order metrics to correlate with dynamics.

7.2 Continuation of polydispersity studies

In Chapter 3, we addressed the problems with taking an effective one-component picture of a polydisperse mixture. We did this by analyzing a continuously polydisperse sample exactly in the dilute limit and as a 60-component fluid at finite densities. The success of this study brings forth new questions. The most obvious question is how finely binned would a polydisperse fluid need to be to reproduce the exact fluid behavior? We have demonstrated that a one-component description is inadequate and a 60-component description seems sufficient. If we vary the number of effective components, how quickly will we approach each extreme? This could be useful for looking at descriptions of polydisperse fluids through confocal microscopy, where the amount of data collected is already pushing the current limits of sampling for a one-component fluid. Could we get better information through a coarse binning of effective components?

7.3 Continuous approximation to the SW-SRA fluid

The correlations in Chapters 2, 4, 5 and 6 were developed by analyzing fluids with repulsive interparticle potentials. In order to expand this to a fluid

that has a large role of attractions in its structural and dynamic behavior, we examined a continuously-varying approximation to the square-well short-ranged-attractive fluid studied in Chapter 3:

$$\mathcal{V}_{ij}(r) = \begin{cases} \infty & r_{ij} \leq (1-\lambda)\sigma_{ij} \\ \epsilon\left(r_{\text{eff}}^{-36} + \frac{1}{2}\left(\tanh\left(20\left(r_{\text{eff}} - 2\right)\right) - 1\right)\right) & r_{ij} > (1-\lambda)\sigma_{ij} \end{cases} \tag{7.2}$$

where $r_{\text{eff}} \equiv \left(\left(r_{ij}/\sigma_{ij}\right) - (1-\lambda)\right)/\lambda$. We chose $\lambda = 0.05$ to be the width of the attractive well. These parameters generated a system that demonstrated an attractions-dominated regime of the fluid's structuring and dynamics. We studied this system through molecular dynamics simulations, Brownian dynamics simulations and Monte Carlo simulations to gather the phase-space behavior of this fluid.

Unfortunately, we were not able to construct a coherent and consistent narrative tying the structure and dynamics of this fluid with an attractive regime. However, since we have collected a wide range of raw dynamic an structural information about this system, it would be an excellent place to start new research on connections between structure and dynamics in fluids dominated by attractions.

Appendix

Appendix 1

Exact results for polydisperse short-ranged square-well fluid at low particle density

In the limit of low particle density ($\rho \to 0$), some implications of adopting the effective one-component description can be worked out analytically for a continuously polydisperse SW fluid with pair interaction $\mathcal{V}_{ij}(r)$,

$$\mathcal{V}_{ij}(r) = \begin{cases} \infty & r \leq \sigma_{ij} \\ -\epsilon & \sigma_{ij} < r \leq (1+\lambda)\sigma_{ij} \\ 0 & r > (1+\lambda)\sigma_{ij} \end{cases} \tag{1.1}$$

and a Gaussian distribution of particle diameters with mean σ and variance $\upsilon^2\sigma^2$, i.e., $p(\sigma_i) = (2\pi\upsilon^2\sigma^2)^{-1/2}\exp[-(\sigma_i-\sigma)^2/2\upsilon^2\sigma^2]$. Note that, for this system, the probability distribution for the interaction diameter, $f(\sigma_{ij})$ is also a Gaussian with mean σ and variance $\nu^2\sigma^2/2$. In the low density limit, the PRDFs are known exactly, i.e.,

$$g_{ij}(r) = \begin{cases} 0 & r \leq \sigma_{ij} \\ e^{\epsilon/k_{\mathrm{B}}T} & \sigma_{ij} < r \leq (1+\lambda)\sigma_{ij} \\ 1 & r > (1+\lambda)\sigma_{ij} \end{cases} \tag{1.2}$$

Substituting eq. 1.2 into the continuous polydispersity limit of eq. 3.5, $-s^{(2)}/k_{\mathrm{B}} = (\rho/2)\int d\sigma_{ij} f(\sigma_{ij}) \int d\mathbf{r}[g_{ij}(r)\ln g_{ij}(r) - g_{ij}(r) + 1]$, noting that $\langle\sigma_{ij}^3\rangle = \sigma^3(1 + 3\nu^2/2)$, and evaluating yields

$$-\frac{s^{(2)}}{k_{\mathrm{B}}\rho\sigma^3} = \frac{2\pi}{3}\left\{1+\frac{3\nu^2}{2}\right\}\left\{1+\left[(1+\lambda)^3-1\right]\left[e^{\epsilon/k_{\mathrm{B}}T}\left(\frac{\epsilon}{k_{\mathrm{B}}T}-1\right)+1\right]\right\} \tag{1.3}$$

The right-hand-side of eq. 1.3 is equal to $B/\sigma^3 + [d(B/\sigma^3)/d\ln T]$, where B is the second virial coefficient of the fluid. Thus, to leading order in density, we also have $s^{(2)} = s^{\text{ex}}$, as expected. Likewise, substituting eq. 1.2 into the continuous polydispersity limit of eq. 3.7, $\tau = y_c^{-1} \int d\sigma_{ij} f(\sigma_{ij}) \int_0^{y_c} dy |g_{ij}(y) - 1|$, and evaluating gives the following expression

$$\frac{\tau}{\rho^{1/3}\sigma} = \frac{1}{y_c} \left\{ 1 + \lambda \left(e^{\epsilon/k_{\text{B}}T} - 1 \right) \right\} \tag{1.4}$$

As can readily be seen, the right-hand sides of both eq. 1.3 and 1.4 are monotonically increasing functions of $\epsilon/k_{\text{B}}T$. In other words, no structural anomalies appear in the dilute SW fluid according to the exact, multicomponent analysis.

The effective one-component radial distribution $g_{\text{eff}}(r) = \int d\sigma_{ij} f(\sigma_{ij}) g_{ij}(r)$ can also be obtained from knowledge $f(\sigma_{ij})$ and $g_{ij}(r)$ of eq. 1.2; it is given by

$$g_{\text{eff}}(r) = \frac{1}{2} \left[1 + \left(1 - e^{\epsilon/k_{\text{B}}T} \right) \text{erf} \left\{ \frac{r/\sigma - (1+\lambda)}{v(1+\lambda)} \right\} + e^{\epsilon/k_{\text{B}}T} \text{erf} \left\{ \frac{r/\sigma - 1}{v} \right\} \right] \tag{1.5}$$

Substitution of eq. 1.5 into eq. 3.6 and 3.8 allows determination of $-s_{\text{eff}}^{(2)}$ and τ_{eff}, respectively. Note that these quantities, unlike $-s^{(2)}$ and τ, show a minimum at intermediate values of $\epsilon/k_{\text{B}}T$, giving the spurious impression that pair correlations anomalously weaken with attractions at low values of $\epsilon/k_{\text{B}}T$.

As a final point, we note that the single-component system with structure equivalent to that indicated by the effective one-component analysis will have the following pair potential, $\mathcal{V}_{\text{eff}}(r) = -k_{\text{B}}T \ln g_{\text{eff}}(r)$. Polydispersity

makes this potential considerably softer than the SW interaction between any two particles in the polydisperse fluid.

Bibliography

[1] E. H. Abramson and H. West-Foyle. Viscosity of nitrogen measured to pressures of 7 GPa and temperatures of 573 K. *Phys. Rev. E*, 77:041202, 2008.

[2] W. P. Krekelberg, T. Kumar, J. Mittal, J. R. Errington, and T. M. Truskett. Anomalous structure and dynamics of the Gaussian-core fluid. *Phys. Rev. E*, 79:031203–6, 2009.

[3] W. P. Krekelberg, J. Mittal, V. Ganesan, and T. M. Truskett. How short-range attractions impact the structural order, self-diffusivity, and viscosity of a fluid. *J. Chem. Phys.*, 127:044502, 2007.

[4] L. Lopez-Flores, P. Mendoza-Mendez, L. E. Sanchez-Diaz, G. Perez-Angel, M. Chavez-Paez, A. Vizcarra-Rendon, and M. Medina-Noyola. Dynamic equivalence between atomic and colloidal liquids. *arXiv:1106.2475v1*, 2011.

[5] Y. Rosenfeld. Relation between the transport coefficients and the internal entropy of simple systems. *Phys. Rev. A*, 15:2545–2549, 1977.

[6] Y. Rosenfeld. A quasi-universal scaling law for atomic transport in simple fluids. *J. Phys.: Condens. Matter*, 11:5415, 1999.

[7] M. Dzugutov. A univeral scaling law for atomic diffusion in condesed matter. *Nature*, 381:137–139, 1996.

[8] U. Bengtzelius, W. Gotze, and A. Sjolander. Dynamics of supercooled liquids and the glass transition. *J. Phys. C: Solid State Phys.*, 17(33):5915, 1984.

[9] G. Jacucci and I. R. McDonald. Structure and diffusion in mixtures of rare-gas liquids. *Physica A*, pages 607–625, 1975.

[10] E. H. Abramson. Viscosity of water measured to pressures of 6 GPa and temperatures of 300 C. *Phys. Rev. E*, 76:051203, 2007.

[11] E. H. Abramson. Viscosity of carbon dioxide measured to a pressure of 8 GPa and temperature of 673 K. *Phys. Rev. E*, 80:021201, 2009.

[12] J. L. Carmer, G. Goel, M. J. Pond, J. R. Errington, and T. M. Truskett. Enhancing tracer diffusivity by tuning interparticle interaction and solvation shell structure. *in prep.*, 2011.

[13] H. Löwen. Melting, freezing and colloidal suspensions. *Phys. Rep.*, 237:249–324, 1994.

[14] C. N. Likos. Effective interactions in soft condensed matter physics. *Phys. Rep.*, 348(4-5):267 – 439, 2001.

[15] C. N. Likos. Soft matter with soft particles. *Soft Matter*, 2:478–498, 2006.

[16] M. Schmiedeberg, T. K. Haxton, S. R. Nagel, and A. J. Liu. Mapping the glassy dynamics of soft spheres onto hard-sphere behavior. *arXiv:1107.2583v1*, 2011.

[17] M. P. Allen and D. J. Tildesley. *Computer Simulations of Liquids*. Oxford University Press, New York, 1987.

[18] J. Mittal, J. R. Errington, and T. M. Truskett. Thermodynamics Predicts How Confinement Modifies the Dynamics of the Equilibrium Hard-Sphere Fluid. *Phys. Rev. Lett.*, 96:177804, 2006.

[19] J. Mittal, J. R. Errington, and T. M. Truskett. Relationship between thermodynamics and dynamics of supercooled liquids. *J. Chem. Phys.*, 125:076102, 2006.

[20] Y. D. Fomin, V. N. Ryzhov, and N. V. Gribova. Breakdown of excess entropy scaling for systems with thermodynamic anomalies. *Phys. Rev. E*, 81(6):1–12, 2010.

[21] J. J. Hoyt, M. Asta, and B. Sadigh. Test of the Universal Scaling Law for the Diffusion Coefficient in Liquid Metals. *Phys. Rev. Lett.*, 85:594–597, 2000.

[22] A. Samanta, S. M. Ali, and S. K. Ghosh. Universal Scaling Laws of Diffusion in a Binary Fluid Mixture. *Phys. Rev. Lett.*, 87:245901, 2001.

[23] C. Mayer, F. Sciortino, C. N. Likos, P. Tartaglia, H. Löwen, and E. Zaccarelli. Multiple Glass Transitions in Star Polymer Mixtures: Insights from Theory and Simulations. *Macromolecules*, 42(1):423–434, 2009.

[24] A. J. Archer and R. Evans. Binary Gaussian core model: Fluid-fluid phase separation and interfacial properties. *Phys. Rev. E*, 64:041501, 2001.

[25] T. O. Pangburn and M. A. Bevan. Role of polydispersity in anomalous interactions in electrostatically levitated colloidal systems. *J. Chem. Phys.*, 123(17):174904, 2005.

[26] J. J. Salacuse and G. Stell. Polydisperse systems: Statistical thermodynamics, with applications to several models including hard and permeable spheres. *J. Chem. Phys.*, 77(7):3714–3725, 1982.

[27] S. Auer and D. Frenkel. Suppression of crystal nucleation in polydisperse colloids due to increase of the surface free energy. *Nature*, 413(6857):711–713, 2001.

[28] H. J. Schope, G. Bryant, and W. van Megen. Effect of polydispersity on the crystallization kinetics of suspensions of colloidal hard spheres when approaching the glass transition. *J. Chem. Phys.*, 127(8):084505–7, 2007.

[29] P. Salgi and R. Rajagopalan. Polydispersity in colloids: implications to static structure and scattering. *Adv. Colloid Interface Sci.*, 43(2-3):169–288, 1993.

[30] T. O. Pangburn and M. A. Bevan. Anomalous potentials from inverse analyses of interfacial polydisperse attractive colloidal fluids. *J. Chem. Phys.*, 124(5):054712, 2006.

[31] A. M. Puertas, M. Fuchs, and M. E. Cates. Simulation study of nonergodicity transitions: Gelation in colloidal systems with short-range attractions. *Phys. Rev. E*, 67:031406, 2003.

[32] W. G. McMillan and J. E. Mayer. The Statistical Thermodynamics of Multicomponent Systems. *J. Chem. Phys.*, 13:276–305, 1945.

[33] J. G. Kirkwood and F. P. Buff. The Statistical Mechanical Theory of Solutions. I. *J. Chem. Phys.*, 19(6):774–777, 1951.

[34] P. J. Flory and W. R. Krigbaum. Statistical Mechanics of Dilute Polymer Solutions. II. *J. Chem. Phys*, 18:1086–1094, 1950.

[35] C. N. Likos, A. Lang, M. Watzlawek, and H. Löwen. Criterion for determining clustering versus reentrant melting behavior for bounded interaction potentials. *Phys. Rev. E*, 63:031206, 2001.

[36] D. L. Ermak. A computer simulation of charged particles in solution. I. Technique and equilibrium properties. *J. Chem. Phys.*, 62:4189, 1975.

[37] J. F. Brady and G. Bossis. The rheology of concentrated suspensions of spheres in simple shear flow by numerical simulation. *J. Fluid Mech.*, 155:105–129, 1985.

[38] P. J. Hoogerbrugge and J. M. V. A. Koelman. Simulating Microscopic Hydrodynamic Phenomena with Dissipative Particle Dynamics. *Europhys. Lett.*, 19:155–160, 1992.

[39] A. Malevanets and R. Kapral. Mesoscopic model for solvent dynamics. *J. Chem. Phys*, 110:8605–8613, 1999.

[40] M. J. Pond, W. P. Krekelberg, V. K. Shen, J. R. Errington, and T. M. Truskett. Composition and concentration anomalies for structure and dynamics of Gaussian-core mixtures. *J. Chem. Phys.*, 131:161101, 2009.

[41] M. J. Pond, J. R. Errington, and T. M. Truskett. Implications of the effective one-component analysis of pair correlations in colloidal fluids with polydispersity. *arXiv:1107.4996v1*, 2011.

[42] W. P. Krekelberg, M. J. Pond, G. Goel, V. K. Shen, J. R. Errington, and T. M. Truskett. Generalized Rosenfeld scalings for tracer diffusivities in not-so-simple fluids: Mixtures and soft particles. *Phys. Rev. E*, 80(6):61205, 2009.

[43] M. J. Pond, J. R Errington, and T. M. Truskett. Generalizing Rosenfeld's excess-entropy scaling to predict long-time diffusivity in dense fluids of Brownian particles: From hard to ultrasoft interactions. *J. Chem. Phys*, 134:081101, 2011.

[44] M. J. Pond, J. R. Errington, and T. M. Truskett. Mapping between long-time molecular and Brownian dynamics. *arXiv:1108:1038v1*, 2011.

[45] F. H. Stillinger and D. K. Stillinger. Negative thermal expansion in the Gaussian core model. *Physica A*, 244:358–369, 1997.

[46] A. Lang, C. N. Likos, M. Watzlawek, and H. Löwen. Fluid and solid phases of the Gaussian core model. *J. Phys.: Condens. Matter*, 12:5087–5108, 2000.

[47] A. A. Louis, P. G. Bolhuis, and J. P. Hansen. Mean-field fluid behavior of the Gaussian core model. *Phys. Rev. E*, 62:7961–7972, 2000.

[48] S. Prestipino, F. Saija, and P. V. Giaquinta. Phase diagram of softly repulsive systems: The Gaussian and inverse-power-law potentials. *J. Chem. Phys.*, 123:144110, 2005.

[49] P. V. Giaquinta and F. Saija. Re-entrant Melting in the Gaussian-Core Model: The Entropy Imprint. *ChemPhysChem*, 6:1768–1771, 2005.

[50] P. Mausbach and H. O. May. Static and dynamic anomalies in the Gaussian core model liquid. *Fluid Phase Equilib.*, 249:17–23, 2006.

[51] C. E. Zachary, F. H. Stillinger, and S. Torquato. Gaussian core model phase diagram and pair correlations in high Euclidean dimensions. *J. Chem. Phys.*, 128:224505, 2008.

[52] H. H. Wensink, H. Löwen, M. Rex, C. N. Likos, and S. van Teeffelen. Long-time self-diffusion for Brownian Gaussian-core particles. *Comput. Phys. Commun.*, 179:77 – 81, 2008.

[53] F. H. Stillinger. Phase transitions in the Gaussian core system. *J. Chem. Phys.*, 65:3968–3974, 1976.

[54] F. H. Stillinger and T. A. Weber. Study of melting and freezing in the Gaussian core model by molecular dynamics simulation. *J. Chem. Phys.*, 68:3837–3844, 1978.

[55] J. Mittal, J. R. Errington, and T. M. Truskett. Relationships between Self-Diffusivity, Packing Fraction, and Excess Entropy in Simple Bulk and Confined Fluids. *J. Phys. Chem. B*, 111:10054–10063, 2007.

[56] J. R. Errington and P. G. Debenedetti. Relationship between structural order and the anomalies of liquid water. *Nature*, 409:318–321, 2001.

[57] J. R. Errington, T. M. Truskett, and J. Mittal. Excess-entropy-based anomalies for water like fluid. *J. Chem. Phys.*, 125:244502, 2006.

[58] J. Mittal, J. R. Errington, and T. M. Truskett. Quantitative Link between Single-Particle Dynamics and Static Structure of Supercooled Liquids. *J. Phys. Chem. B*, 110:18147–18150, 2006.

[59] J. A. Hernando. Thermodynamic potentials and distribution functions. *Mol. Phys.*, 69:319–326(8), 1990.

[60] T. M. Truskett, S. Torquato, and P. G. Debenedetti. Towards a quantification of disorder in materials: Distinguishing equilibrium and glassy sphere packings. *Phys. Rev. E*, 62:993, 2000.

[61] E. Dickinson. Polydisperse suspensions of spherical colloidal particles: analogies with multicomponent molecular liquid mixtures. *Ind. Eng. Chem. Prod. Res. Dev.*, 25(1):82–87, 1986.

[62] J. L. Barrat and J. P. Hansen. On the stability of polydisperse colloidal crystals. *J. Phys. France*, 47(9):1547–1553, 1986.

[63] P. G. Bolhuis and D. A. Kofke. Monte Carlo study of freezing of polydisperse hard spheres. *Phys. Rev. E*, 54(1):634, 1996.

[64] W. van Megen, T. C. Mortensen, S. R. Williams, and J. Müller. Measurement of the self-intermediate scattering function of suspensions of hard spherical particles near the glass transition. *Phys. Rev. E*, 58(5):6073–6085, 1998.

[65] S.-E. Phan, W. B. Russel, J. Zhu, and P. M. Chaikin. Effects of polydispersity on hard sphere crystals. *J. Chem. Phys.*, 108(23):9789–9795, 1998.

[66] P. Bartlett and P. B. Warren. Reentrant Melting in Polydispersed Hard Spheres. *Phys. Rev. Lett.*, 82(9):1979, 1999.

[67] R. P. Sear. Phase separation and crystallisation of polydisperse hard spheres. *Europhys. Lett.*, 44(4):531, 1998.

[68] D. J. Lacks and J. R. Wienhoff. Disappearances of energy minima and loss of order in polydisperse colloidal systems. *J. Chem. Phys.*, 111(1):398–401, 1999.

[69] P. Sollich. Predicting phase equilibria in polydisperse systems. *J. Phys.: Condens. Matter*, 14, 2002.

[70] P. Sollich, P. B. Warren, and M. E. Cates. *Moment Free Energies for Polydisperse Systems*, pages 265–336. John Wiley & Sons, Inc., 2007.

[71] P. N. Pusey, E. Zaccarelli, C. Valeriani, E. Sanz, W. C. K. Poon, and M. E. Cates. Hard spheres: crystallization and glass formation. *Phil. Trans. R. Soc. A*, 367(1909):4993–5011, 2009.

[72] P. Sollich and N. B. Wilding. Polydispersity induced solid-solid transitions in model colloids. *Soft Matter*, 7(9):4472–4484, 2011.

[73] J. K. Phalakornkul, A. P. Gast, R. Pecora, G. Nägele, A. Ferrante, B. Mandl-Steininger, and R. Klein. Structure and short-time dynamics of polydisperse charge-stabilized suspensions. *Phys. Rev. E*, 54(1):661–675, 1996.

[74] G. M. Whitesides and B. Grzybowski. Self-Assembly at All Scales. *Science*, 295(5564):2418–2421, 2002.

[75] V. N. Manoharan and D. J. Pine. Building Materials by Packing Spheres. *MRS Bulletin*, 29:91–95, 2004.

[76] D. Frydel and S. A. Rice. Influence of polydispersity on the effective interaction in a quasi-two-dimensional pseudo-one-component colloid fluid. *Phys. Rev. E*, 71(4):041403, 2005.

[77] L. Blum and G. Stell. Polydisperse systems. I. Scattering function for polydisperse fluids of hard or permeable spheres. *J. Chem. Phys.*, 71(1):42–46, 1979.

[78] M. Kotlarchyk and S.-H. Chen. Analysis of small angle neutron scattering spectra from polydisperse interacting colloids. *J. Chem. Phys.*, 79(5):2461–2469, 1983.

[79] B. D'Aguanno and R. Klein. Structural effects of polydispersity in charged colloidal dispersions. *J. Chem. Soc., Faraday Trans.*, 87(3):379–390, 1991.

[80] F. Lado. Static structure of polydisperse colloidal monolayers. *J. Chem. Phys.*, 108(15):6441–6446, 1998.

[81] B. J. Anderson, V. Gopalakrishnan, S. Ramakrishnan, and C. F. Zukoski. Scattering for mixtures of hard spheres: Comparison of total scattering intensities with model. *Phys. Rev. E*, 73(3):031407, 2006.

[82] D. Frenkel, R. J. Vos, C. G. de Kruif, and A. Vrij. Structure factors of polydisperse systems of hard spheres: A comparison of Monte Carlo simulations and Percus–Yevick theory. *J. Chem. Phys.*, 84(8):4625–4630, 1986.

[83] P. van Beurten and A. Vrij. Polydispersity effects in the small-angle scattering of concentrated solutions of colloidal spheres. *J. Chem. Phys.*, 74(5):2744–2748, 1981.

[84] M. Ginoza and M. Yasutomi. Measurable Structure Factor of a Multi-Species Polydisperse Percus-Yevick Fluid with Schulz Distributed Diameters. *J. Phys. Soc. Japan*, 68:2292–2297, 1999.

[85] J. G. Briano and E. D. Glandt. Statistical thermodynamics of polydisperse fluids. *J. Chem. Phys.*, 80(7):3336–3343, 1984.

[86] D. A. Kofke and E. D. Glandt. Infinitely polydisperse fluids. *J. Chem. Phys.*, 90(1):439–447, 1989.

[87] S. E. Abraham and B. Bagchi. Suppression of the rate of growth of dynamic heterogeneities and its relation to the local structure in a supercooled polydisperse liquid. *Phys. Rev. E*, 78(5):051501, 2008.

[88] J. C. Crocker and D. G. Grier. Methods of Digital Video Microscopy for Colloidal Studies. *J. Colloid Interface Sci.*, 179(1):298 – 310, 1996.

[89] C. P. Royall, M. E. Leunissen, and A. van Blaaderen. A new colloidal model system to study long-range interactions quantitatively in real space. *J. Phys.: Condens. Matter*, 15(48):S3581, 2003.

[90] P. Varadan and M. J. Solomon. Direct Visualization of Long-Range Heterogeneous Structure in Dense Colloidal Gels. *Langmuir*, 19(3):509–512, 2003.

[91] V. Prasad, D. Semwogerere, and E. R. Weeks. Confocal microscopy of colloids. *J. Phys.: Condens. Matter*, 19(11):113102, 2007.

[92] C. R. Iacovella, R. E. Rogers, S. C. Glotzer, and M. J. Solomon. Pair interaction potentials of colloids by extrapolation of confocal microscopy measurements of collective suspension structure. *J. Chem. Phys.*, 133(16):164903, 2010.

[93] M. A. Bevan and S. L. Eichmann. Optical microscopy measurements of kT-scale colloidal interactions. *Curr. Opin. Colloid Interface Sci.*, 16(2):149 – 157, 2011.

[94] T. Eckert and E. Bartsch. Re-entrant Glass Transition in a Colloid-Polymer Mixture with Depletion Attractions. *Phys. Rev. Lett.*, 89:125701, 2002.

[95] K. N. Pham, A. M. Puertas, J. Bergenholtz, S. U. Egelhaaf, A. Moussaïd, P. N. Pusey, A. B. Schofield, M. E. Cates, M. Fuchs, and W. C. K. Poon. Multiple Glassy States in a simple Model System. *Science*, 296:104, 2002.

[96] F. Sciortino. One liquid, two glasses. *Nat. Mater.*, 1:145, 2002.

[97] E. Zaccarelli. Colloidal gels: equilibrium and non-equilibrium routes. *J. Phys.: Condens. Matter*, 19(32):323101, 2007.

[98] D. A. Kofke and E. D. Glandt. Monte Carlo simulation of multicomponent equilibria in a semigrand canonical ensemble. *Mol. Phys.*, 64(6):1105–1131, 1988.

[99] G. C. Rutledge. Modeling experimental data in a Monte Carlo simulation. *Phys. Rev. E*, 63:021111, 2001.

[100] N. B. Wilding and P. Sollich. Grand canonical ensemble simulation studies of polydisperse fluids. *J. Chem. Phys.*, 116(16):7116–7126, 2002.

[101] N. B. Wilding. A nonequilibrium Monte Carlo approach to potential refinement in inverse problems. *J. Chem. Phys.*, 119:12163, 2003.

[102] J. R. Errington, P. G. Debenedetti, and S. Torquato. Quantification of order in the Lennard-Jones system. *J. Chem. Phys.*, 118:2256–2263, 2003.

[103] J. R. Errington. Direct calculation of liquid–vapor phase equilibria from transition matrix Monte Carlo simulation. *J. Chem. Phys.*, 118:9915–9925, 2003.

[104] J. R. Errington and V. K. Shen. Direct evaluation of multicomponent phase equilibria using flat-histogram methods. *J. Chem. Phys.*, 123(16):164103, 2005.

[105] A. P. Lyubartsev, A. A. Martsinovski, S. V. Shevkunov, and P. N. Vorontsov-Velyaminov. New approach to Monte Carlo calculation of the free energy: Method of expanded ensembles. *J. Chem. Phys.*, 96:1776–1783, 1992.

[106] E. C. Cichowski, T. R. Schmidt, and J. R. Errington. Determination of Henry's law constants through transition matrix Monte Carlo simulation. *Fluid Phase Equilib.*, 236(1-2):58–65, 2005.

[107] J. R. Errington and D. A. Kofke. Calculation of surface tension via area sampling. *J. Chem. Phys.*, 127:174709, 2007.

[108] S. Asakura and F. Oosawa. On Interaction between Two Bodies Immersed in a Solution of Macromolecules. *J. Chem. Phys.*, 22:1255, 1954.

[109] H. Reiss, H. L. Frisch, and J. L. Lebowitz. Statistical mechanics of rigid spheres. *J. Chem. Phys.*, 31:369, 1959.

[110] T. M. Truskett, S. Torquato, S. Sastry, P. G. Debenedetti, and F. H. Stillinger. Structural precursor to freezing in the hard-disk and hard-sphere systems. *Phys. Rev. E*, 58:3083–3088, 1998.

[111] R. Chopra, T. M. Truskett, and J. R. Errington. On the Use of Excess Entropy Scaling to Describe the Dynamic Properties of Water. *J. Phys. Chem. B*, 114(32):10558–10566, 2010.

[112] J. Mittal, J. R. Errington, and T. M. Truskett. Does confining the hard-sphere fluid between hard walls change its average properties? *J. Chem. Phys.*, 126:244708, 2007.

[113] J. Mittal, V. K. Shen, J. R. Errington, and T. M. Truskett. Confinement, entropy, and single-particle dynamics of equilibrium hard-sphere mixtures. *J. Chem. Phys.*, 127:154513, 2007.

[114] G. Goel, W. P. Krekelberg, M. J. Pond, J. Mittal, V. K. Shen, J. R. Errington, and T. M. Truskett. Available states and available space:

static properties that predict self-diffusivity of confined fluids. *J. Stat. Mech.*, page P04006, 2009.

[115] G. Goel, W. P. Krekelberg, J. R. Errington, and T. M. Truskett. Tuning Density Profiles and Mobility of Inhomogeneous Fluids. *Phys. Rev. Lett.*, 100:106001, 2008.

[116] M. S. Shell, P. G. Debenedetti, and A. Z. Panagiotopoulos. Molecular structural order and anomalies in liquid silica. *Phys. Rev. E*, 66:011202, 2002.

[117] T. M. Truskett and K. A. Dill. A Simple Statistical Mechanical Model of Water. *J. Phys. Chem. B*, 106:11829–11842, 2002.

[118] P. Kumar, S. V. Buldyrev, F. Sciortino, E. Zaccarelli, and H. E. Stanley. Static and dynamic anomalies in a repulsive spherical ramp liquid: Theory and simulation. *Phys. Rev. E*, 72:021501, 2005.

[119] R. Esposito, F. Saija, A. M. Saitta, and P. V. Giaquinta. Entropy-based measure of structural order in water. *Phys. Rev. E*, 73:040502(R), 2006.

[120] P. A. Netz, S. V. Buldyrev, M. C. Barbosa, and H. E. Stanley. Thermodynamic and dynamic anomalies for dumbbell molecules interacting with a repulsive ramplike potential. *Phys. Rev. E*, 73:061504, 2006.

[121] L. Xu, S. V. Buldyrev, C. A. Angell, and H. E. Stanley. Thermodynamics and dynamics of the two-scale spherically symmetric Jagla ramp model of anomalous liquids. *Phys. Rev. E*, 74:031108, 2006.

[122] R. Sharma, S. N. Chakraborty, and C. Chakravarty. Entropy, diffusivity, and structural order in liquids with waterlike anomalies. *J. Chem. Phys.*, 125:204501, 2006.

[123] A. B. de Oliveira, M. C. Barbosa, and P. A. Netz. Interplay between structure and density anomaly for an isotropic core-softened ramp-like potential. *Physica A*, 386:744–747, 2007.

[124] Z. Yan, S. V. Buldyrev, P. Kumar, N. Giovambattista, P. G. Debenedetti, and H. E. Stanley. Structure of the first- and second-neighbor shells of simulated water: Quantitative relation to translational and orientational order. *Phys. Rev. E*, 76:051201, 2007.

[125] M. M. Szortyka and M. C. Barbosa. Diffusion anomaly in an associating lattice gas model. *Physica A*, 380:27–35, 2007.

[126] A. B. de Oliveira, G. Franzese, P. A. Netz, and M. C. Barbosa. Waterlike hierarchy of anomalies in a continuous spherical shouldered potential. *J. Chem. Phys.*, 128:064901, 2008.

[127] W. P. Krekelberg, J. Mittal, V. Ganesan, and T. M. Truskett. Structural anomalies of fluids: Origins in second and higher coordination shells. *Phys. Rev. E*, 77:041201, 2008.

[128] Z. Yan, S. V. Buldyrev, and H. E. Stanley. Relation of water anomalies to the excess entropy. *Phys. Rev. E*, 78:051201, 2008.

[129] A. Chaimovich and M. S. Shell. Anomalous waterlike behavior in spherically-symmetric water models optimized with the relative entropy. *Phys. Chem. Chem. Phys.*, 11:1901–1915, 2009.

[130] W. G. Hoover. *Computational Statistical Mechanics*, pages 172–173. Elsevier Science Pub Co, 1991.

[131] N. Gnan, T. B. Schrøder, U. R. Pedersen, N. P. Bailey, and J. C. Dyre. Pressure-energy correlations in liquids. IV. Isomorphs in liquid phase diagrams. *J. Chem. Phys.*, 131:234504, 2009.

[132] P. Mausbach and H.-O. May. Transport Anomalies in the Gaussian Core Model Fluid. *Z. Phys. Chem.*, 223(9):1035–1046, 2009.

[133] S. Chapman and T. G. Cowling. *The Mathematical Theory of Non-uniform Gases*. Cambridge University Press, 3rd edition, 1970.

[134] K. Tankeshwar and F. Ould-Kaddour. Tracer diffusion in a simple liquid. *J. Phys.: Condens. Matter*, 4:3349–3360, 1992.

[135] S. K. Sharma and K. Tankeshwar. Self-diffusion coefficients of expanded rubidium. *J. Phys.: Condens. Matter*, 8:10839–10845, 1996.

[136] K. Tankeshwar, B. Singla, and K. N. Pathak. A simple model for the calculation of self-diffusion. *J. Phys.: Condens. Matter*, 3:3173–3182, 1991.

[137] B. Widom and J. S. Rowlinson. New Model for the Study of Liquid–Vapor Phase Transitions. *J. Chem. Phys*, 52:1670–1684, 1970.

[138] D. C. Rapaport. *The Art of Molecular Dynamic Simulation*. Cambridge University Press, Cambridge, 2nd edition, 2004.

[139] V. K. Shen and J. R. Errington. Determination of Surface Tension in Binary Mixtures Using Transition-Matrix Monte Carlo. *J. Chem. Phys.*, 124:024721, 2006.

[140] Vincent K. Shen and Jeffrey R. Errington. Determination of fluid-phase behavior using transition-matrix monte carlo: binary lennard-jones mixtures. *J. Chem. Phys.*, 122:064508, 2005.

[141] T. Boublik. Hard-Sphere Equation of State. *J. Chem. Phys.*, 53:471, 1970.

[142] G. A. Monsoori, N. F. Carnahan, K. E. Starling, and T. W. Leland. Equilibrium Thermodynamic Properties of the Mixture of Hard Spheres. *J. Chem. Phys.*, 54:1523, 1971.

[143] I. Biazzo, F. Caltagirone, G. Parisi, and F. Zamponi. Theory of Amorphous Packings of Binary Mixtures of Hard Spheres. *Phys. Rev. Lett.*, 102:195701, 2009.

[144] S. Yerazunis, S. W. Cornell, and B. Wintner. Dense Random Packing of Binary Mixtures of Spheres. *Nature*, 207:835, 1965.

[145] P. N. Pusey and W. van Megen. Phase behaviour of concentrated suspensions of nearly hard colloidal spheres. *Nature*, 320:340, 1986.

[146] E. R. Weeks, J. C. Crocker, A. C. Levitt, A. Schofield, and D. A. Weitz. Three-Dimensional Direct Imaging of Structural Relaxation Near the Colloidal Glass Transition. *Science*, 287:627–631, 2000.

[147] H. Löwen. Fun with hard spheres. In K. R. Mecke and D. Stoyan, editors, *Statistical Physics and Spatial Statistics*, volume 554 of *Lecture Notes in Physics*, page 295. Springer, Berlin, 2000.

[148] M. Watzlawek, C. N. Likos, and H. Löwen. Phase Diagram of Star Polymer Solutions. *Phys. Rev. Lett.*, 82:5289–5292, 1999.

[149] C. N. Likos, M. Watzlawek, and H. Löwen. Freezing and clustering transitions for penetrable spheres. *Phys. Rev. E*, 58:3135–3144, 1998.

[150] S. Prestipino, F. Saija, and P. V. Giaquinta. Phase diagram of the Gaussian-core model. *Phys. Rev. E*, 71:050102, 2005.

[151] B. M. Mladek, D. Gottwald, G. Kahl, M. Neumann, and C. N. Likos. Formation of polymorphic cluster phases for a class of models of purely repulsive soft sphere. *Phys. Rev. Lett.*, 96:045701, 2006.

[152] F. Lo Verso, C. N. Likos, and L. Reatto. Star polymers with tunable attractions: cluster formation, phase separation, reentrant crystallization. *Progr. Colloid Polym. Sci.*, 133:78–87, 2006.

[153] A. J. Moreno and C. N. Likos. Diffusion and relaxation dynamics in cluster crystals. *Phys. Rev. Lett.*, 99:107801, 2007.

[154] M. Mladek, D. Gottwald, G. Kahl, M. Neumann, and C. N. Likos. Clustering in the absence of attractions: density functional theory and computer simulations. *J. Phys. Chem. B*, 111:12799–12808, 2007.

[155] F. Saija, S. Prestipino, and P. V. Giaquinta. Evaluation of phenomenological one-phase criteria for the melting and freezing of softly repulsive particles. *J. Chem. Phys.*, 124:244504, 2006.

[156] G. Foffi, F. Sciortino, P. Tartaglia, E. Zaccarelli, F. Lo Verso, L. Reatto, K. A. Dawson, and C. N. Likos. Structural Arrest in Dense Star-Polymer Solutions. *Phys. Rev. Lett.*, 90:238301, 2003.

[157] J. C. Pamies, A. Cacciuto, and D. Frenkel. Phase diagram of Hertzian spheres. *J. Chem. Phys.*, 131, 2009.

[158] L. A. Shall and S. A. Egorov. Structural and dynamical anomalies of a Gaussian core fluid: A mode-coupling theory study. *J. Chem. Phys.*, 132(18):184504, 2010.

[159] H. Jacquin and L. Berthier. Anomalous structural evolution of soft particles: equibrium liquid state. *Soft Matter*, 6:29702974, 2010.

[160] L. Berthier, A. J. Moreno, and G. Szamel. Increasing the density melts ultrasoft colloidal glasses. *Phys. Rev. E*, 82:060501, 2010.

[161] M. Schmidt. An ab initio density functional for penetrable spheres. *J. Phys: Condens. Matter*, 11:10163–10169, 1999.

[162] A. Jusufi and C. N. Likos. Colloquium: Star-branched polyelectrolytes: the physics of their conformations and interactions. *Rev. Mod. Phys.*, 81:1753 – 1772, 2009.

[163] M.f Medina-Noyola. Long-time self-diffuison in concentrated colloidal dispersions. *Phys. Rev. Lett.*, 60(26):2705, 1988.

[164] D. S. Dean and A. Lefèvre. Self-diffusion in a system of interacting Langevin particles. *Phys. Rev. E*, 69:061111, 2004.

[165] L. Berthier, E. Flenner, H. Jacquin, and G. Szamel. Scaling of the glassy dynamics of soft repulsive particles: A mode-coupling approach. *Phys. Rev. E*, 81:031505, 2010.

[166] A. Ikeda and K. Miyazaki. Glass Transition of the Monodisperse Gaussian Core Model. *Phys. Rev. Lett.*, 106:015701, 2011.

[167] S.-H. Suh, C.-H. Kim, S.-C. Kim, and A. Santos. Molecular dynamics simulation study of self-diffusion for penetrable-sphere model fluids. *Phys. Rev. E*, 82:051202, 2010.

[168] G. K. Batchelor. Brownian diffusion of particles with hydrodynamic interaction. *J. Fluid Mech.*, 74:1–29, 1976.

[169] G. K. Batchelor. Diffusion in a dilute polydisperse system of interacting spheres. *J. Fluid Mech.*, 131:155–175, 1983.

[170] H. N. W. Lekkerkerker and J. K. G. Dhont. On the calculation of the self-diffusion coefficient of interacting Brownian particles. *J. Chem. Phys*, 80(11):5790, 1984.

[171] J. K. G. Dhont. *An Introduction to Dynamics of Colloids*. Elsevier, Burlington, 1996.

[172] D. Ben-Amotz and G. Stell. Reformulation of Weeks-Chandler-Andersen Perturbation Theory Directly in Terms of a Hard-Sphere Reference System. *J. Phys. Chem. B*, 108:6877–6882, 2004.

[173] E. M. Grzelak and J. R. Errington. Nanoscale Limit to the Applicability of Wenzels Equation. *Langmuir*, 26(16):1329713304, 2010.

[174] R. Chopra, T. M. Truskett, and J. R. Errington. On the Use of Excess Entropy Scaling To Describe Single-Molecule and Collective Dynamic Properties of Hydrocarbon Isomer Fluids. *J. Phys. Chem. B*, 114(49):16487–16493, 2010.

[175] D. M. Heyes and A. C. Brańka. Molecular and Brownian Dynamics Simulations of Self-Diffusion in Inverse Power Fluids. *Physics and Chemistry of Liquids*, 28(2):95–115, 1994.

[176] H. Löwen, J.-P. Hansen, and J.-N. Roux. Brownian dynamics and kinetic glass transition in colloidal suspensions. *Phys. Rev. A*, 44:1169–1181, 1991.

[177] T. Gleim, W. Kob, and K. Binder. How Does the Relaxation of a Supercooled Liquid Depend on Its Microscopic Dynamics? *Phys. Rev. Lett.*, 81:4404–4407, 1998.

[178] G. Foffi, K. A. Dawson, S. V. Buldyrev, F. Sciortino, E. Zaccarelli, and P. Tartaglia. Evidence for an unusual dynamical-arrest scenario in short-ranged colloidal system. *Phys. Rev. E*, 65:050802(R), 2002.

[179] E. Lange, J. B. Caballero, A. M. Puertas, and M. Fuchs. Comparison of structure and transport properties of concentrated hard and soft sphere fluids. *J. Chem. Phys*, 130:174903–8, 2009.

[180] C. N. Likos, H. Löwen, M. Watzlawek, B. Abbas, O. Jucknischke, J. Allgaier, and D. Richter. Star Polymers Viewed as Ultrasoft Colloidal Particles. *Phys. Rev. Lett.*, 80(20):4450–4453, 1998.

[181] H. Löwen, T. Palberg, and R. Simon. Dynamical criterion for freezing of colloidal liquids. *Phys. Rev. Lett.*, 70:1557–1560, 1993.

[182] I. M. de Schepper, E. G. D. Cohen, P. N. Pusey, and H. N. W. Lekkerkerker. Long time diffusion in suspensions of interacting charged colloids. *J. Phys.: Condens. Matter*, 1(36):6503, 1989.

[183] P. N. Pusey, H. N. W. Lekkerkerker, E. G. D. Cohen, and I. M. de Schepper. Analogies between the dynamics of concentrated charged colloidal suspensions and dense atomic liquids. *Physica A*, 164(1):12 – 27, 1990.

[184] E. G. D. Cohen and I. M. de Schepper. Note on transport processes in dense colloidal suspensions. *J. Stat. Phys.*, 63:241–248, 1991.

Vita

Mark Jeffrey Pond was born in Aurora, Colorado in 1984, the son of Dr. L. Page Pond and Kimberly Pond. He received a Bachelor of Science in Chemical Engineering degree in Chemical Engineering and a Bachelor of Arts degree in Mathematics from Rice University in May 2006. From there he was accepted into the graduate program at the University of Texas at Austin and started his graduate studies in August, 2006.

Permanent address: 9866 Carmel Court
Lone Tree, CO 80124

This dissertation was typeset with LaTeX[†] by the author.

[†]LaTeX is a document preparation system developed by Leslie Lamport as a special version of Donald Knuth's TeX Program.